

**A 2500 YEAR LAKE SEDIMENT RECORD OF DROUGHT AND HUMAN ACTIVITY
FROM SOUTHWESTERN CHINA**

by

Aubrey L. Hillman

B.S., University of Maryland Baltimore County, 2009

B.A., University of Maryland Baltimore County, 2009

Submitted to the Graduate Faculty of
Arts and Sciences in partial fulfillment
of the requirements for the degree of
Master of Science

University of Pittsburgh

2011

UNIVERSITY OF PITTSBURGH
FACULTY OF ARTS AND SCIENCES

This thesis was presented

by

Aubrey L. Hillman

It was defended on

March 30, 2011

and approved by

Daniel Bain, Ph.D., Assistant Professor

Patrick Manning, Ph.D., World History Center Director

Michael Rosenmeier, Ph.D., Assistant Professor

Thesis Director: Mark Abbott, Ph.D., Associate Professor

Copyright © by Aubrey L. Hillman

2011

**A 2500 YEAR LAKE SEDIMENT RECORD OF DROUGHT AND HUMAN
ACTIVITY FROM SOUTHWESTERN CHINA**

Aubrey L. Hillman, M.S.

University of Pittsburgh, 2011

The delivery of precipitation to southwestern China is largely through monsoon circulation which has evolved with changing insolation forcing during the Holocene and will likely continue to change in response to greenhouse gas increases. Additionally, southwestern China has a long history of human activity including mining, metallurgy, agriculture, and pollution. Here, high-resolution sampling of a sediment core from Lake Xing Yun in the Yunnan Province (24°10'N, 102°46'E), a drought sensitive lake that behaves as a closed basin, provides a sub-decadal record of changing climate and human activity in the late Holocene. We use $\delta^{18}\text{O}$ and $\delta^{13}\text{C}$ measurements of authigenic precipitated from the lake water and magnetic susceptibility values to document the timing, direction, and magnitude of moisture changes associated with variations in monsoon strength. We use $\delta^{13}\text{C}$ and $\delta^{15}\text{N}$ measurements on organic matter and carbon to nitrogen ratios to assess the impact of human activity on the Xing Yun watershed and sediment trace metal concentrations in investigate regional mining and smelting intensity.

The 2,500 year record highlights several transition periods related to both human and climate forcing. The rise of metallurgy and intensive mining practices occurs at 900 AD, much later than historical records indicate. A number of proxies including $\delta^{13}\text{C}$ values and C/N ratio show a marked shift at 1600 AD, the time in which many Han immigrants from the north settled and worked land in the Yunnan Province. The most pronounced feature of the record is a rapid

transition to a substantially drier climate that took place over 50 years and persisted from 1360-1880 AD as an expression of the Little Ice Age (LIA). This project demonstrates that complex human and climate interactions have been taking place for thousands of years and have the potential to illuminate discontinuities in Chinese historical records and learn lessons that might apply to future climate change.

TABLE OF CONTENTS

LIST OF TABLES	VIII
LIST OF FIGURES	IX
PREFACE.....	XII
1.0 INTRODUCTION.....	1
1.1 CLIMATE	1
1.2 SETTING.....	5
1.3 HISTORY	8
2.0 A 2500 YEAR HISTORY OF DROUGHT IN SOUTHWESTERN CHINA.....	18
2.1 INTRODUCTION	18
2.2 METHODS.....	21
2.3 RESULTS	25
2.4 DISCUSSION.....	35
2.4.1 Environmental Isotopes	35
2.4.2 Covariance.....	37
2.4.3 Other Climate Comparisons.....	39
2.5 CONCLUSION	45
3.0 A 2500 YEAR HISTORY OF HUMAN ACTIVITY IN SOUTHWESTERN CHINA	47

3.1	INTRODUCTION	47
3.2	METHODS.....	48
3.3	RESULTS.....	52
3.4	DISCUSSION.....	57
3.5	CONCLUSION	63
4.0	THE INTERACTION BETWEEN HUMAN ACTIVITY AND LANDSCAPE DEVELOPMENT	65
	APPENDIX A- TABLE OF DATA FOR DRIVE 1.....	68
	APPENDIX B- TABLE OF DATA FOR DRIVE 2.....	75
	APPENDIX C- TABLE OF DATA FOR DRIVE 3.....	80
	APPENDIX D- TABLE OF TRACE METAL DATA.....	84
	APPENDIX E- TABLE OF CARBON TO NITROGEN RATIO DATA	96
	BIBLIOGRAPHY.....	99

LIST OF TABLES

Table 2-1- Radiocarbon dates	26
Table 3-1- Measured elements and detection limits.	50
Table 3-2- Radiocarbon dates	53
Appendix A- Table of Data for Drive 1.....	68
Appendix B- Table of Data for Drive 2.....	75
Appendix C- Table of Data for Drive 3.....	80
Appendix D- Table of Trace Metal Data.....	84
Appendix E- Table of Carbon to Nitrogen Ratio Data.....	96

LIST OF FIGURES

Figure 1-1- Oxygen isotopes from Xing Yun compared to summer insolation at 20°N. Image adapted from Hodell et al. (1999).	3
Figure 1-2- Map of Yunnan Province adapted from ESRI 2010 with Chinese border highlighted for emphasis. The approximate location of Xing Yun is circled.	4
Figure 1-3- Map of Xing Yun lake and watershed adapted from ESRI 2010. Areas of low relief are light in color. The boundaries of the watershed are traced.	6
Figure 1-4- Bathymetry of Xing Yun Lake. Star indicates the location where core A-09 was taken.	7
Figure 1-5- Map of archaeological sites of interest in the Yunnan Province adapted from ESRI 2010. All sites are from the Dian culture mentioned in Higham (1996). Lijiashan is located between Xing Yun and Fuxian.	9
Figure 1-6- Map of pre-20 th century copper mines in the Yunnan province adapted from Golas (1999). The square is the approximate location of Xing Yun.	11
Figure 1-7- Map of pre-20 th century silver mines in the Yunnan province adapted from Golas (1999). The square is the approximate location of Xing Yun.	12
Figure 1-8- Map of pre-20 th century tin and lead mines in the Yunnan province adapted from Golas (1999). The square is the approximate location of Xing Yun.	13

Figure 1-9- Estimates of silver taxation in the Yunnan Province during the Ming dynasty adapted from Yang (2009). Dots represent the percent of the national silver tax where data was available. The year 1504 A.D. was a year of low silver taxation, but nonetheless Yunnan constitutes 100% of the silver taxed during that year.	14
Figure 1-10- Estimates of yearly copper production in Yunnan adapted from Yang (2009).	15
Figure 2-1- ^{210}Pb ages from Xing Yun A-09 using the CRS model. Error bars represent one standard deviation.	25
Figure 2-2- Age depth model for Xing Yun A-09. Circles denote ^{14}C dates, the square denotes ^{137}Cs date, and the triangle denotes the ^{210}Pb date at 1880 AD.	26
Figure 2-3 – Selected X-ray diffraction peaks for Xing Yun A-09 drive 1. Intensity is unitless. Calcite peaks are marked with a C, quartz peaks are marked with a Q.	28
Figure 2-4- X-ray diffraction peaks for Xing Yun A-09 drive 2. Intensity is unitless. Calcite peaks are marked with a C, quartz peaks are marked with a Q.	29
Figure 2-5- X-ray diffraction peaks for Xing Yun A-09 drive 3. Intensity is unitless. Calcite peaks are marked with a C, quartz peaks are marked with a Q.	30
Figure 2-6- Euhedral calcite from Xing Yun A-09 drive 1 4 cm.	31
Figure 2-7- Subhedral calcite from Xing Yun A-09 drive 1 130 cm.	32
Figure 2-8- From left to right: % organic matter in dashed line, % carbonate in solid line, % residual mineral matter in dotted line, stable isotopes, and magnetic susceptibility of Xing Yun A-09.	33
Figure 2-9- Carbon to nitrogen ratio in Xing Yun A-09.	35
Figure 2-10- Covariance for Xing Yun A-09 grouped into 4 time periods. 1- 400 BC to 1360 AD. 2- 1360 to 1880 AD. 3- 1880 to 1970 AD. 4- 1970 AD to present.	38

Figure 2-11- Calculated $\Delta\delta^{18}\text{O}$ values compared with Xing Yun A-09 oxygen isotope record...	40
Figure 2-12- Xing Yun A-09 oxygen isotopes compared to Dongge and Wanxiang Cave oxygen isotopes. Highlighted areas show the transition into the wet period of 1140-1360 AD, the transition into the dry LIA, and the transition out of the dry LIA.	42
Figure 2-13- Cook et al. (2010) PDSI reconstruction compared to Xing Yun A-09 oxygen isotopes. Highlighted areas indicate potential periods of agreement.....	43
Figure 2-14- Braganza et al. (2009) ENSO reconstruction compared to Xing Yun A-09 oxygen isotopes. Highlighted areas are potential periods of anti-correlation.	45
Figure 3-1- ^{210}Pb ages from Xing Yun A-09 using the CRS model. Error bars represent one standard deviation.	52
Figure 3-2- Age depth model for Xing Yun A-09. Circles denote ^{14}C dates, the square denotes ^{137}Cs date, and the triangle denotes the ^{210}Pb date at 1880 AD.	53
Figure 3-3- Metal concentration for selected elements from Xing Yun A-09.....	55
Figure 3-4- Biplot of PCA loadings for 23 measured elements from Xing Yun A-09.....	56
Figure 3-5- Carbon to nitrogen ratio in Xing Yun A-09.....	57
Figure 3-6- Calculated metal flux for selected elements from Xing Yun A-09. Shaded areas represent periods where there was no unified empire. Lines represent transitions into climate units III and IV.	59
Figure 3-7- From top to bottom: stratigraphic column indicating red color and presence of pyrite in light pattern, dark color and lack of pyrite in dark pattern, carbon to nitrogen ratio, calculated sedimentation rate, and magnetic susceptibility for Xing Yun A-09.	60
Figure 3-8- Fifty six samples plotted with component 1 and 2 scores from Xing Yun A-09.	63

PREFACE

A number of people have been instrumental in the success of this project. First and foremost I have to thank my parents and husband-to-be who have been constant sources of support and encouragement. I want to thank Mark Abbott for taking me on and letting me run with this project. Mark has pushed me harder than I thought possible and I've come a long way in two years. I also want to thank all of my other committee members who have been a never ending source of advice and guidance. Thanks to all of the other graduate students working under Mark: Byron Steinman, Matt Finkenbinder, and a special thanks to Dave Pompeani who has been a sounding board for all of my ideas and has helped with just about every aspect of this project. I would like to thank the various universities that have run my samples: University of Pittsburgh for stable isotopes, ^{210}Pb dating, SEM, and XRD, University of California at Irvine for radiocarbon, University of Alberta for trace metals, Duquesne University for XRD, and Idaho State University for C/N.

1.0 INTRODUCTION

In this study, a sediment profile from the Xing Yun basin provides a high-resolution, accelerator mass spectrometry (AMS) ^{14}C -dated record of late Holocene climate change and human impact in southwestern China. Xing Yun Lake records the regional variation in the Asian Monsoon over millennial time scales at a sub-decadal resolution. The record from Xing Yun substantiates several other paleoclimate records in the region. The region surrounding Xing Yun offers an interesting perspective on Chinese history; however, historical records are limited. Using a variety of proxies on lake sediments from Xing Yun such as trace metal concentration, magnetic susceptibility, oxygen and carbon isotopic composition, and carbon to nitrogen ratios, has the potential to clarify gaps in the historical records and substantiate historical records. Additionally, the aim of this project is to quantify recent human disturbance to the watershed and assess the extent of environmental degradation.

1.1 CLIMATE

Asia is the world's largest land mass with a total population of roughly 2 billion people. Precipitation in southeast Asia is highly seasonal because it is delivered by summer monsoon circulation. Changes in the timing and strength of the summer monsoon impacts water resources and the people who depend on it. Kunming ($25^{\circ}20'\text{N}$, $102^{\circ}43'\text{E}$), the capital of the Yunnan

province in the People's Republic of China, receives 70% of its annual precipitation during the months of June, July, August, and September. Increased radiative forcing caused by human activities is likely to change summer monsoon patterns, affecting the lives of as much as a third of the world's population. In order to better understand how the Asian monsoon (AM) has changed in the past and might respond to increasing greenhouse gas concentrations, we look to Asian paleoclimate data preserved in ice cores, speleothems, lake sediments, and tree rings (Cook et al., 2010; Dykoski et al., 2005; Hodell et al., 1999; Yafeng et al., 1999).

There has been a great amount of interest in understanding how monsoonal systems vary over millennial time scales because of the AM's influence on densely populated regions. The AM is strongly influenced by precessional insolation forcing, as demonstrated in a number of paleoclimate studies (Dykoski et al., 2005; Hodell et al., 1999; Zhang et al., 2008). During the last glacial maximum, precessional forcing was low in the Northern Hemisphere summer, causing the summer portion of AM to weaken and the winter monsoon to strengthen (Figure 1-1) (Hodell et al., 1999). This changed around 12,000 years BP when summer monsoon strength increased until 8,000 years BP. Thereafter, in the middle to late Holocene, data show summer monsoon strength weakening. Although precessional forcing is clearly a major factor impacting the strength of the AM over millennial timescales there are clearly other factors that affect precipitation intensity in the part of the world that operate on decadal to century timescales that can be detected by lake sediment studies.

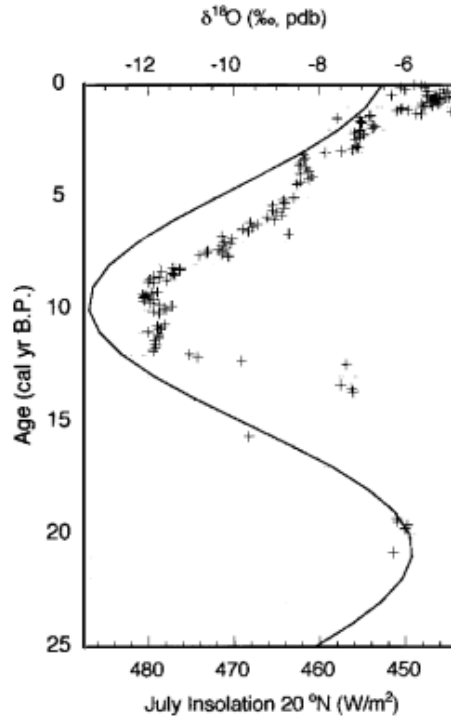


Figure 1-1- Oxygen isotopes from Xing Yun compared to summer insolation at 20°N. Image adapted from Hodell et al. (1999).

The AM, El Niño Southern Oscillation (ENSO), and North Atlantic Oscillation (NAO) are connected in complex ways with wide-reaching consequences that vary over decadal to century timescales. A number of studies have sought to understand the complexity of the AM as related to other climate patterns through computer modeling (Kinter et al., 2002; Lau and Nath, 2006; Wang et al., 2000; Yim et al., 2008). In an attempt to realize the changing relationship between the AM and ENSO, Kinter et al. (2002) used historical data from the last 50 years and produced computer simulations of the yearly interactions between the Indian monsoon rainfall index, the Webster and Yang monsoon index, the tropical-wide oscillation index, and the Southern Oscillation Index (SOI). The results of the study showed that prior to 1976, ENSO cycles were preceded by a period of a strong AM. After 1976, AM strength was no longer a

reliable indicator of ENSO and cause and effect become difficult to separate. Possible causes for the change in this relationship are still being investigated, but one possibility is the cycling of the NAO.

The Asian monsoon has two components, South Asian and East Asian, of which the East Asian component is frequently investigated because it is linked to other climate phenomena, such as the West Pacific monsoon in the United States, ENSO, and the Australian summer monsoon (Chang, 2004). The East Asian monsoon affects southwestern China including the provinces of Yunnan, Sichuan, Guizhou, Guangxi, and Hunan (Figure 1-2). The Yunnan Province is well suited for a paleoclimate study because it has lakes that preserve authigenic calcium carbonate which record changes in the precipitation-evaporation (P-E) balance over many thousands of years.

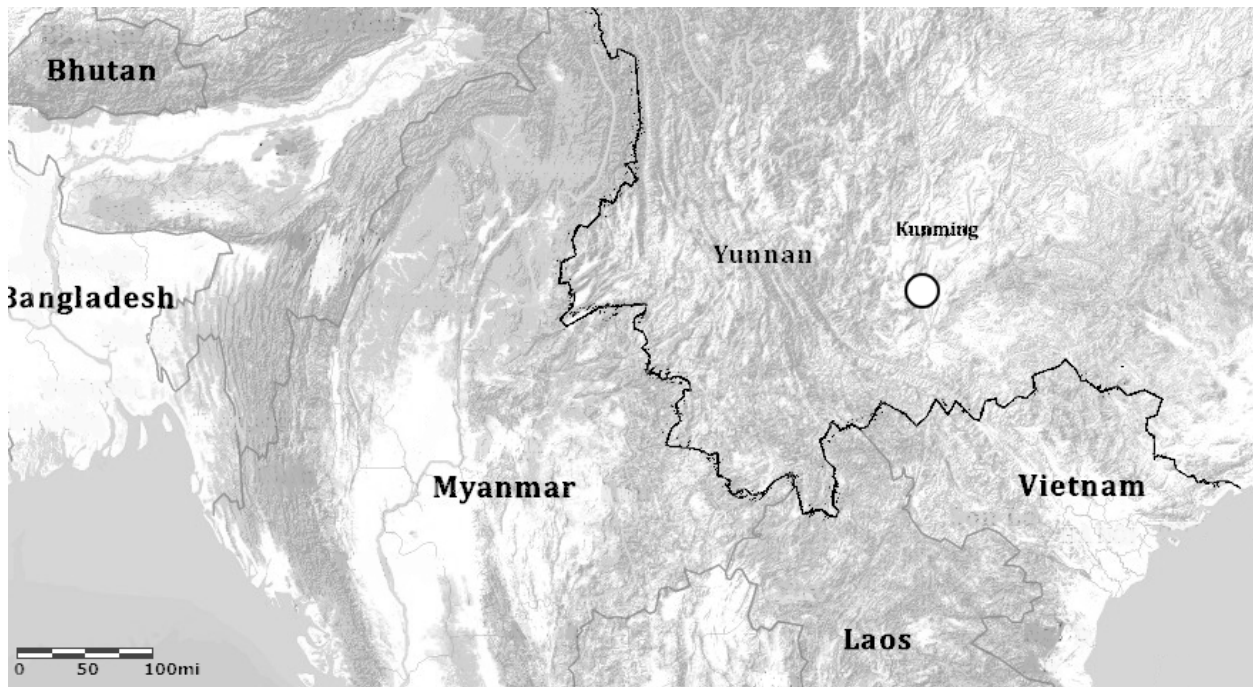


Figure 1-2- Map of Yunnan Province adapted from ESRI 2010 with Chinese border highlighted for emphasis.

The approximate location of Xing Yun is circled.

1.2 SETTING

The Yunnan Province lies in southwestern China, east of Tibet, and north of Myanmar, Laos, and Vietnam. Xing Yun Lake (24°10'N, 102°46'E, 1723 m) is in the Yunnan Province, underlain by Paleozoic limestone which has several mineral deposits of economic interest including marble (Golas, 1999). Xing Yun is connected to Fuxian Lake by a small stream and sits 3 m higher than Fuxian (Figure 1-3) (Li et al., 2007). Xing Yun is a relatively small lake with an area of 34.7 km², a catchment area of 383 km², and a mean depth of 5.9 m (Figure 1-4) (Li et al., 2007). The origin of Xing Yun is unknown, but it was likely formed by tectonic faulting and Fuxian is much larger and the result of tectonic faulting (Whitmore et al., 1997). Xing Yun has several inflowing and one outflowing stream into Fuxian that has been artificially widened several times. In 1923 AD and again in 1956 AD, the outflowing river was dredged and the channel that connects Xing Yun and Fuxian today widened and deepened. This allowed water to flow from Xing Yun into Fuxian and dropped Xing Yun Lake level by 2.0 m in 1923 AD and an additional 1.0 m in 1956 AD.

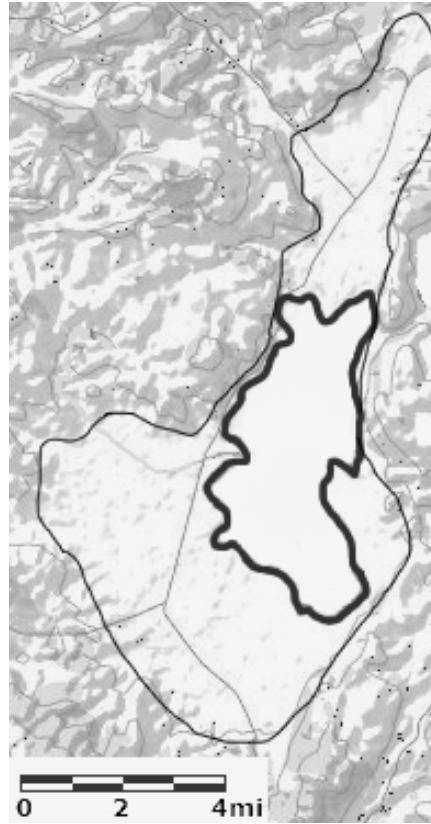


Figure 1-3- Map of Xing Yun lake and watershed adapted from ESRI 2010. Areas of low relief are light in color. The boundaries of the watershed are traced.

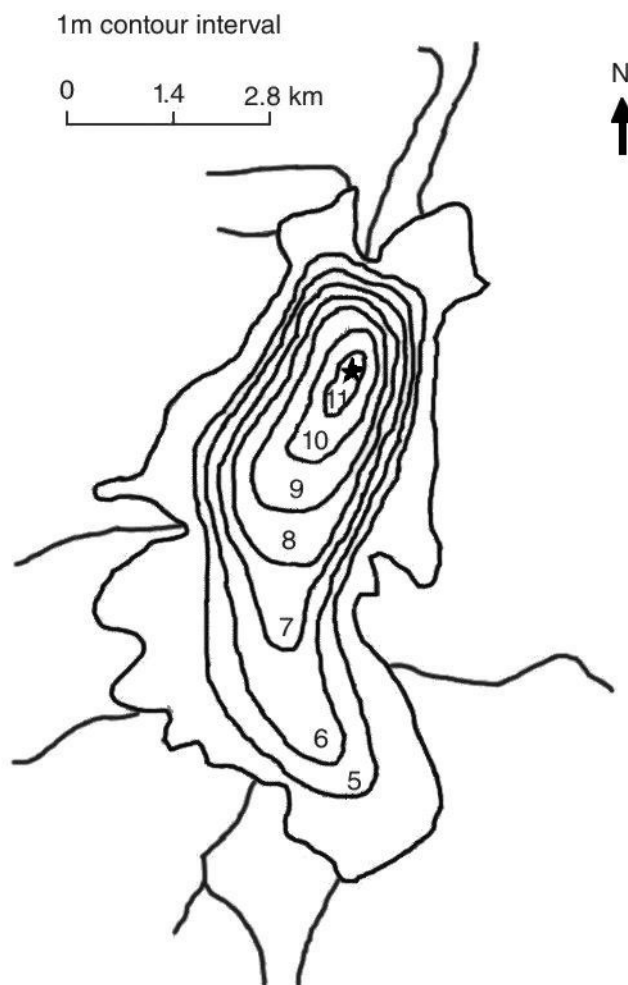


Figure 1-4- Bathymetry of Xing Yun Lake. Star indicates the location where core A-09 was taken.

Xing Yun and the entire region of southwestern China is strongly influenced by the AM, specifically the Eastern AM. Kunming (25°20'N, 102°43'E, 6200 km) is 70 km away from Xing Yun and receives 70% of its annual precipitation during the months of June to September. The months from December to March account for only 5% of the annual precipitation. Thus the annual water budget in this area is controlled by annual summer monsoon strength. Based on precipitation amount and measured values of δD and $\delta^{18}O$ of rainfall, precipitation falling on the Xing Yun watershed should have a δD value of -66.2‰ and a $\delta^{18}O$ value of -9.6‰, which places

it on the global meteoric water line (GMWL); however, measured values of δD and $\delta^{18}O$ of lake water plot to the right of the GMWL, indicating enrichment of $\delta^{18}O$ through evaporation. For this reason, Xing Yun is sensitive to changes in the P-E balance because it loses most of its water through evaporation. This is confirmed through stable isotopic analysis of surface water resulting in $\delta^{18}O$ values of -5.7‰ in 1997 and samples collected in August of 2009 that measured -4.3‰ (Whitmore et al., 1997). Since lake waters are enriched in $\delta^{18}O$ through evaporation, precipitate minerals such as $CaCO_3$ are also enriched in $\delta^{18}O$ and can be used to document the timing, direction, duration, extent, and possible magnitude of changes in the moisture balance.

1.3 HISTORY

The earliest hominid occupation of China likely occurred in northern regions approximately 1 million years ago (Zhu and R., 2003). Modern humans occupied the Yunnan province by 40,000 years ago on the basis of genetic evidence (Zhong et al., 2010). A few archaeological sites from the Dali region have been radiocarbon dated to 3000-1800 BC while many more sites throughout the Yunnan Province are dated to 1800-1000 BC (Yao, 2010). The region where Xing Yun Lake is situated has several archaeological sites of interest. Shell mounds and other evidence of fishing and hunting are located near many lake basins such as Fuxian and Dian (Yao, 2010).

During the Bronze Age, the archaeological evidence of bronze production in Yunnan is disputed, mainly on the basis of radiocarbon dates. Sites of bronze mining and manufacturing at Haimenkou and Nagu have radiocarbon dates of 1000 BC, which are rejected by some scholars (Yao, 2010). Further investigation in 2008 confirmed these dates with supported stratigraphic

evidence (Yao, 2010). Little archaeological information is available between the first tentative bronze mining and the emergence of the Dian culture around 800 BC surrounding Lake Dian (Higham, 1996). The site closest to Xing Yun Lake is Lijiashan, which was rich in bronze artifacts and was likely related to the Dian culture (Figure 1-5) (Higham, 1996). Artifacts from Lijiashan have been radiocarbon dated to 830-400 BC; however, archaeologists argue that the culture of the artifacts suggest a younger date (Higham, 1996).

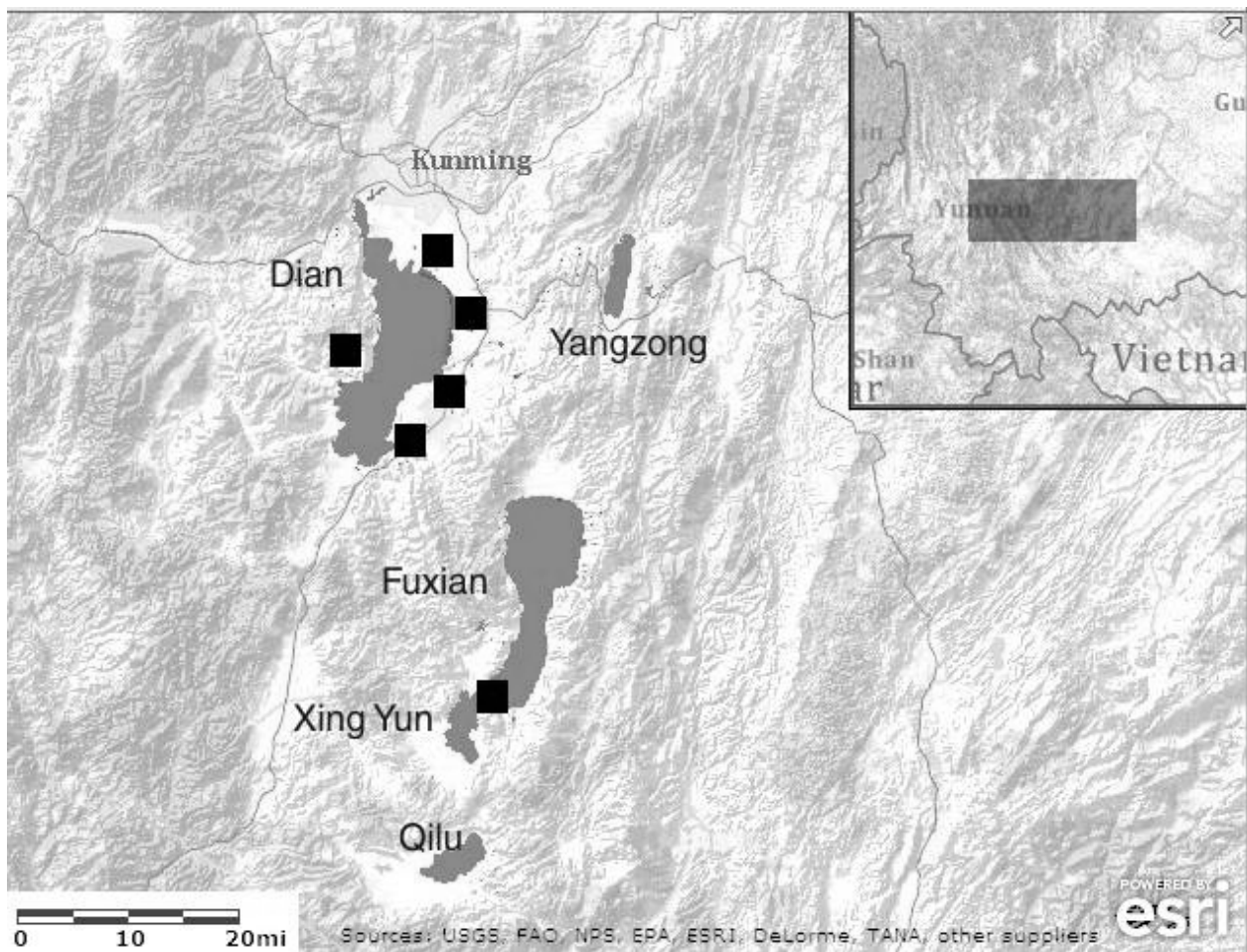


Figure 1-5- Map of archaeological sites of interest in the Yunnan Province adapted from ESRI 2010. All sites are from the Dian culture mentioned in Higham (1996). Lijiashan is located between Xing Yun and Fuxian.

Subsequent history of Yunnan, in relation to the history of China, is difficult to unravel since Yunnan has frequently broken off from Chinese government and remained independent. James Scott (2009) describes Yunnan and much of southeast Asia as a region called “Zomia”, characterized by populations that avoid government and are fairly self-contained. Self-containment is possible through the conscious use of escape agriculture in direct opposition to the monoculture agriculture typically used by the state. Escape agriculture is typified by shifting methods of cultivation where diverse crops are planted continuously leading to staggered crop maturity. Staggered maturity allows crops to remain in the ground for long periods of time while providing a constant food supply to the population. Typical crops that fit this requirement include sorghum, barley, cotton, buckwheat, and pearl millet.

This style of agriculture was pursued in the Yunnan Province with little to moderate interaction with the Chinese government. However, the Chinese dynasties had an interest in Yunnan because of its mineral deposits such as gold, tin, lead, copper, and silver (Figure 1-6) (Figure 1-7) (Figure 1-8) (Yang, 2009). Of particular interest was the mineral chalcocite (Cu_2S) because it yields up to 79.9% Cu, which is twice as much copper as most ores (Golas, 1999). As early as the first century AD, Yunnan was well-known for its metal and continued to be mined throughout history (Yang, 2009). Yunnan was so prodigious in metal deposits that beginning with the Yuan Dynasty in 1300 AD, copper and silver were taxed. Tax records show that Yunnan was producing approximately half of all silver in China. Similar levels of mining and taxation continued through the Ming Dynasty with Yunnan taxation accounting for as much as 80% of China’s total silver taxation during some years (Figure 1-9). These figures probably underestimate actual silver production since regional mining activities were not recorded or taxed. The method of extracting silver was through a process known as cupellation where the

ore was heated, oxidizing waste materials such as lead, and leaving valuable metals such as silver in a useable state (Needham and Gwei-djen, 1974). This method was likely used as early as the Warring States period in 600 BC, but explicit mention of it in historical records did not occur until roughly 900 AD (Golas, 1999).

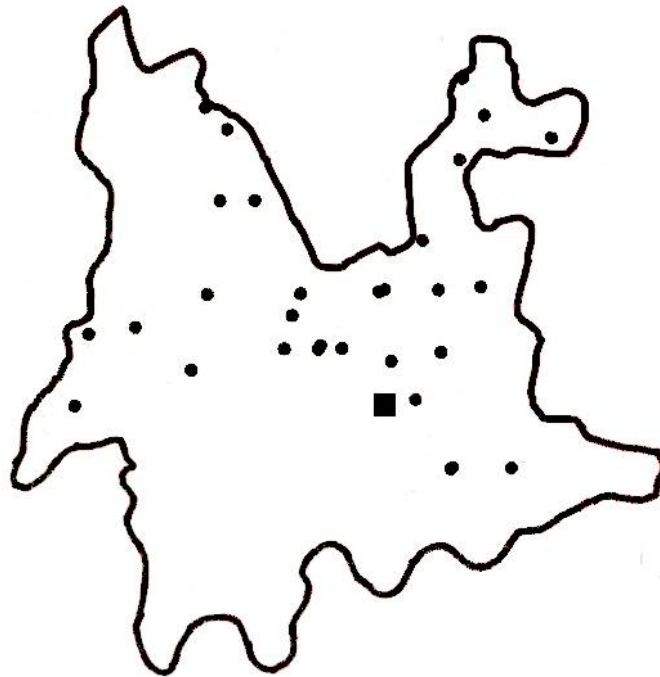


Figure 1-6- Map of pre-20th century copper mines in the Yunnan province adapted from Golas (1999). The square is the approximate location of Xing Yun.

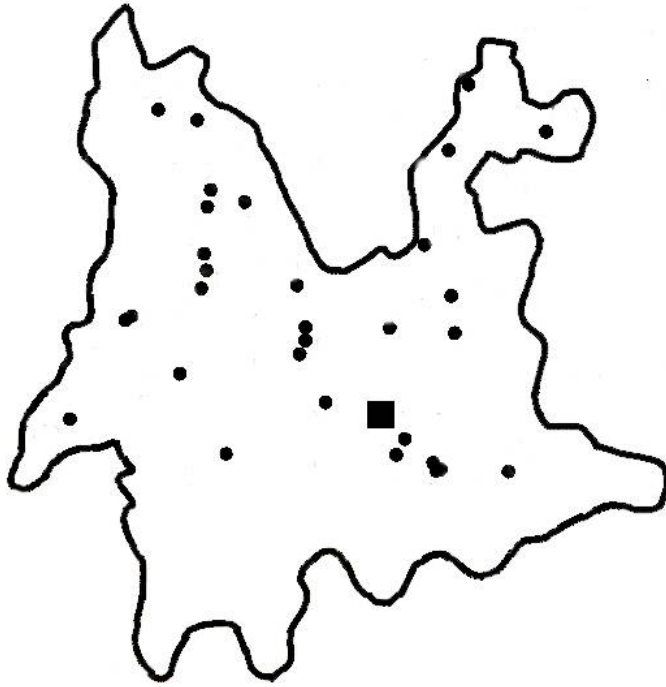


Figure 1-7- Map of pre-20th century silver mines in the Yunnan province adapted from Golas (1999). The square is the approximate location of Xing Yun.

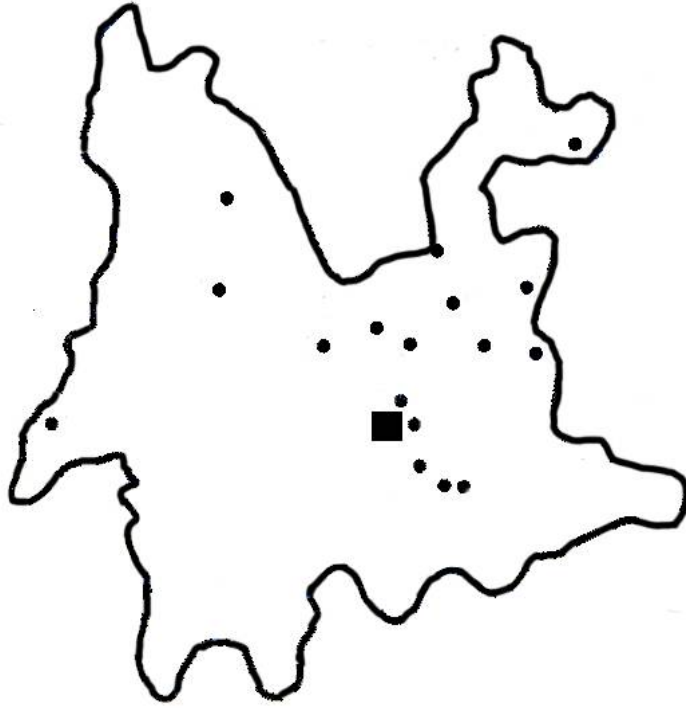


Figure 1-8- Map of pre-20th century tin and lead mines in the Yunnan province adapted from Golas (1999).

The square is the approximate location of Xing Yun.

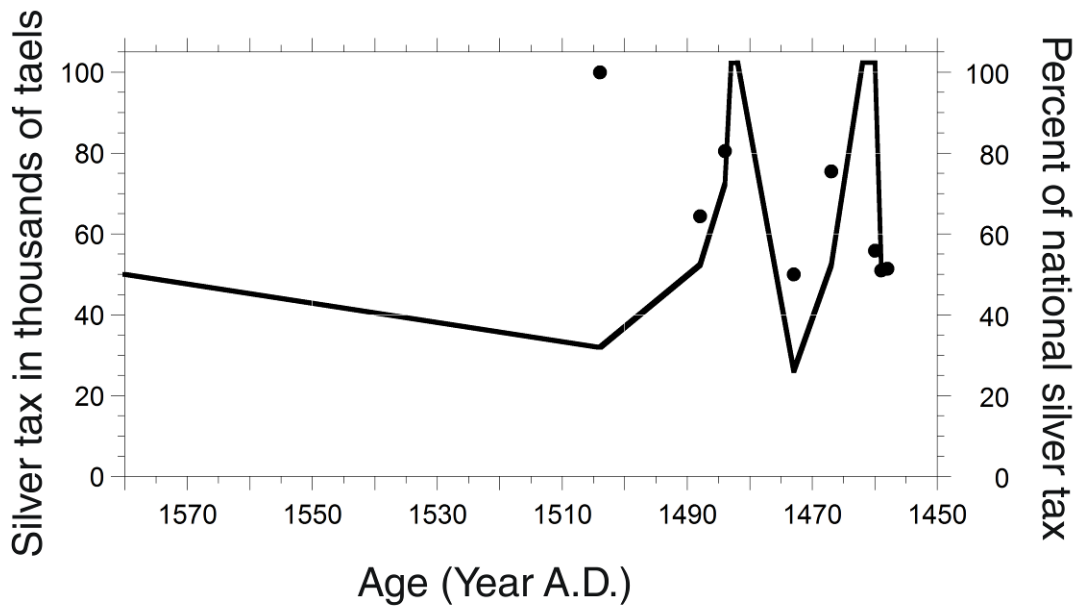


Figure 1-9- Estimates of silver taxation in the Yunnan Province during the Ming dynasty adapted from Yang (2009). Dots represent the percent of the national silver tax where data was available. The year 1504 A.D. was a year of low silver taxation, but nonetheless Yunnan constitutes 100% of the silver taxed during that year.

With the beginning of the Qing Dynasty in 1644 AD, Yunnan experienced sweeping cultural and economic changes. A rapidly growing population led immigrants to settle further into the Yunnan Province, spurred by government tax exemption and grants (Yang, 2009). Unlike previous immigrants during the Ming Dynasty, immigrants from the Qing Dynasty were able to push into mountainous areas previously only accessed by the native populations (Yang, 2009). Immigrants transformed the mountainous regions by practicing slash and burn agriculture and introducing new agricultural techniques like terracing (Giersch, 2006). The old crops of escape agriculture were replaced by New World crops such as maize, sweet potatoes, peanuts, tobacco, and opium (Giersch, 2006). The influx of workers led to the intensification of mining, particularly copper (Yang, 2009). Copper mining in Yunnan became so important that a great

deal of the Qing economy depended on Yunnan meeting production quotas set by the Chinese government. The Qing dynasty's copper was supplied by Japan until Japan implemented trading regulations that limited the amount of copper China could buy. By the mid to late 1700's, the Yunnan province entered the peak of mining (Figure 1-10).

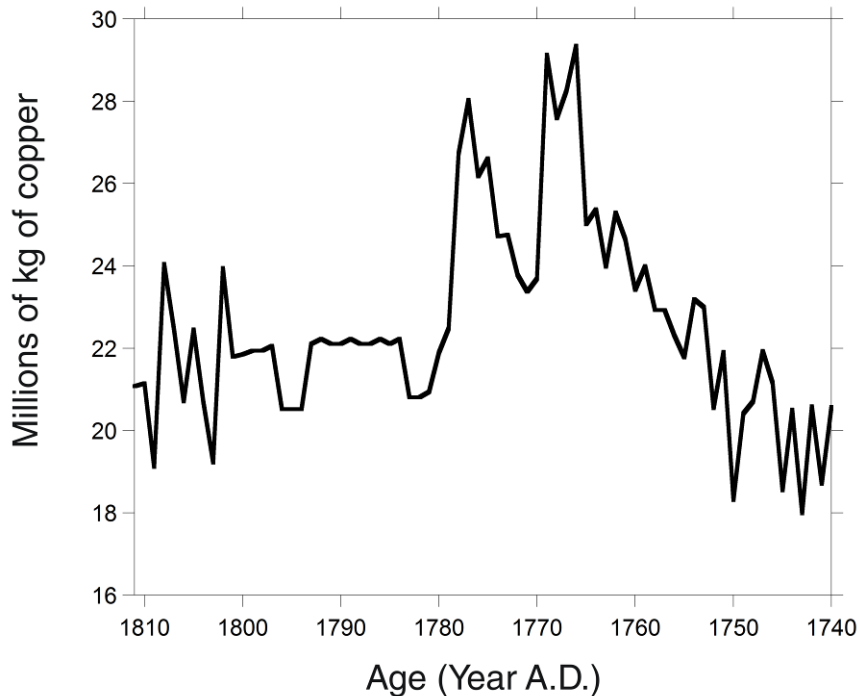


Figure 1-10- Estimates of yearly copper production in Yunnan adapted from Yang (2009).

The opportunity for jobs and government tax credits led to huge growth in Yunnan and surrounding areas. Yunnan and Guizhou Provinces had a population of 5 million in 1700 AD and 20 million in 1850 AD (Lee, 1982). Early demographics for this region of China before the Ming Dynasty are not always included in Chinese historical documents and those census records that are available are often inaccurate since women, children, and certain minority groups were not counted (Lee, 1982). Historical records and demographic extrapolation estimate the

population of Yunnan in the sixteenth century to be around 2 million with regions around Dian Lake being densely populated (Lee, 1982). The Ming Dynasty encouraged immigration into the Yunnan Province before the Qing Dynasty, however it was not as successful and most immigration was concentrated on the western edge of the province (Lee, 1982). Consequently, the population grew sporadically with slow overall growth and Yunnan likely reached a population of 3 million by 1740 AD (Lee, 1982). By 1850 AD the population in Yunnan was 10 million with increased urbanization and perhaps as much as 10% of the population living in the city (Lee, 1982).

By the nineteenth century, Yunnan's ores generated much conflict. The French and British empires attempted to make inroads to the Yunnan province to access the ores (Fairbank and Liu, 1980). The Han and Muslim Chinese fought over control of the silver mines, eventually erupting into a series of several rebellions (Fairbank and Liu, 1980). By 1900 AD, Yunnan had one of the few minting operations that were permitted to create the silver dollar (Fairbank and Liu, 1980). As the political situation in China became tumultuous and the Chinese Republic was founded, the situation in Yunnan became increasingly chaotic with numerous rebellions (Fairbank, 1983). Some scholars contend that Chinese mining did not witness any technological innovations during thousands of years of activity as a result of a preponderance of manual labor (Golas, 1999). A miner in the Yunnan province in 900 AD would not find the technology much changed by 1900 AD (Golas, 1999).

The river basins of the Yunnan Province continued to play an important role in human agriculture and irrigation. In 1923 AD and again in 1956 AD, the only outflowing river of Xing Yun lake was dredged and the channel that connects Xing Yun and Fuxian today widened and deepened (Whitmore et al., 1994). This allowed water to flow from Xing Yun into Fuxian and

dropped Xing Yun Lake level by 2.0 m in 1923 AD and an additional 1.0 m in 1956 AD (Whitmore et al., 1994).

The following chapters explore the interpretation of oxygen and carbon isotopes and trace metal data from sediment cores collected in Xing Yun Lake in August 2009. Chapter 2 and 3 are intended for publication and therefore contain redundancies in the introductory text, methods, and results.

2.0 A 2500 YEAR HISTORY OF DROUGHT IN SOUTHWESTERN CHINA

2.1 INTRODUCTION

Paleoclimate research in southwestern China has largely been concentrated on cave deposits and the analysis of oxygen isotopic composition. High resolution speleothems provide data for comparison with lake sediments including Shihua Cave (39°90'N, 116°40'E), Dongge Cave (25°17'N, 108°50'E), Heshang Cave (30°27'N, 110°25'E), and Wanxiang Cave (33°19'N, 105°00'E) (Dykoski et al., 2005; Hu et al., 2008; Qian and W., 2002; Zhang et al., 2008). Speleothem records are extensively used because they can be accurately dated using $^{238}\text{U}/^{232}\text{Th}$. However, $\delta^{18}\text{O}$ of precipitated calcite in caves is influenced by a number of complicating factors: atmospheric temperature and humidity, groundwater mixing and infiltration, cave humidity, and kinetic fractionation (Lachniet, 2009). In order for any speleothem to be interpreted in terms of paleoclimate, annual measurements of drip water should be taken in order to ensure minimal kinetic fractionation and to assess the seasonality of calcite precipitation. The effects of altitude and continentality on cave conditions are not well understood, yet many of the speleothem records from China are located in high altitude areas, creating another confounding factor for interpretation.

Wanxiang Cave, situated in central China, has valuable data regarding monsoonal strength variability for the last 1,800 years (Zhang et al., 2008). Oxygen isotope fluctuations are

small with 0.5 to 1.0‰ changes during transition periods. In this record the period from 530 to 930 AD is characterized by declining monsoon strength with a sharp drop at 860 A D. Thereafter, monsoon strength increases to a peak at 1020 A D. $\delta^{18}\text{O}$ values remain high with moderate variations until 1360 AD. A sudden drop in monsoon strength occurs at 1360 AD and remains low until 1880 AD which the authors believe is the influence of the Little Ice Age (LIA). The authors connect AM strength to North Atlantic temperatures and solar variability, though they note several periods where the record lags behind these factors, such as during the LIA.

Zhang et al. (2008) note that periods of weak (strong) monsoons correlate with the decline (rise) of several Chinese dynasties. The period of weak monsoon strength from 850-940 AD corresponds to when the Tang Dynasty ended and ushered in a period of political chaos known as the Five Dynasties and Ten Kingdoms. Conversely, the strong monsoon strength from 960-1020 AD occurred synchronously with the flourishing of the Song Dynasty. However, other authors have questioned this interpretation for several reasons. Wanxiang Cave is strongly influenced by AM precipitation; since precipitation is a very local phenomenon, it may not be appropriate to apply such records to the whole of China (DeEr et al., 2009). Additionally, there are several periods of history which are contradictory; the Ming Dynasty thrived when the AM was weak and the Qing Dynasty fell irrespective of AM strength. Correlating $\delta^{18}\text{O}$ isotopic composition with AM strength and cultural history oversimplifies some of the subtleties of Chinese history.

Paleolimnological analyses have been performed on a few lakes of the Yunnan Province. These include closed basin lakes Qilu (24°10'N, 102°45'E) and Xing Yun (24°10'N, 102°46'E) and open basin Lake Erhai (25°45'N, 100°11'E). Closed basin lakes provide an opportunity for paleoclimatic analysis because they record evaporative losses through authigenic calcite. Both

Qilu and Xing Yun Lakes have outflow to surrounding sources, so they are not considered topographically closed basin (Hodell et al., 1999). However, they can be considered “effectively” closed basin because they lose most of their water to evaporation. Erhai is an open basin lake and is not as sensitive to evaporation variability; however, Erhai can serve as a control for precipitation falling over the region.

Erhai has been the subject of much study because it is one of the larger lakes in the Yunnan Province and has a long record of human occupation, which makes it useful in an effort to quantify human disturbance to the watershed. A multi-proxy study covering the last 7,500 years BP, which included analysis of pollen, sediment particle size, carbon isotopic composition of organic matter, magnetic susceptibility, mineral assemblage, and trace metal concentration, found that as early as 7,000 years BP, sediments record a disturbed vegetation pattern likely due to deforestation and irrigation (Dearing et al., 2008). Human disturbance continues until roughly 2,000 years BP when erosion and hydraulic engineering show another significant change in the watershed hydrology (Dearing et al., 2008). This is confirmed by a pollen assessment of Erhai Lake where pollen from pine and deciduous trees decrease significantly after 1,100 years BP (Shen et al., 2006).

The basis for this study of Xing Yun comes from a study by Hodell et al. (1999) of Xing Yun and Qilu Lakes. In Hodell’s study the age model is not very robust since bulk sediments and shells were used for ^{14}C measurements which are prone to hard water lake effects (Deevey et al., 1954). Thus, the timing of certain events is not clear; however Hodell’s study provides a firm basis for this study of Xing Yun. Hodell’s analyses of the sediments included percent organic and inorganic carbon, grain size, magnetic susceptibility, and stable isotopic analysis of $\delta^{18}\text{O}$ of authigenic carbonate every 3-5 cm. Hodell showed that during the last glacial maximum,

$\delta^{18}\text{O}$ values were high, suggesting a weak summer monsoon and a strong winter monsoon. The last glacial maximum also had high magnetic susceptibility values which were the result of detrital magnetic particles delivered to the lake by winter monsoon winds.

Carbonate deposition increased in Qilu Hu and Xing Yun after 12,000 years BP, coincident with decreased $\delta^{18}\text{O}$ values and lower magnetic susceptibility, suggesting increasing temperatures. The $\delta^{18}\text{O}$ values cannot be solely explained by increased productivity due to warming and must be attributed, in part, to increasing summer monsoon strength until 8,000 years BP. Hodell suggested that decreased carbonate deposition and higher $\delta^{18}\text{O}$ values after 8,000 years BP were the result of gradual weakening of the summer monsoon associated with precessional forcing. Increasing magnetic susceptibility beginning 3,000 years BP is explained as human disturbance to the watershed.

In this study, a sediment profile from the Xing Yun basin provides a high-resolution, accelerator mass spectrometry ^{14}C -dated record of late Holocene climate change and human impacts in southwestern China. The Xing Yun Lake record was compared with data from regional cave deposits as well as PDSI and ENSO reconstructions.

2.2 METHODS

Xing Yun cores were taken in August 2009. Surface sediments (core A-09 drive 1) were taken with a piston core fitted with a 5.5 cm diameter removable polycarbonate tube and 133.5 cm of sediments were recovered. The upper 56 cm of core A-09 drive 1 was extruded in the field at 0.5 cm intervals. Deeper sediments (cores A-09 drive 2 and drive 3) were collected with

a modified square-rod piston corer (Livingston core) and extruded in the field (Wright et al., 1984). The cores measure 92 cm and 96 cm respectively. Altogether these three cores produce a total record of 2.64 m. Cores A-09 drive 1 and drive 2 overlap by 47.5 cm and cores A-09 drive 2 and drive 3 overlap by 10 cm on the basis of field notes and stratigraphic comparison of oxygen isotopes, carbon isotopes, and magnetic susceptibility values.

Sediment ages were determined by radiocarbon, ^{210}Pb , and ^{137}Cs measurements. The 56 cm of extruded sediments from core A-09 drive 1 were used for ^{210}Pb and ^{137}Cs measurements. Samples were freeze dried and equilibrated in a cold storage room at the University of Pittsburgh. ^{210}Pb , ^{137}Cs , and ^{214}Pb activities were measured on a Canberra Germanium Detector BE2020 at the University of Pittsburgh for 23 hours to detect γ radiation. Sediment ages were determined on the basis of the constant rate of supply model (Appleby and Oldfield, 1983). Accelerator mass spectrometer radiocarbon dating was performed on 6 samples which were pretreated using the standard acid, base, acid procedure of Abbott and Stafford (1996). Samples were measured at the Kleck Center for Accelerator Mass Spectrometry at the University of California Irvine.

Three samples in drive 1 (4 cm, 70 cm, 130 cm) were examined by scanning electron microscopy (SEM) at the University of Pittsburgh's Department of Mechanical Engineering and Material Science. The SEM is a Philips XL-30 field emission scanning electron microscope, equipped with detectors for SE and BSE imaging and elemental composition analyses by energy-dispersive X-ray spectroscopy (EDS). X-ray diffraction analysis (XRD) was performed on 19 samples evenly spaced from all 3 cores using a Philips X'pert X-ray diffractometers for powder diffraction. XRD results from drive 1 presented in Figure 2-3 were analyzed at Duquesne

University (16.0, 16.5, 40, 80, 110 cm). XRD results from the remaining samples of drive 1, and drives 2 and 3 were analyzed at the University of Pittsburgh.

Bulk density samples measuring 1 g cm^{-3} were determined every 2 cm down the entire length of the core less than 24 hours after the core had been opened. These were weighed immediately and again after 36 hours in a drying oven at 60°C . Weight percent organic matter and carbonate content within these same samples was determined by loss-on-ignition (LOI) analysis at 550°C and 1000°C , respectively, following the methods of Dean (1974).

Sediment core magnetic susceptibility was measured on split cores using a Bartington® Instruments Ltd. ME2EI surface-scanning sensor equipped with a TAMISCAN-TSI automatic logging conveyer. Cores were sampled continuously at a 0.5 cm interval and stored in scintillation vials. Samples were disaggregated with 7% H_2O_2 and sieved through a $63 \mu\text{m}$ screen to remove biological carbonate. Samples were soaked in 50% bleach and 50% DI water mixture for 6-8 hours, rinsed, and freeze dried. Bulk carbonate samples were reacted in $\sim 100\%$ phosphoric acid at 90°C , and measured using a dual-inlet GV Instruments, Ltd. (now IsoPrime, Ltd., a subsidiary of Elementar Analysensysteme GmbH) IsoPrime™ stable isotope ratio mass spectrometer and MultiPrep™ inlet module at the University of Pittsburgh. Oxygen and carbon isotope results are expressed in conventional delta (δ) notation as the per mil (‰) deviation from the Vienna Peedee Belemnite standard (VPBD). Analytical uncertainties are within $\pm 0.10\%$. Isotopic measurements were replicated every 10 cm and analyzed two to three times to ensure accurate results. Repeated measurements of $\delta^{18}\text{O}$ and $\delta^{13}\text{C}$ have an average standard deviation of 0.10 and 0.20‰ (VPBD), respectively.

Weight percent carbon and nitrogen was sampled every 2 cm for the length of each drive. Samples were covered in 1 M HCl for 24 hours to dissolve organic carbon. Samples were then

freeze dried at the University of Pittsburgh and analyzed at Idaho State University. Samples were analyzed using ECS 4010 (Elemental Combustion System 4010) interfaced to a Delta V advantage mass spectrometer through the ConFlo IV system. The elemental analysis was done by an evolutionary "flash combustion/chromatographic separation techniques". The furnace temperature was kept at 1000°C; while the reduction oven was 650°C. The gases generated from the combustion of the samples were carried in a helium stream into a GC column held at 60°C. The gases then separate before being diluted in the ConFlo IV and passed to the mass spectrometer for analysis. Isotope ratios of $\delta^{13}\text{C}$ are reported as ‰ values relative to the VPDB scale; whereas $\delta^{15}\text{N}$ values are reported as ‰ values relative to air- N_2 . Three in-house standards (ISU Peptone, Costech Acetanilide and DORM-2) which are directly calibrated against international standards (IAEA-N-1, IAEA-N-2, USGS-25, USGS-40, USGS-41, USGS-24, IAEA-600) were used to create a two point calibration curve (normalization curve) to correct the raw data. ISU Peptone and Costech Acetanilide were used to set up a two-point calibration line (normalization curve). A third standard (DORM-2) was used to monitor the accuracy of the data. The final data was corrected using a three-point calibration curve (normalization curve). At least 1 standard was run for every 6 or 7 samples. Samples were measured for weight percent nitrogen, weight percent organic carbon, $\delta^{15}\text{N}$, $\delta^{13}\text{C}$ of organic carbon, and C (%)/N (%).

In order to compare Xing Yun's stable isotope results with other cave records, $\Delta\delta^{18}\text{O}$ was calculated, which is the difference between Xing Yun $\delta^{18}\text{O}$ values and speleothem $\delta^{18}\text{O}$ values, as a technique for removing secondary controls on $\delta^{18}\text{O}$ fractionation and quantifying precipitation (Hu et al., 2008). Oxygen isotope values from Dongge cave published by Wang et al. (2006) were interpolated at one year resolution using MatLab 7.10.0. Xing Yun $\delta^{18}\text{O}$ values were subtracted from Dongge $\delta^{18}\text{O}$ values for years in which there was data from Xing Yun.

2.3 RESULTS

^{210}Pb ages were calculated on the basis of the constant rate of supply (CRS) model (Figure 2-1) (Appleby and Oldfield, 1983). Radiocarbon dates were calibrated using Calib 6.0 (Table 2-1) (Stuiver et al., 2010). On basis of these 2 dating techniques, the following age-depth model was produced (Figure 2-2).

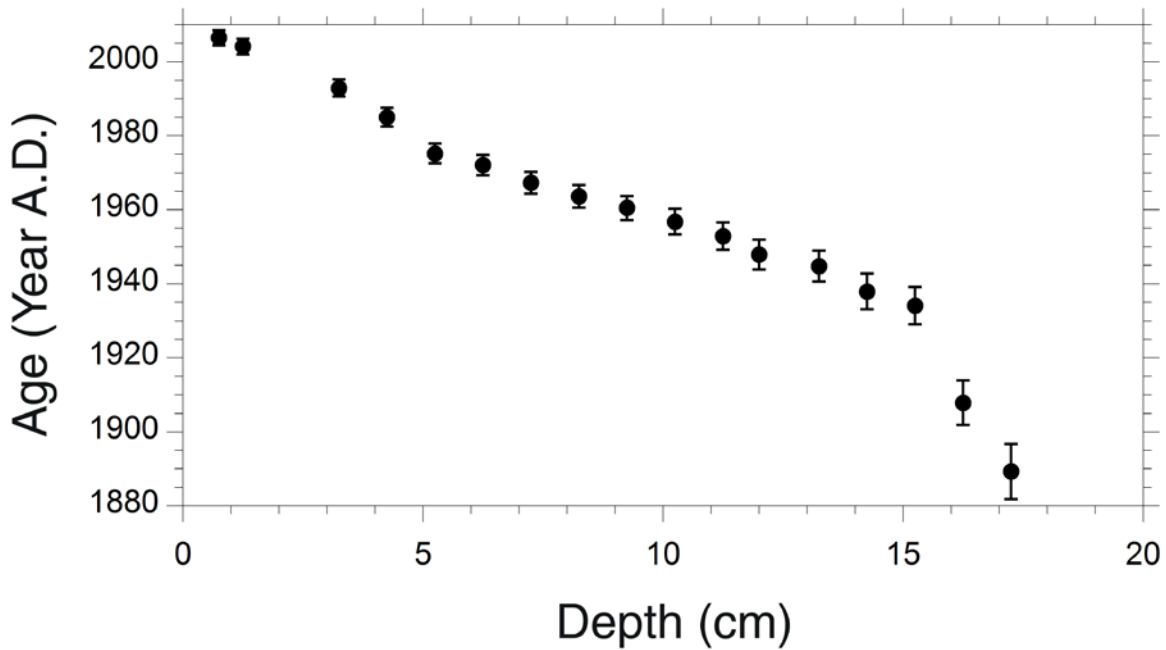


Figure 2-1- ^{210}Pb ages from Xing Yun A-09 using the CRS model. Error bars represent one standard deviation.

Table 2-1- Radiocarbon dates.

Core	Drive Depth (cm)	Total Depth (cm)	Material	¹⁴ C age (BP)	¹⁴ C age error	Median calibrated age (cal years BP)	2-sigma calibrated age range (cal years BP)
A-09 D1	35.5	35.5	Wood	110	25	110	0-270
A-09 D1	37.5	37.5	Charcoal	110	50	120	0-280
A-09 D1	59.0	59.0	Charcoal	130	25	120	0-270
A-09 D2	59.0	145.0	Charcoal	1060	25	960	930-1050
A-09 D3	82.0	250.0	Wood	2105	20	2080	2000-2140
A-09 D3	95.0	263.0	Charcoal	2220	20	2230	2150-2350

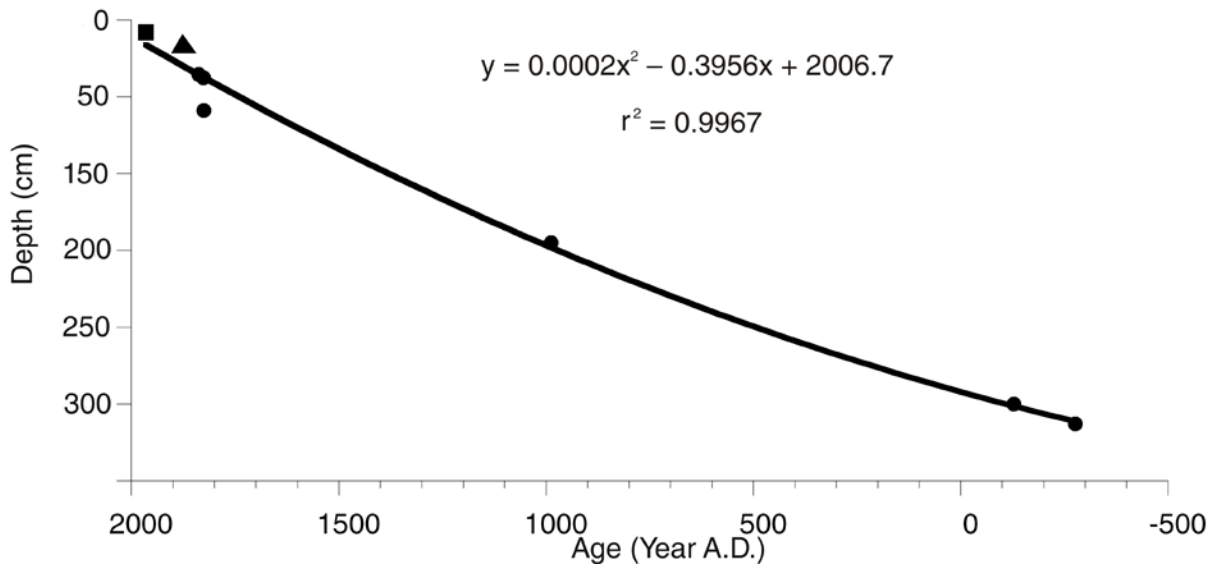


Figure 2-2- Age depth model for Xing Yun A-09. Circles denote ¹⁴C dates, the square denotes ¹³⁷Cs date, and the triangle denotes the ²¹⁰Pb date at 1880 AD.

XRD results revealed that the predominant minerals are calcite and hexagonal quartz. Drive 1 samples are mostly quartz with some calcite (Figure 2-3). Drive 2 samples are evenly

mixed quartz and calcite, with calcite increasing down core (Figure 2-4). Samples in drive 3 are dominated by calcite with some small amounts of quartz (Figure 2-5). XRD analysis indicates that the precipitated carbonate crystals are nearly pure calcite. This analysis is confirmed by the results of the SEM which show euhedral to subhedral calcite (Figure 2-6, Figure 2-7). SEM results indicate that the carbonate crystals are formed by precipitation from the water body.

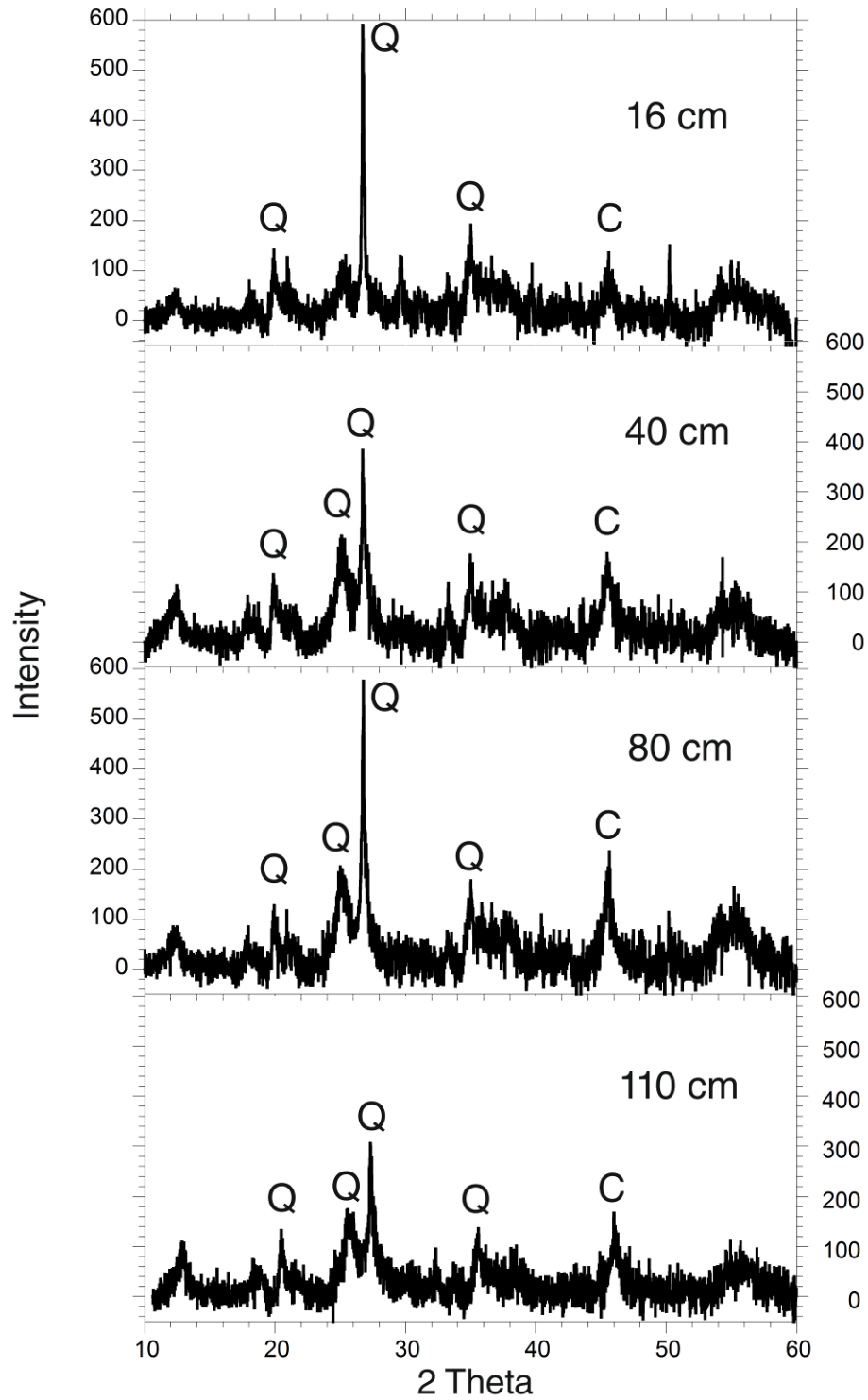


Figure 2-3 – Selected X-ray diffraction peaks for Xing Yun A-09 drive 1. Intensity is unitless. Calcite peaks are marked with a C, quartz peaks are marked with a Q.

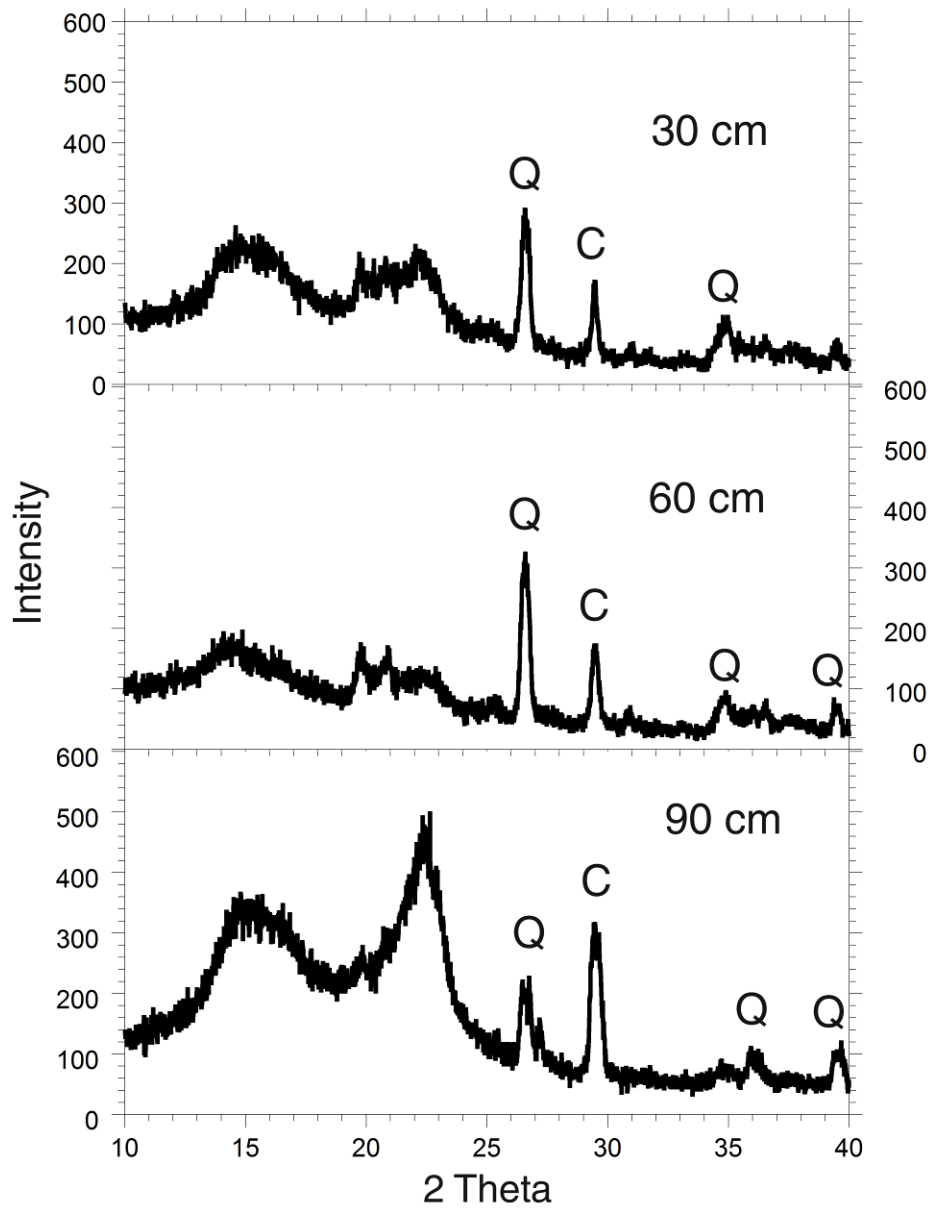


Figure 2-4- X-ray diffraction peaks for Xing Yun A-09 drive 2. Intensity is unitless. Calcite peaks are marked with a C, quartz peaks are marked with a Q.

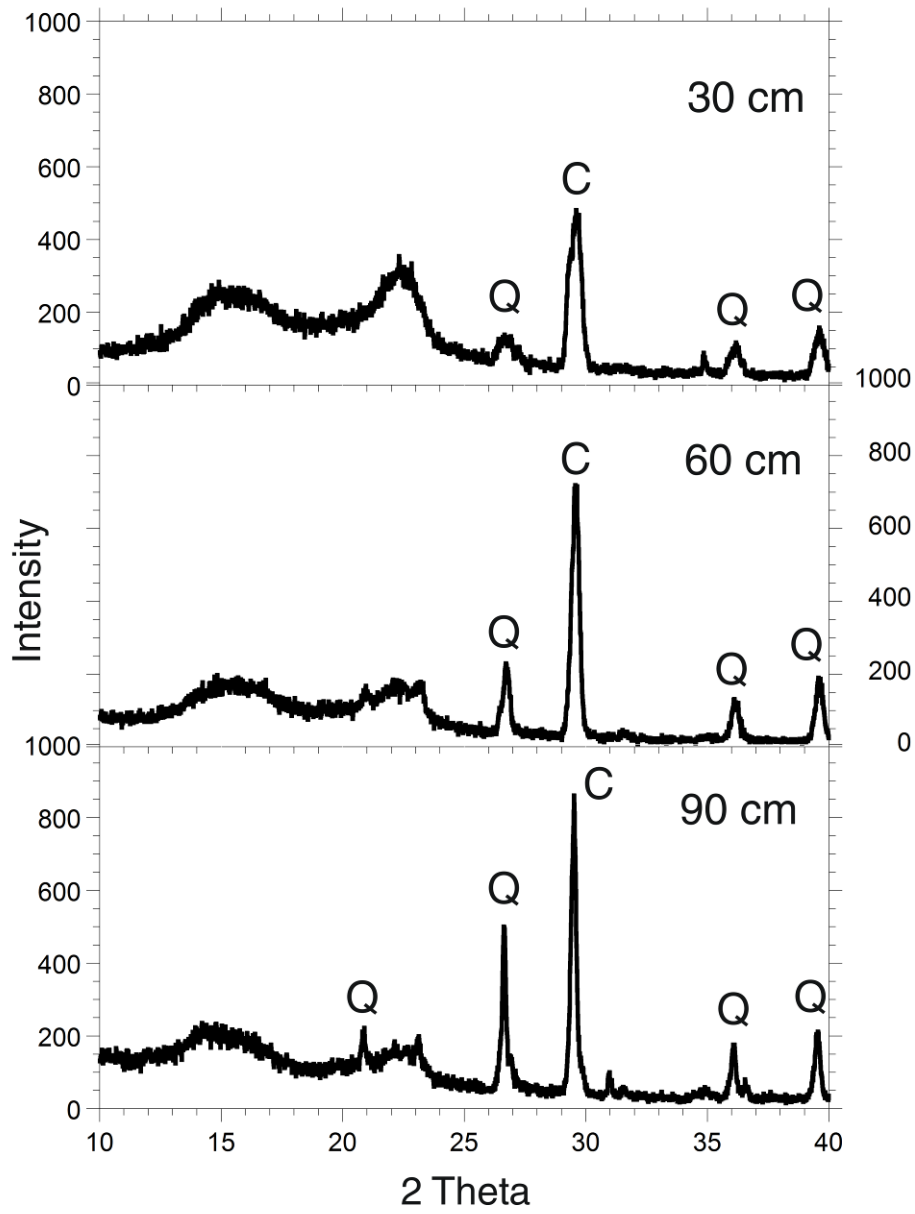


Figure 2-5- X-ray diffraction peaks for Xing Yun A-09 drive 3. Intensity is unitless. Calcite peaks are marked with a C, quartz peaks are marked with a Q.

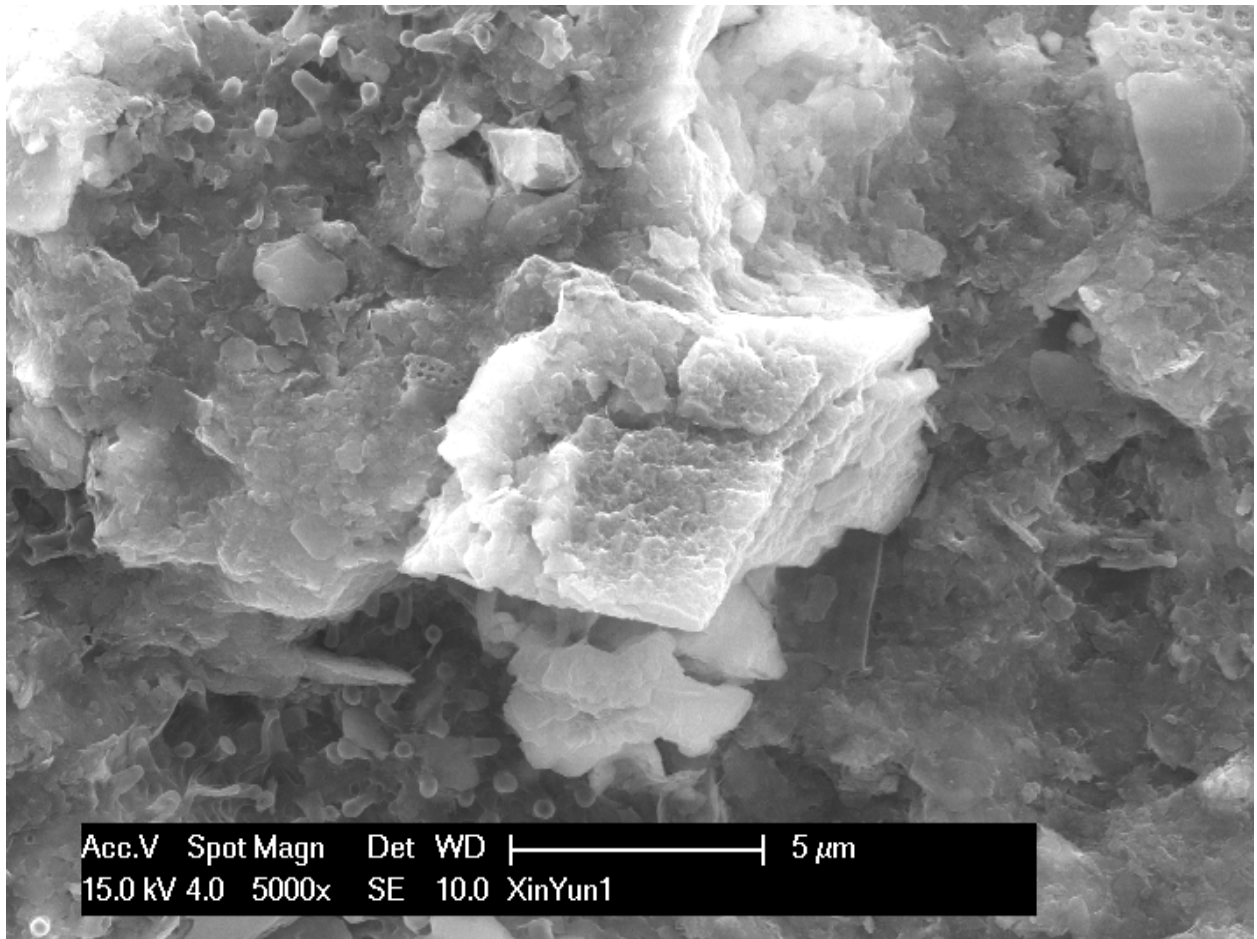


Figure 2-6- Euhedral calcite from Xing Yun A-09 drive 14 cm.

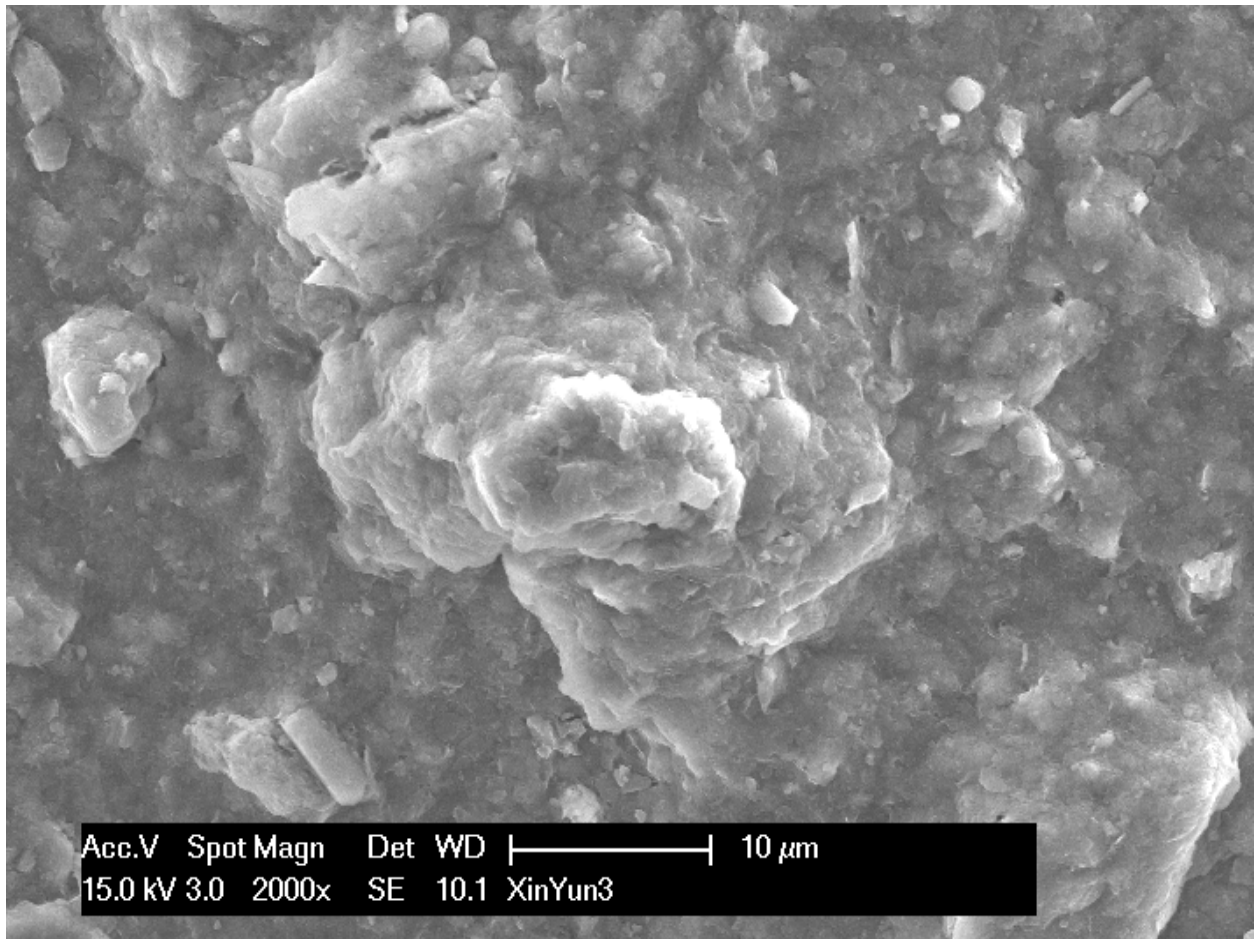


Figure 2-7- Subhedral calcite from Xing Yun A-09 drive 1 130 cm.

The results of both $\delta^{18}\text{O}$ and $\delta^{13}\text{C}$ exhibit a wide range of variability in the span of 2,640 years BP or to the year 430 BC. Oxygen isotopic values reach a minimum of -8.5‰, a maximum of -4.3‰, and have a range of 4.2‰. Carbon isotopic values reach a minimum of -5.3‰, a maximum of 1.3‰, and have a range of 6.6‰. The record can be split into 5 distinct units (Figure 2-8).

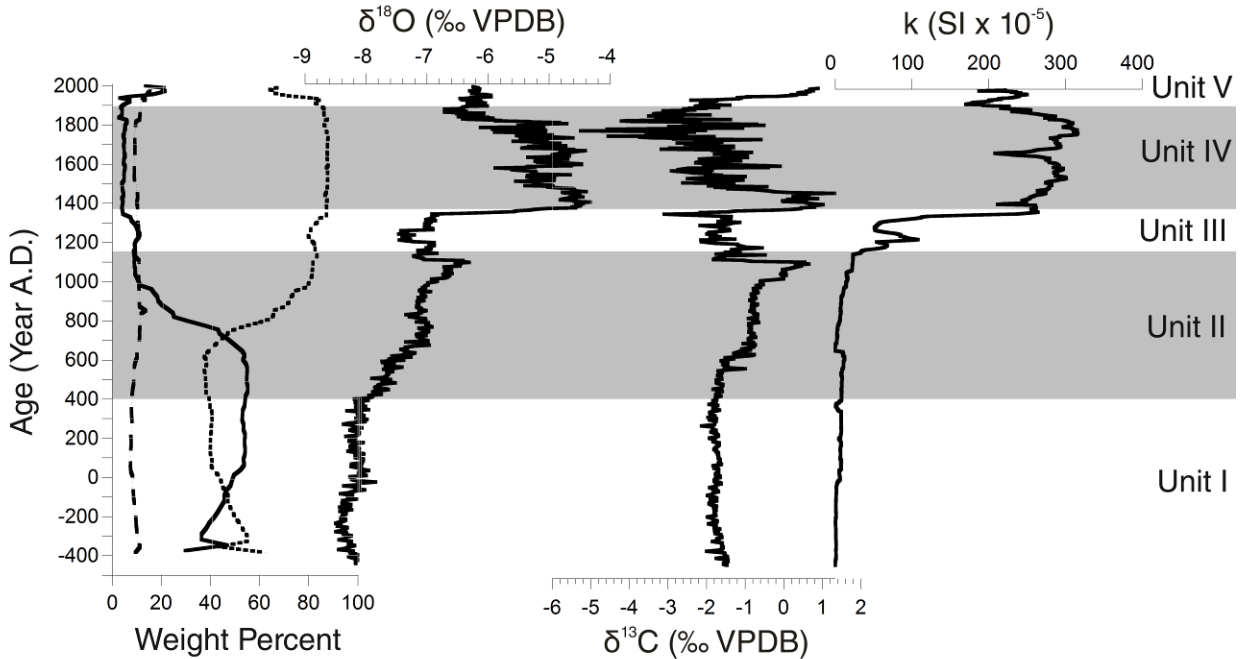


Figure 2-8- From left to right: % organic matter in dashed line, % carbonate in solid line, % residual mineral matter in dotted line, stable isotopes, and magnetic susceptibility of Xing Yun A-09.

Unit I spans the period from 430 BC to 400 AD and is characterized by limited change with 40-60% carbonate, 5-12% organic matter, and magnetic susceptibility values ranging from 0.0-8.0 SI. Oxygen isotopic values are stable and range from -8.5‰ to -7.8‰, as are $\delta^{13}\text{C}$ values which range from -2.1‰ to -1.4‰.

Unit II occurs from 400 to 1140 AD and shows gradual change with carbonate content slowly decreasing from roughly 60% to 10%. Values of both $\delta^{18}\text{O}$ and $\delta^{13}\text{C}$ become more positive and shift by approximately 1.0‰ and 1.5‰, respectively. There is little change in magnetic susceptibility.

Unit III is marked by abrupt change occurring over roughly 220 years from 1140-1360 AD. Carbonate content remains relatively stable around 10%. Therefore, relatively large samples were needed for mass spectrometer analysis. Magnetic susceptibility briefly increases

to 107.7 SI. Oxygen isotopic values become more negative with a minimum of -7.5‰ and $\delta^{13}\text{C}$ values more negative with a minimum of -3.1‰.

Unit IV is a period of rapid change over approximately 50 years during which both $\delta^{18}\text{O}$ and $\delta^{13}\text{C}$ shift to the more positive values by 3.5‰. Unit IV spans the period from 1360-1880 AD and is characterized by $\delta^{18}\text{O}$ values that reach a maximum of -4.3‰ and $\delta^{13}\text{C}$ values that reach a minimum of -5.3‰. Unit IV also has a rapid increase in magnetic susceptibility with values consistently higher than 150 SI and a maximum of 316.3 SI.

Unit V represents the period from 1880-2005 AD and is characterized by slightly more negative isotope values. Oxygen isotopic values remain consistent around -6.2‰ and $\delta^{13}\text{C}$ values remains nearly constant around 0.5‰. Carbonate content increases to roughly 15-20%. Magnetic susceptibility values reach a low point of 170 SI at the beginning of Unit V and then increase to roughly 250 SI.

The carbon to nitrogen ratio is low through the entire record. The ratio fluctuates between 10 and 12 from 400 BC to 1000 AD (Figure 2-9). Thereafter, the C/N ratio fluctuates, but generally decreases until 1400 AD. From 1400 to 1800 AD, the C/N ratio declines to 7, suggesting a nearly pure aquatic source of organic matter. From 1800 AD to present day, the ratio fluctuates between 8 and 10. These results, coupled with organic matter $\delta^{13}\text{C}$ values between -25 and -30‰ indicate that the dominant organic matter source is lacustrine algae, especially from the time period 1400 to 1800 AD (Myers, 1994).

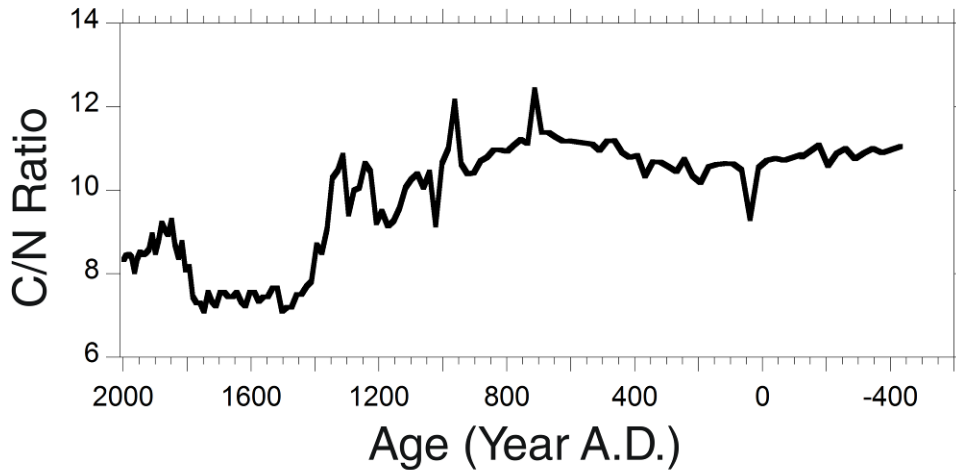


Figure 2-9- Carbon to nitrogen ratio in Xing Yun A-09.

2.4 DISCUSSION

2.4.1 Environmental Isotopes

The validity of the isotope record is confirmed by the fact that the Xing Yun $\delta^{18}\text{O}$ values match very closely with the record previous work by Hodell et al. (1999), albeit this work has a higher resolution of 5-6 years and better age control. The cores recovered in 2009 from Xing Yun are restricted to the last 2,500 years so it is difficult to identify Holocene scale monsoonal patterns. However, when compared to the study by Hodell, Unit I corresponds to a period of moderate monsoon strength. Unit II's gradual change in isotopic composition is evidence of changing monsoon strength likely in response to changing precession. It is only in the uppermost section of Unit II that abrupt change occurs as seen in the isotope records.

During the whole of Unit III, $\delta^{18}\text{O}$ shifts to more negative values by about -1.0‰ and $\delta^{13}\text{C}$ values shift to more negative values by about -2.5‰. These negative oxygen isotope values indicate wet conditions with increased monsoon strength during a time when orbital precession should be decreasing the strength of the summer monsoon (Hodell et al., 1999). Unit III spans the time period of 1140-1360 AD, which too late to be considered part of the Medieval Climate Anomaly (MCA). One hypothesis is that this time period reflects a rise in lake level, possibly due to human activity. However, further investigation into historical records is needed.

The rapid change that occurs in Unit IV is characterized by more positive $\delta^{18}\text{O}$ values which indicates drier conditions associated with a weaker summer monsoon. The LIA occurred from 1500-1850 AD, so Unit IV is part of this climate shift in southwestern China. Such a large shift in isotopic composition is unique in the Xing Yun sediment record, since many other speleothem records do not record such a large magnitude change. This means that the LIA in southwestern China must have been exceptionally dry. This interpretation of the LIA is supported by many other paleoclimate records (DeEr et al., 2009; Mann et al., 2009; Qian and W., 2002). However, what makes Xing Yun's record unique is that the drought is far more severe than other record suggest.

It is not until roughly 1880 AD that the LIA ends in southwestern China and transitions to Unit V, modern day values. Put into the perspective of 2,500 years, recent monsoon strength is quite weak. The average $\delta^{18}\text{O}$ value for the last 120 years is -6.2‰, compared to an average of -6.7‰ for the entire record. Magnetic susceptibility values are also quite high which is interpreted as increasing human disturbance to the watershed in Hodell's study and which is also the most plausible explanation in this study (see page 57 for more detail).

2.4.2 Covariance

The results for the $\delta^{13}\text{C}$ values are unusual because Xing Yun is effectively a closed basin lake. Closed basin lakes on short time scales (less than 5,000 years) with low alkalinity usually exhibit covariance between $\delta^{13}\text{C}$ and $\delta^{18}\text{O}$ isotopes in a 1:1 relationship (Li and Ku, 1997). The sediments of Xing Yun show four distinct modes (Figure 2-10). Cluster one is the largest and spans the longest time period from 400 BC to 1360 AD. The line of best fit for cluster one is $y = 0.88902x + 5.4838$, which is close to 1 and suggests closed basin conditions (Li and Ku, 1997). Cluster two is from 1360 to 1880 AD, which takes place during Unit IV and is a period of weakened monsoon strength. The line of best fit for cluster two is $y = 1.8277x + 7.8085$. Cluster three is from 1880 to 1970 AD and covers Xing Yun's transition out of the LIA. The line of best fit for cluster three is $y = 2.6986x + 14.932$. Cluster four is from 1970 AD to present and is in line with cluster one. However, cluster four is differentiated from cluster one on the basis of more positive carbon isotope values. If the future isotopic composition of Xing Yun's lake water shows more negative carbon isotope values, then the lake water is likely returning to the state it was in cluster one.

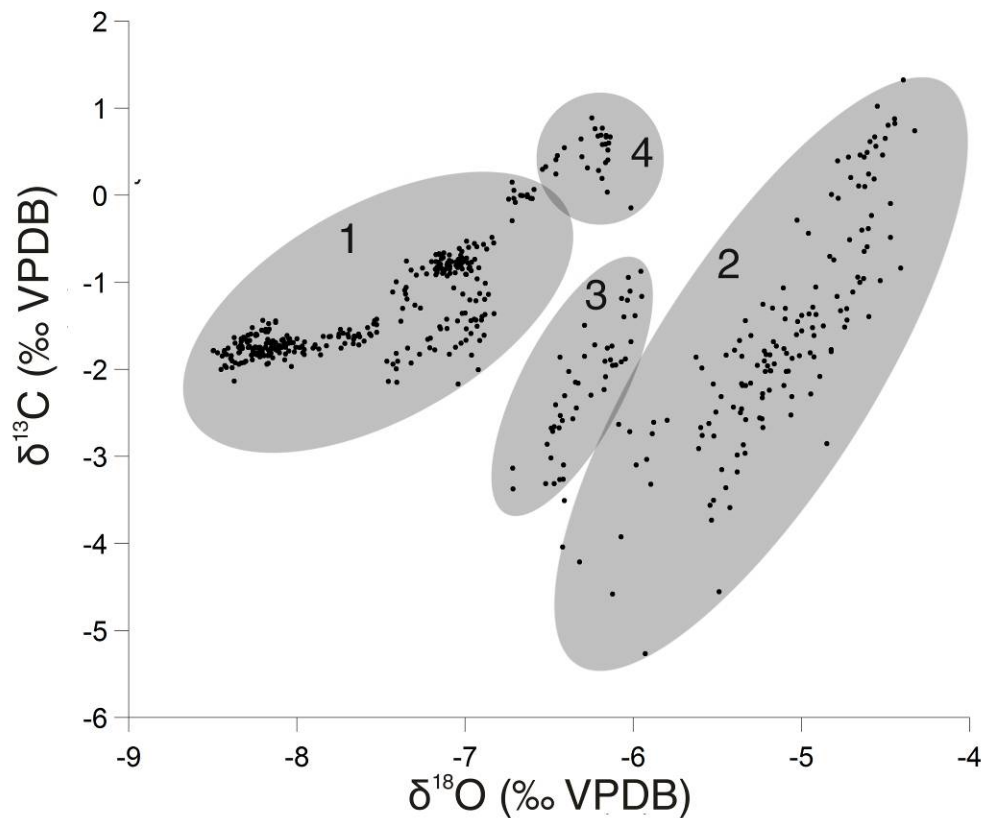


Figure 2-10- Covariance for Xing Yun A-09 grouped into 4 time periods. 1- 400 BC to 1360 AD. 2- 1360 to 1880 AD. 3- 1880 to 1970 AD. 4- 1970 AD to present.

The clustering of surface water isotopic values suggests that the isotopic changes are not random phenomena. The isotopic evolution of Xing Yun’s lake water appears to be influenced by human activity. Beginning with the Yuan Dynasty around 1300 AD, people began large scale exploitation of the copper and silver ores in the province (Yang, 2009). Mining activity and smelting continued to increase which impacted the lake water because of increased atmospheric pollution. An even more drastic change to the landscape occurred during the Qing Dynasty, when the government began encouraging Han people to immigrate into the Yunnan Province (Yang, 2009). These immigrants brought a new style of agriculture and new crops such as maize, sweet potatoes, peanuts, tobacco, and opium (Giersch, 2006). A rapid expansion in not

only the scale of agricultural activities, but also the carbon pathway of the plants had an impact on the soil. Erosion of soil from the catchment into Xing Yun Lake might cause $\delta^{13}\text{C}$ to diverge from $\delta^{18}\text{O}$. The C/N ratio also changes during this time, suggesting the same conclusion (Figure 2-9). After 1360 AD, the data points show wide variability across the $\delta^{13}\text{C}$ (‰ VPDB) axis (Figure 2-10). This is evidence that human activity likely had a profound impact on the watershed of Xing Yun as early as 1360 AD and that environmental degradation of the landscape has not been confined to the nineteenth century and onwards.

2.4.3 Other Climate Comparisons

One of the most reliable paleoclimate records for comparison with Xing Yun is the speleothem record from Dongge Cave, which is roughly 550 km east from Xing Yun. The Dongge Cave record spans a similar time period and has a similar resolution of 5-6 years, so we performed interpolation and subsequently calculated $\Delta\delta^{18}\text{O}$. Oxygen isotope values from Dongge cave published by Wang et al. (2006) were interpolated at one year resolution using MatLab 7.10.0. Xing Yun $\delta^{18}\text{O}$ values were subtracted from Dongge $\delta^{18}\text{O}$ values for years in which there was data from Xing Yun. The calculated values of $\Delta\delta^{18}\text{O}$ are very similar to the $\delta^{18}\text{O}$ record of Xing Yun (Figure 2-11).

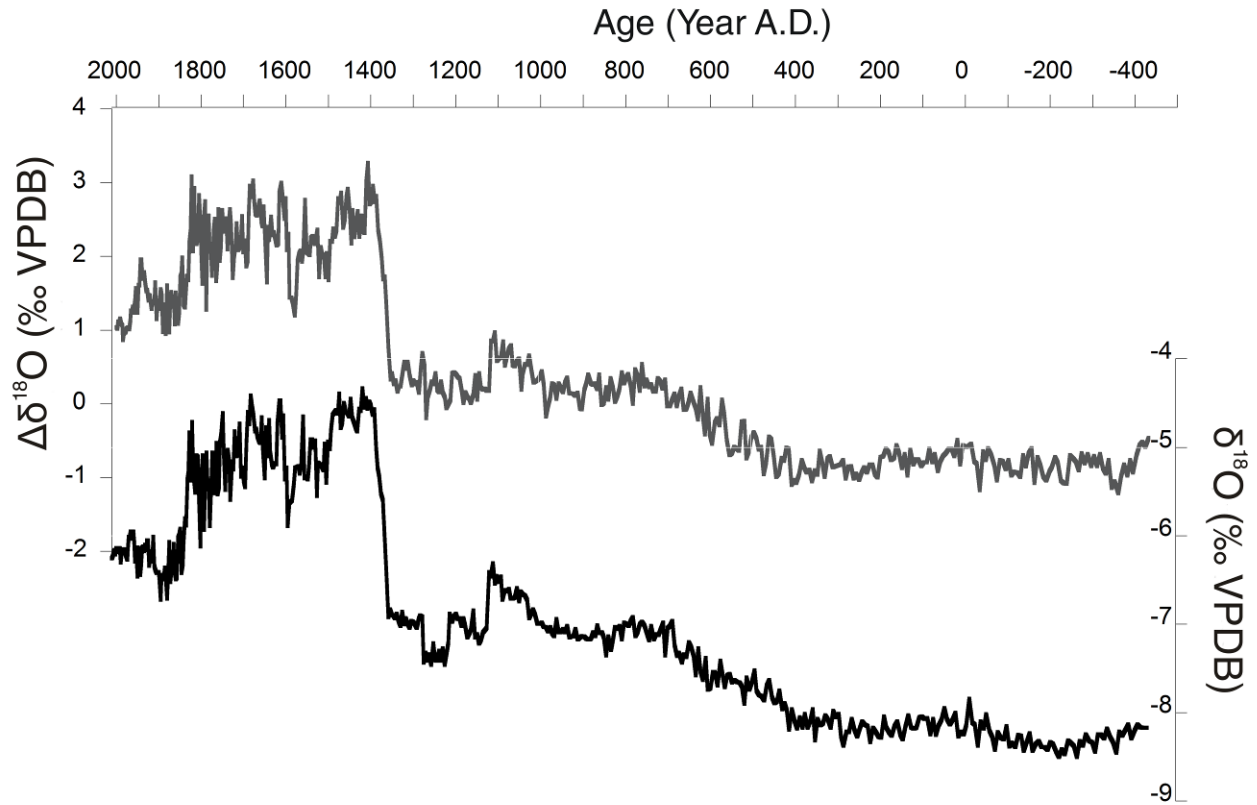


Figure 2-11- Calculated $\Delta\delta^{18}\text{O}$ values compared with Xing Yun A-09 oxygen isotope record.

As discussed in the previous section, Xing Yun shows a decrease of 3.0‰ in oxygen isotope values during the LIA, suggesting that the effects of evaporation on the lake are significant. However, the speleothem records, which are interpreted to not be affected by evaporation, do seem to show the same transition periods that are found in the Xing Yun record, though smaller in magnitude (Figure 2-12). Wanziang is located in more central China, roughly 1,000 km away from Xing Yun, and spans the last 1,800 years. The transition into and out of the LIA is marked by shifts of as much as 1.0‰ (Zhang et al., 2008). It also appears that Wanziang contains the transition into the period of increased AM strength from 1140-1360 AD, but subsequent $\delta^{18}\text{O}$ values do not show a wet period as Xing Yun does.

Dongge Cave is the speleothem record that is located closest to Xing Yun. This speleothem sampled at a 5-6 year resolution shows more variability in oxygen isotopes than Wanxiang (Wang et al., 2006). However, when Dongge and Xing Yun are compared, there is little resemblance. Dongge does appear to document the transition into the LIA with $\delta^{18}\text{O}$ values during the LIA being more positive. There is also some potential agreement during the wet period from 1140-1360 AD, yet given the proximity of Dongge Cave and the similar climate regime, more agreement is expected.

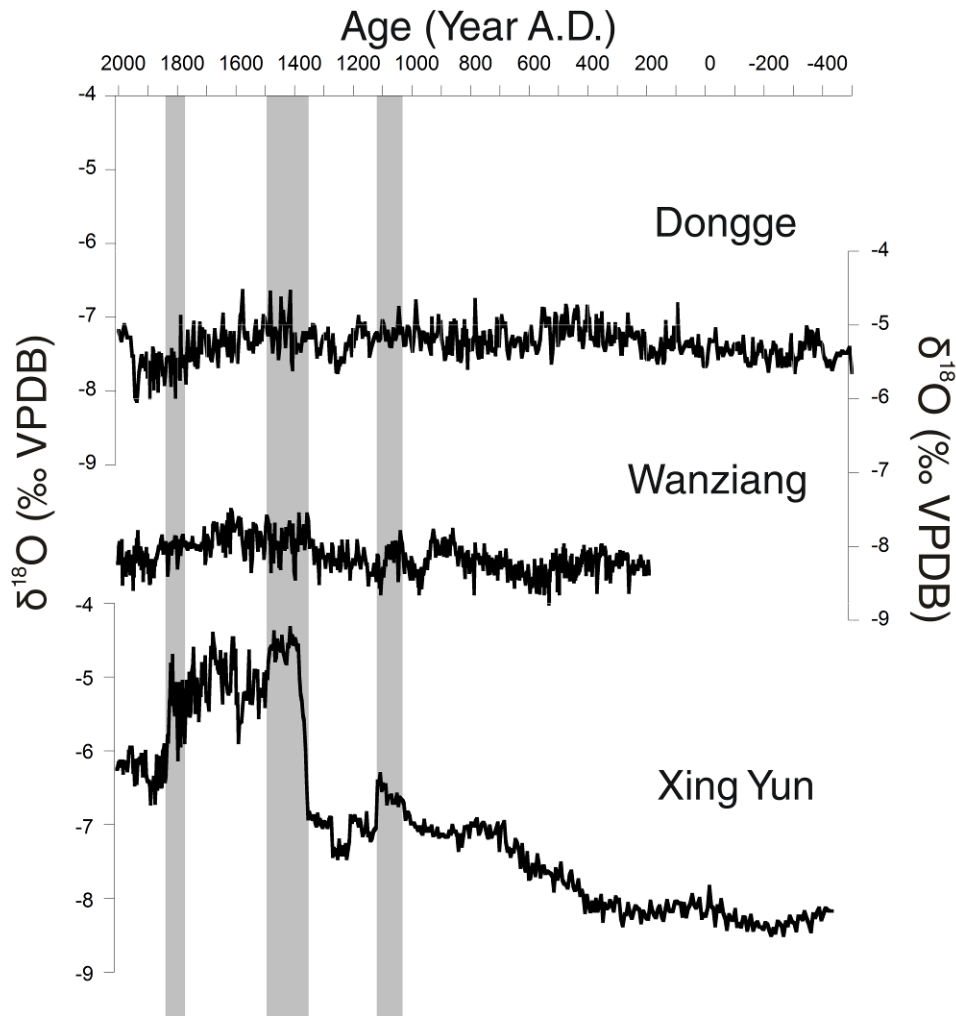


Figure 2-12- Xing Yun A-09 oxygen isotopes compared to Dongge and Wanxiang Cave oxygen isotopes. Highlighted areas show the transition into the wet period of 1140-1360 AD, the transition into the dry LIA, and the transition out of the dry LIA.

Tree rings were used to reconstruct the PDSI (Palmer Severity Drought Index) for southwest China for the past 700 years using gridded computer models (Cook et al., 2010). We took the grid point closest to Xing Yun, calculated a 10 year running average of PDSI and compared it to Xing Yun (Figure 2-13). Periods where PDSI was greater than 1.0 are often times of high $\delta^{18}\text{O}$ values in Xing Yun. While Xing Yun shows persistent drought throughout the LIA, the PDSI reconstruction only shows short periods of drought. The majority of the last 700 years

were dominated by the LIA so the PDSI record gives little long term context. Dendrochronology has been invaluable in understanding short term climate signals; however, long term cooling trends, such as the LIA, are difficult to capture in tree rings due to biological complications, the short life span of trees, and the statistical methods used to produce long records (Esper et al., 2007; Nelson et al., 2011). This is likely the reason that the PDSI record does not show the substantial drought during the LIA that is found in the Xing Yun record.

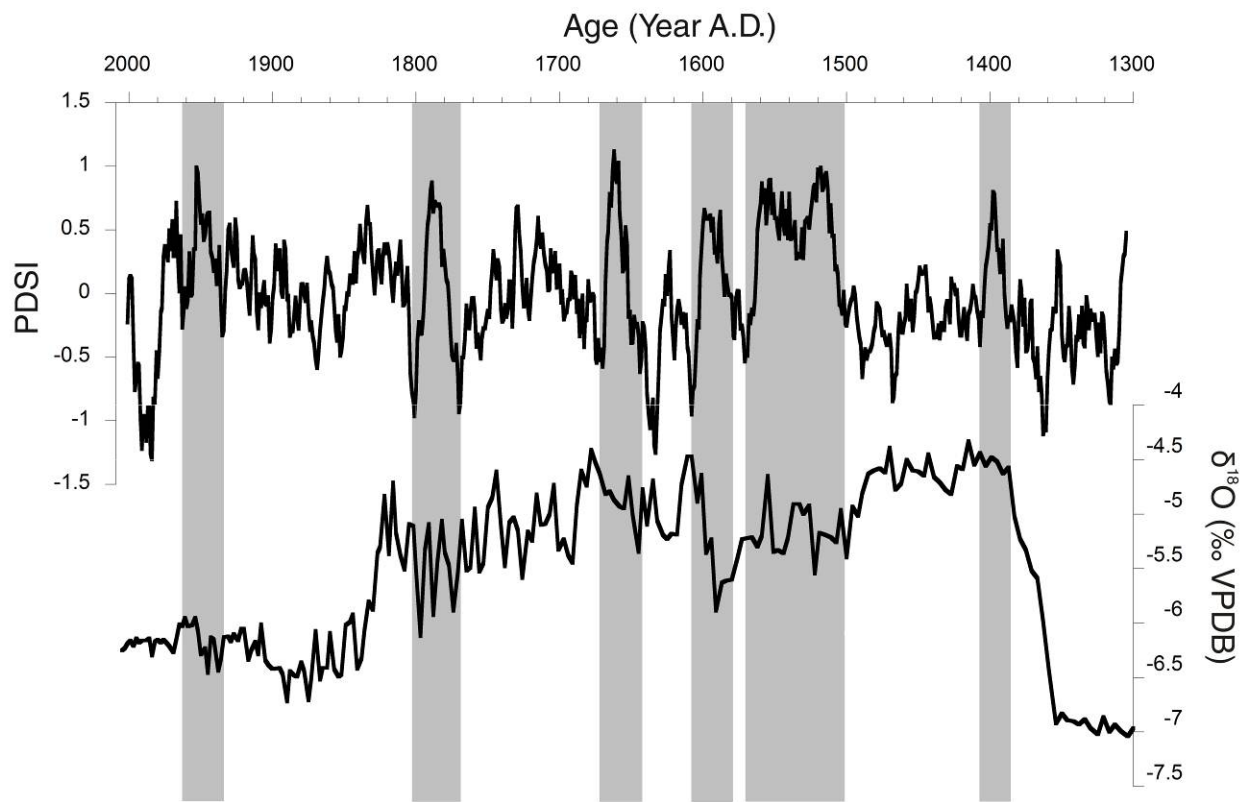


Figure 2-13- Cook et al. (2010) PDSI reconstruction compared to Xing Yun A-09 oxygen isotopes.

Highlighted areas indicate potential periods of agreement.

Lastly, because the AM is known to have a complex relationship with ENSO, Xing Yun was compared to a multi-proxy ENSO reconstruction that dates to 1500 AD (Braganza et al.,

2009). Xing Yun's oxygen isotopes are anti-correlated with ENSO strength at certain time periods, which is confirmed by other studies (Figure 2-14) (Kinter et al., 2002). The most notable period of anti-correlation occurs late in 1500 AD when an unusually strong ENSO is linked to a moderately wet period in Xing Yun during the LIA. In this period, as in other periods of anti-correlation, it appears that the ENSO cycle slightly precedes the shift in $\delta^{18}\text{O}$ isotopes of Xing Yun. This runs counter to previous findings about the linkage between ENSO and the AM since Kinter et al. (2002) found that the AM tends to precede an ENSO event. However, most research examining the relationship between the two has concentrated on only the last 100 or so years. Xing Yun potentially shows that the relationship between ENSO and the AM may vary continually through the period of the record.

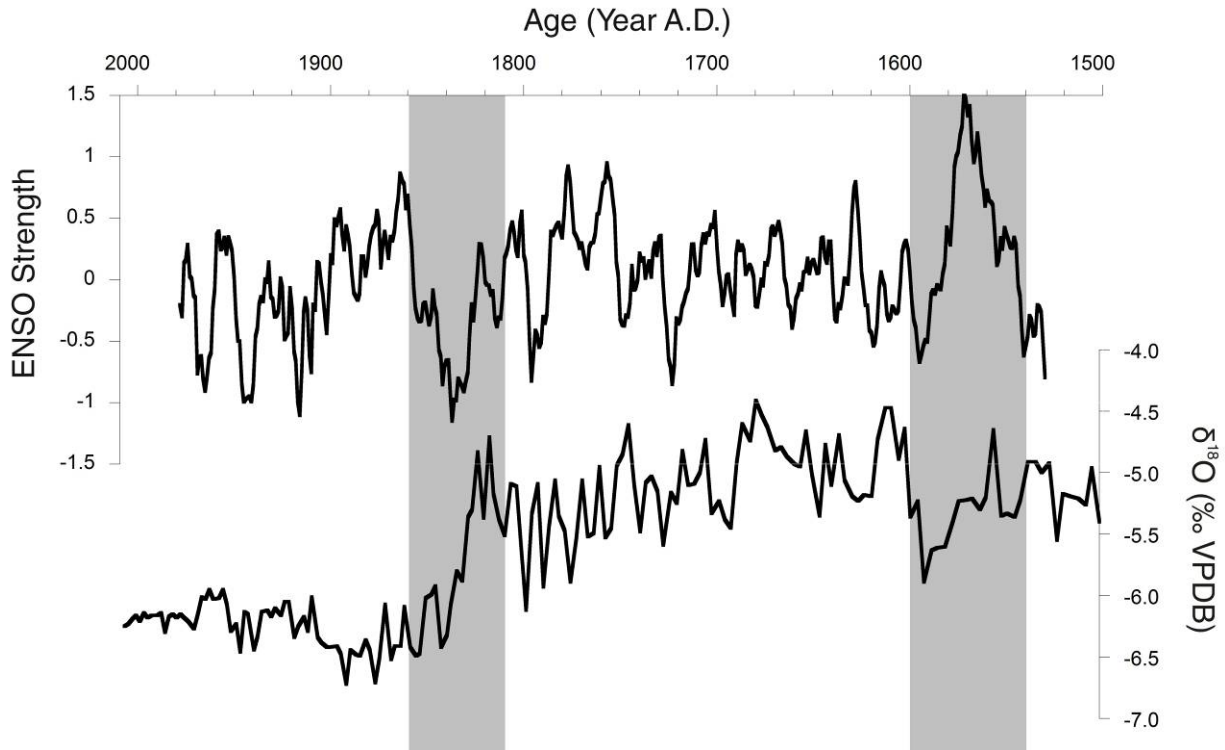


Figure 2-14- Braganza et al. (2009) ENSO reconstruction compared to Xing Yun A-09 oxygen isotopes. Highlighted areas are potential periods of anti-correlation.

2.5 CONCLUSION

Using the authigenic carbonate precipitated from lake sediments in Xing Yun has resulted in a useful paleoclimate record that illuminates the details of climate change in southwestern China. Our record shows good agreement with other existing records in this region, but highlights some important new features. The brief period of increased monsoon strength from 1140-1360 AD in an otherwise weakening monsoonal trend is an unusual feature and warrants further investigation. The LIA was a period of weak monsoons, the strength of which has not been seen before.

Future goals of this project are to investigate the interaction between $\delta^{18}\text{O}$ and $\delta^{13}\text{C}$ isotopes on longer time scales. Extending the record in Xing Yun Lake back many more thousands of years has the potential to reveal longer term patterns. Additionally, Xing Yun is only one of many lakes in Yunnan. Future work will be to retrieve sediment cores from many other lakes in the region and perform stable isotope analysis to identify regional and small scale patterns in monsoon variability.

3.0 A 2500 YEAR HISTORY OF HUMAN ACTIVITY IN SOUTHWESTERN CHINA

3.1 INTRODUCTION

As of 2000 AD, the Yunnan Province is home to 43 million people (Pacific, 2010). Yunnan has suffered cumulative environmental damage that has only recently been quantified. Using historical documents and computer models, a reconstruction of forest coverage rates estimates that in 1850 AD the province was covered in 45% forest and had declined to 30% by 1949 AD (He et al., 2008). Water samples from Xing Yun were taken in 1994 AD and revealed elevated nutrient concentrations which indicate pollution from deforestation and agriculture (Whitmore et al., 1997). More recent water studies also indicate moderate eutrophication and effluent pollution (Li et al., 2007).

The Yunnan province has a unique history since it frequently remained independent of the politics within the Chinese dynasties. While this means that the Yunnan province has an interesting perspective on Chinese history, it also means that historical records are limited. Estimates of population demographics and mining activity are subject to error. Using a variety of proxies on lake sediments from Xing Yun such as trace metal concentration, magnetic susceptibility, carbon and nitrogen isotopic composition, and carbon to nitrogen ratio, has the potential to illuminate gaps in the historical records and substantiate historical records.

Additionally, the aim of this project is to quantify recent human disturbance to the watershed and assess the extent of environmental degradation.

3.2 METHODS

Xing Yun cores were taken in August 2009. Surface sediments (core A-09 drive 1) were taken with a piston core fitted with a 5.5 cm diameter removable polycarbonate tube and 133.5 cm of sediments were recovered. The upper 56 cm of core A-09 drive 1 was extruded in the field at 0.5 cm intervals. Deeper sediments (cores A-09 drive 2 and drive 3) were collected with a modified square-rod piston corer (Livingston core) and extruded in the field (Wright et al., 1984). The cores measure 92 cm and 96 cm respectively. Altogether these three cores produce a total record of 2.64 m. Cores A-09 drive 1 and drive 2 overlap by 47.5 cm and cores A-09 drive 2 and drive 3 overlap by 10 cm on the basis of field notes and stratigraphic comparison of oxygen isotopes, carbon isotopes, and magnetic susceptibility values.

Sediment ages were determined by radiocarbon, ^{210}Pb , and ^{137}Cs measurements. The 56 cm of extruded sediments from core A-09 drive 1 were used for ^{210}Pb and ^{137}Cs measurements. Samples were freeze dried and equilibrated in a cold storage room at the University of Pittsburgh. ^{210}Pb , ^{137}Cs , and ^{214}Pb activities were measured on a Canberra Germanium Detector BE2020 at the University of Pittsburgh for 23 hours to detect γ radiation. Sediment ages were determined on the basis of the constant rate of supply model (Appleby and Oldfield, 1983). Accelerator mass spectrometer radiocarbon dating was performed on 6 samples which were pretreated using the standard acid, base, acid procedure of Abbott and Stafford (1996). Samples

were measured at the Kleck Center for Accelerator Mass Spectrometry at the University of California Irvine.

The entire length of each drive was sampled at a 0.5 cm interval and stored in polycarbonate scintillation vials. Samples for ICP-MS measurements were taken every 6 cm from the depth of 2.12 m to 0.53 m. From the depth of 0.53 m to the top of the core, samples were measured every 1-3 cm. All samples were freeze dried and weighed at the University of Pittsburgh. Elements were extracted using 10 mL of 1 M HNO₃ overnight, a standard method for extracting trace metals from organic lake sediments following the methods of Abbott and Wolfe (2003). Two tenths of a gram of the acid extraction was measured for inductively coupled plasma–mass spectrometer (ICP-MS) analysis for 48 elements at the University of Alberta using a Perkin Elmer Elan6000 quadrupole (Table 3-1). Concentrations in ppm were converted to flux by multiplying sedimentation rate, dry bulk density, and concentration.

Bulk density samples measuring 1 g cm⁻³ were taken every 2 cm down the entire length of the core less than 24 hours after the core had been opened. These were weighed immediately and again after 36 hours in a drying oven at 60°C. Sedimentation rate was calculated as the change in depth in cm divided by the age of the sediment according to the age model.

Table 3-1- Measured elements and detection limits.

Element	Detection Limit (ppm)	Element	Detection Limit (ppm)
Na	0.50	Sn	0.06
Mg	2.00	Sb	0.01
Al	0.20	La	0.03
P	5.00	Ce	0.03
K	6.00	Pr	0.04
Ca	31.00	Nd	0.03
Sc	0.10	Sm	0.04
Ti	0.09	Eu	0.03
V	0.05	Gd	0.03
Cr	0.05	Tb	0.03
Mn	0.03	Dy	0.04
Fe	3.70	Ho	0.02
Co	0.03	Er	0.04
Ni	0.06	Tm	0.06
Cu	0.03	Yb	0.05
Zn	0.08	Lu	0.04
As	0.06	W	0.08
Se	0.20	Os	0.08
Sr	0.03	Ir	0.04
Y	0.02	Au	0.01
Zr	0.09	Tl	0.05
Mo	0.08	Pb	0.03
Ag	0.01	Bi	0.01
Cd	0.06	In	0.03

Principal component analysis was performed using MatLab 7.10.0 in a covariance matrix.

All rare earth metals as well as Sn and Bi were removed from analysis. The following code was used:

```
stdr = std(data);  
sr = data./repmat(stdr,56,1);  
[coefs,scores,variances,t2] = princomp(sr);  
biplot(coefs(:,1:2))  
percent_explained = 100*variances/sum(variances)
```

Weight percent carbon and nitrogen was sampled every 2 cm for the length of each drive. Samples were covered in 1 M HCl for 24 hours to dissolve organic carbon. Samples were then freeze dried at the University of Pittsburgh and analyzed at Idaho State University. Samples were analyzed using ECS 4010 (Elemental Combustion System 4010) interfaced to a Delta V advantage mass spectrometer through the ConFlo IV system. The elemental analysis was done by an evolutionary "flash combustion/chromatographic separation techniques". The furnace temperature was kept at 1000°C; while the reduction oven was 650°C. The gases generated from the combustion of the samples were carried in a helium stream into a GC column held at 60°C. The gases then separate before being diluted in the ConFlo IV and passed to the mass spectrometer for analysis. Isotope ratios of $\delta^{13}\text{C}$ are reported as ‰ values relative to the VPDB scale; whereas $\delta^{15}\text{N}$ values are reported as ‰ values relative to air- N_2 . Three in-house standards (ISU Peptone, Costech Acetanilide and DORM-2) which are directly calibrated against international standards (IAEA-N-1, IAEA-N-2, USGS-25, USGS-40, USGS-41, USGS-24, IAEA-600) were used to create a two point calibration curve (normalization curve) to correct the raw data. ISU Peptone and Costech Acetanilide were used to set up a two-point calibration line (normalization curve). A third standard (DORM-2) was used to monitor the accuracy of the data. The final data was corrected using a three-point calibration curve (normalization curve). At least 1 standard was run for every 6 or 7 samples. Samples were measured for weight percent nitrogen, weight percent organic carbon, $\delta^{15}\text{N}$, $\delta^{13}\text{C}$ of organic carbon, and C (%)/N (%).

3.3 RESULTS

^{210}Pb ages were calculated on the basis of the constant rate of supply (CRS) model (Figure 3-1) (Appleby and Oldfield, 1983). Radiocarbon dates were calibrated using Calib 6.0 (Table 3-2) (Stuiver et al., 2010). On basis of these 2 dating techniques, the following age-depth model was produced (Figure 3-2).

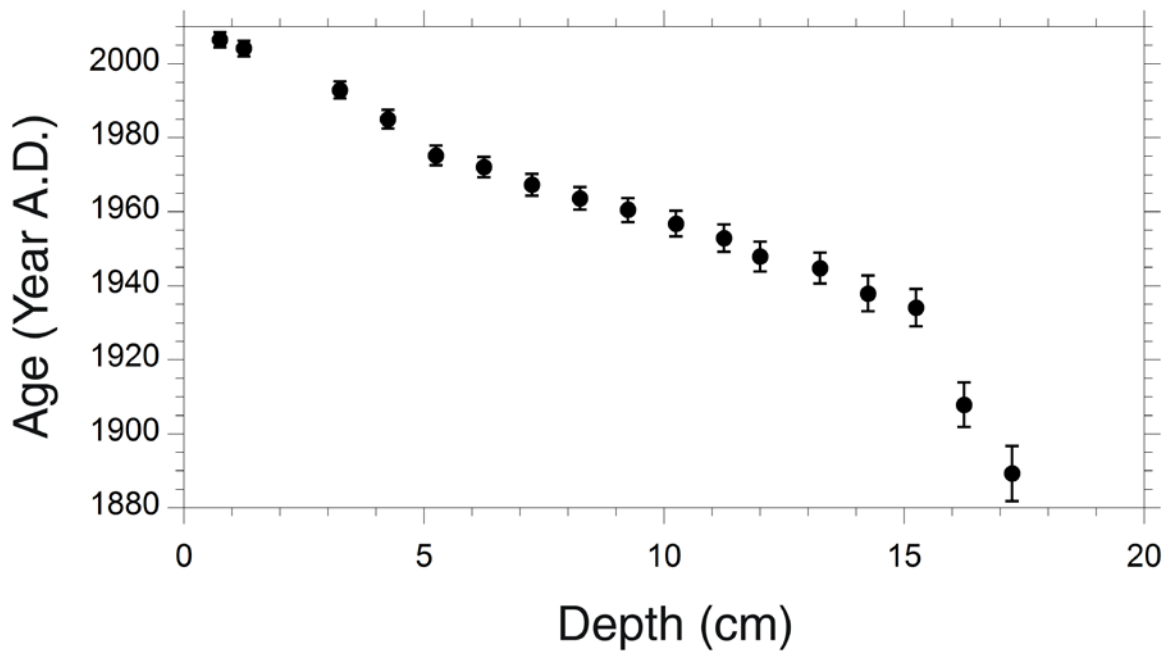


Figure 3-1- ^{210}Pb ages from Xing Yun A-09 using the CRS model. Error bars represent one standard deviation.

Table 3-2- Radiocarbon dates

Core	Drive Depth (cm)	Total Depth (cm)	Material	¹⁴ C age (¹⁴ C BP)	¹⁴ C age error	Median calibrated age (cal years BP)	2-sigma calibrated age range (cal years BP)
A-09 D1	35.5	35.5	Wood	110	25	110	0-270
A-09 D1	37.5	37.5	Charcoal	110	50	120	0-280
A-09 D1	59.0	59.0	Charcoal	130	25	120	0-270
A-09 D2	59.0	145.0	Charcoal	1060	25	960	930-1050
A-09 D3	82.0	250.0	Wood	2105	20	2080	2000-2140
A-09 D3	95.0	263.0	Charcoal	2220	20	2230	2150-2350

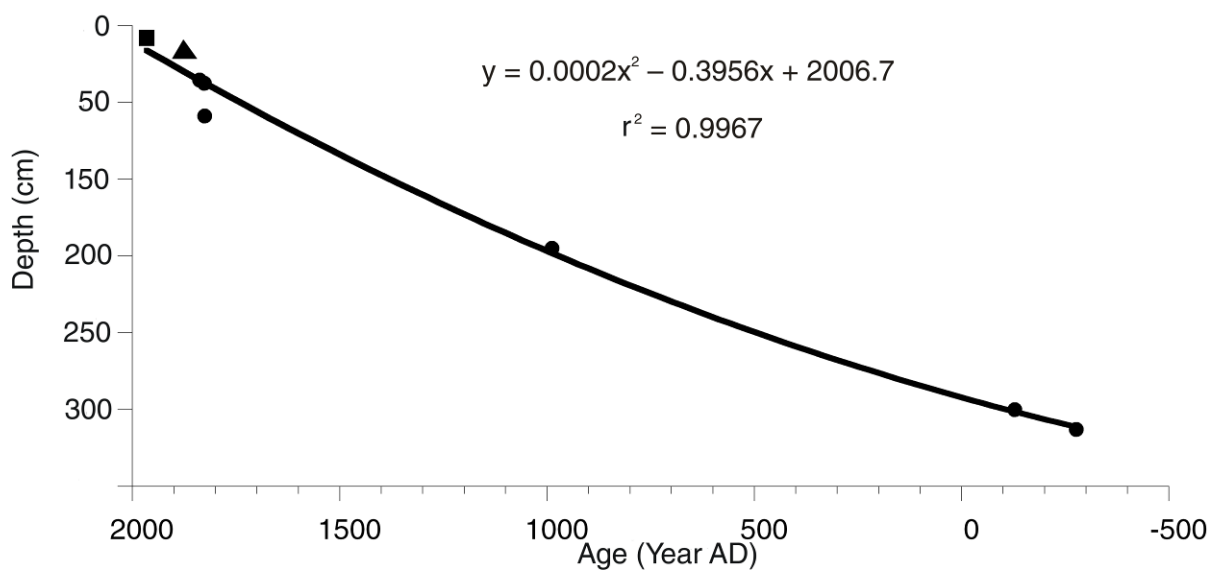


Figure 3-2- Age depth model for Xing Yun A-09. Circles denote ¹⁴C dates, the square denotes ¹³⁷Cs date, and the triangle denotes the ²¹⁰Pb date at 1880 AD.

For the purposes of isolating the effects of local mining and smelting on the landscape, we focus on the trace metal concentrations of Bi, Cr, Pb, Sb, and Zn which have been previously shown to indicate pollution from ores (Abbott and Wolfe, 2003). Lead is particularly useful because it is relatively immobile in sediments (Abbott and Wolfe, 2003). The earliest sample was taken from 2.12 m, corresponding to a cal year of 280 AD. Samples from 280-930 AD have low flux for all elements and represent background levels (Figure 3-3). After 930 AD, all elements show a slow rise in flux with a temporary peak at 1210 AD and fluctuations until 1580 AD. After 1580 AD, flux begins to increase again until a peak is reached at 1790 AD. Lead continues to decrease, Bi, Cr, and Sb fluctuate over the rest of the period, and Zn continues to increase.

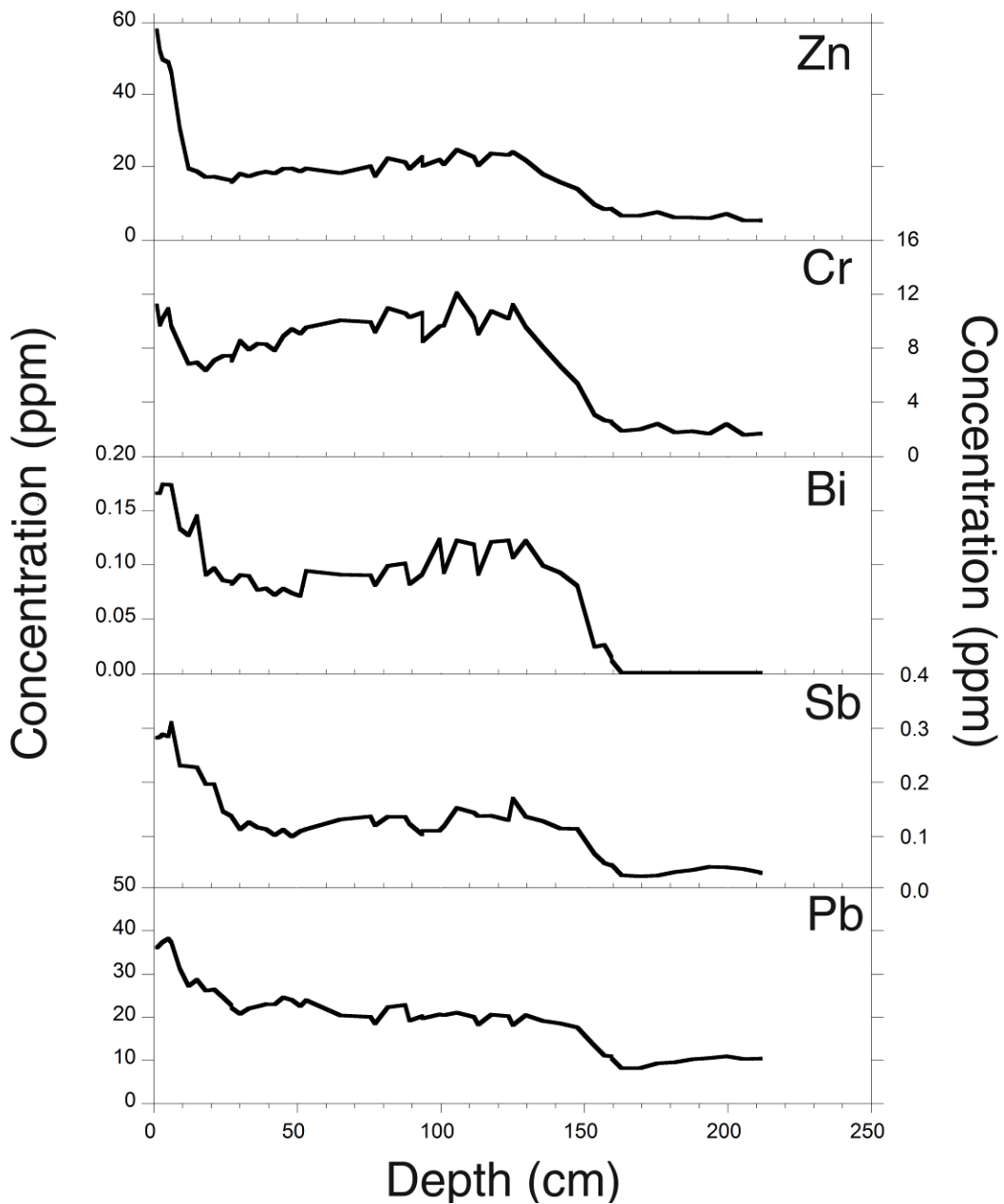


Figure 3-3- Metal concentration for selected elements from Xing Yun A-09.

Principal component analysis revealed that component 1 explained 54.3% of the variance and component 2 explained 33.3% of the variance, for a total of 87.5%. A plot of 23 measured elements reveals that there are 3 distinct groupings (Figure 3-4). Elements associated with

lithogenic inputs plot negatively for component 1 and positively for component 2. Elements associated with metal pollution plot positively for component 1 with both negative and positive scores for component 2.

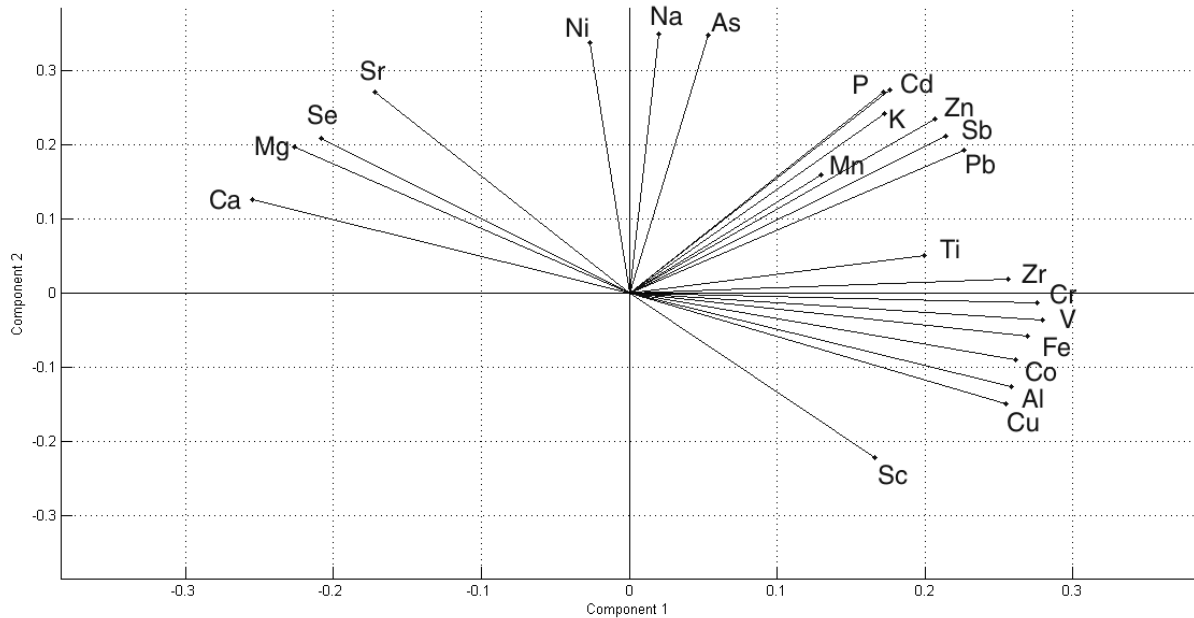


Figure 3-4- Biplot of PCA loadings for 23 measured elements from Xing Yun A-09.

The carbon to nitrogen ratio is low through the entire record. The ratio fluctuates between 10 and 12 from 400 BC to 1000 AD (Figure 3-5). Thereafter, the C/N ratio fluctuates, but generally decreases until 1400 AD. From 1400 to 1800 AD, the C/N ratio declines to 7, suggesting a nearly pure aquatic source of organic matter. From 1800 AD to present day, the ratio fluctuates between 8 and 10. These results, coupled with organic matter $\delta^{13}\text{C}$ values between -25 and -30‰ indicate that the dominant organic matter source is lacustrine algae, especially from the time period 1400 to 1800 AD (Myers, 1994).

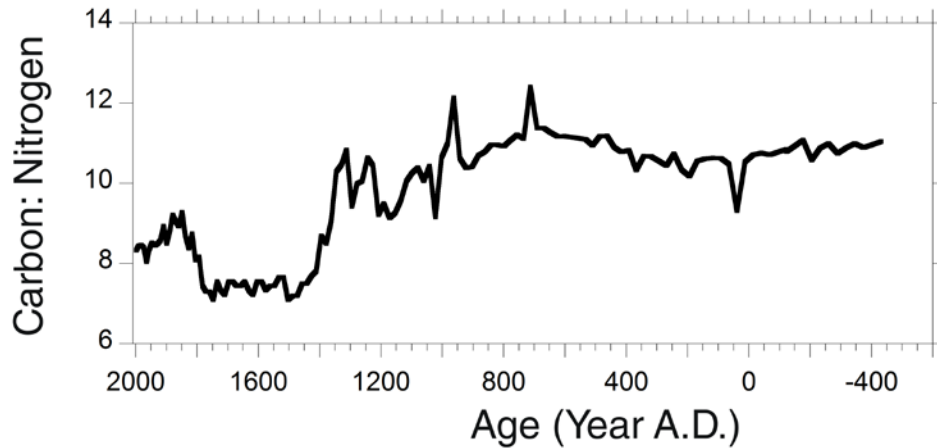


Figure 3-5- Carbon to nitrogen ratio in Xing Yun A-09.

3.4 DISCUSSION

Metal concentrations were converted to flux ($\mu\text{g cm}^{-2} \text{ year}^{-1}$) to investigate metal enrichment over time. Likewise, the age model was used to convert core depths into years for comparison with other sediment and historical records. Periods of Chinese history were noted to see how cultural changes compare with geochemical results (Figure 3-6). The initial rise in metal loadings takes place at the end of the Tang Dynasty and into the period of political instability known as the Five Dynasties and Ten Kingdoms where there was no unified dynasty (Eberhard, 1967). There are several hypotheses that can explain this initial rise in metal enrichment in the sediments of Xing Yun:

- 1) Increased erosional inputs from the watershed.
- 2) Increased deforestation due to population rise and subsequently increased erosional inputs.

- 3) Increased smelting and mining activity that increased atmospheric pollution to the watershed.

Historical records indicate that the population in Yunnan remained relatively stable until roughly 1700 AD, so changes in the watershed would be unrelated to population increase (Lee, 1982). Additionally, reconstruction of forest coverage through historical records and computer modeling suggests that in the last 150 years only 15% of forest was lost and land clearing was not a major operation in the province (He et al., 2008). Calculated sedimentation rates, magnetic susceptibility, and carbon to nitrogen ratio results of Xing Yun also indicate that significant changes to the watershed did not begin until 1400 AD (Figure 3-7). Thus, scenario three, an actual rise in smelting and mining, is the most plausible explanation.

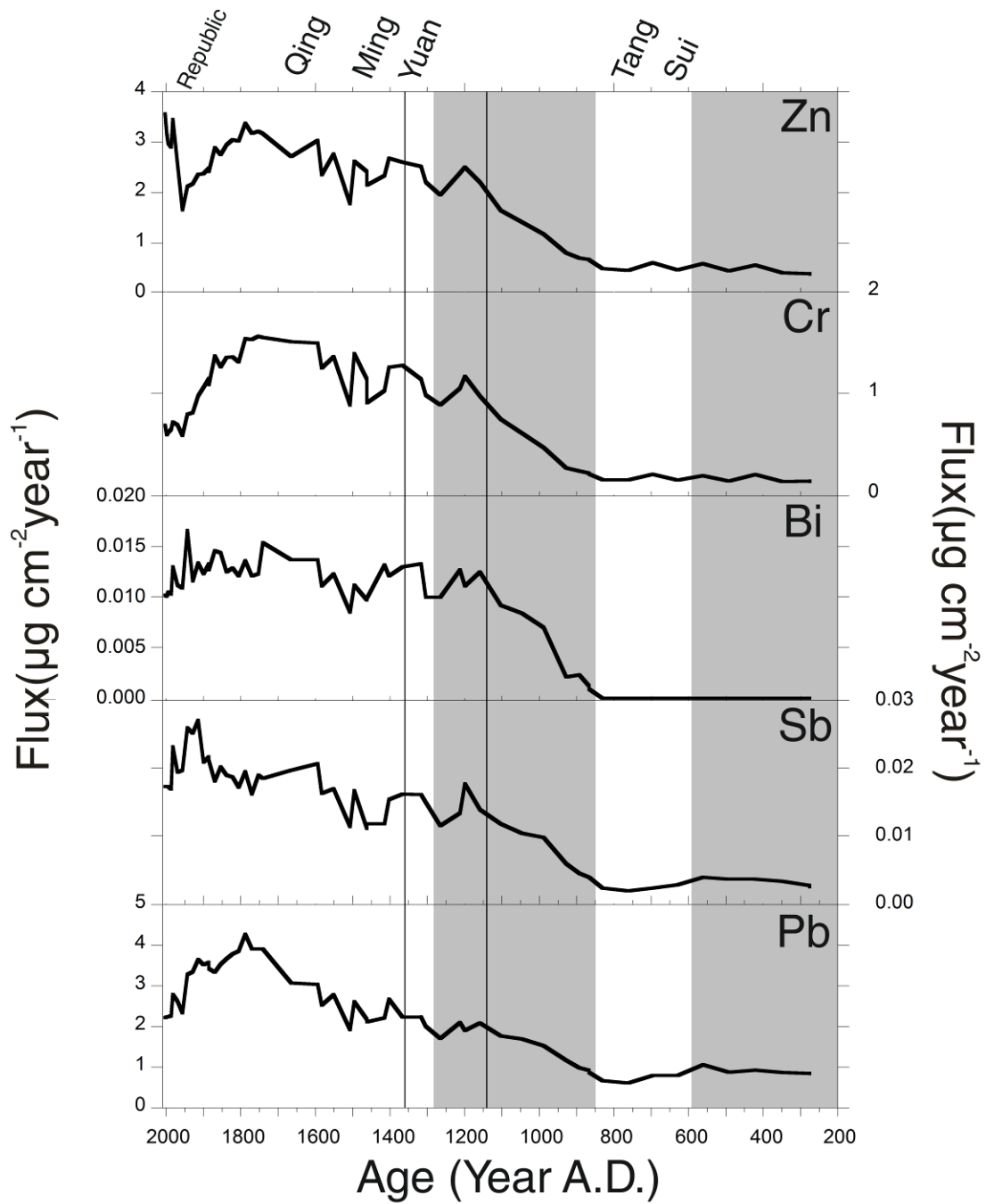


Figure 3-6- Calculated metal flux for selected elements from Xing Yun A-09. Shaded areas represent periods where there was no unified empire. Lines represent transitions into climate units III and IV.

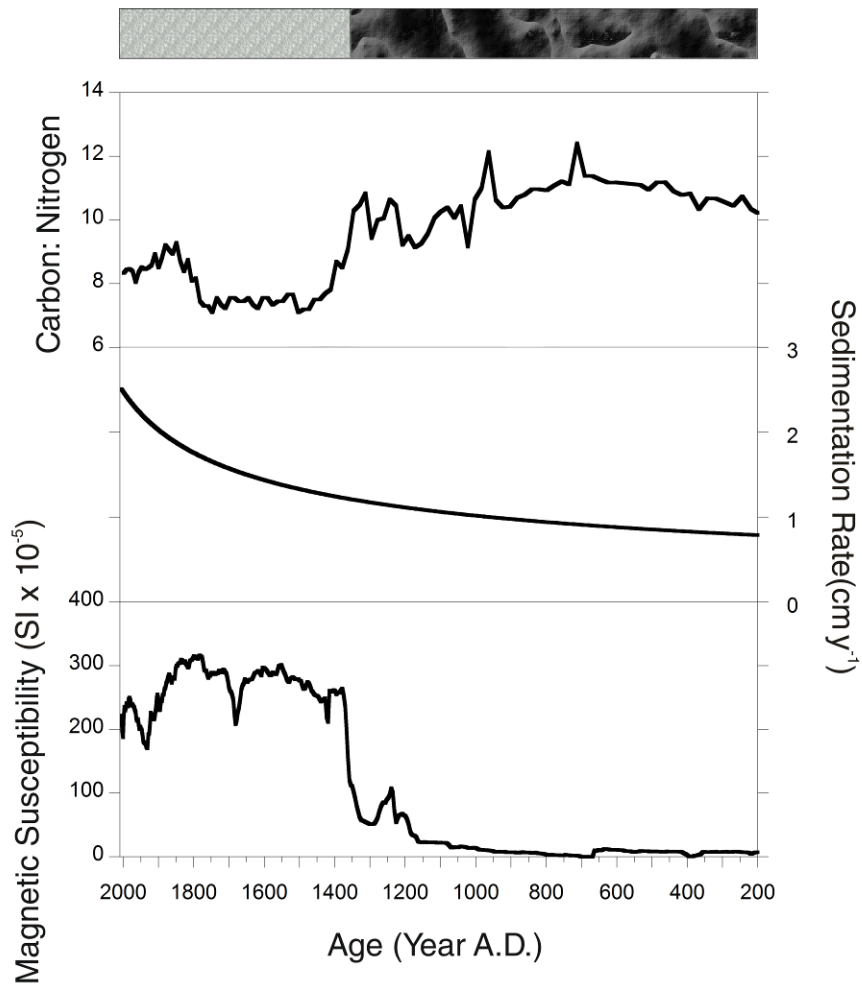


Figure 3-7- From top to bottom: stratigraphic column indicating red color and presence of pyrite in light pattern, dark color and lack of pyrite in dark pattern, carbon to nitrogen ratio, calculated sedimentation rate, and magnetic susceptibility for Xing Yun A-09.

While historical records document mining before 930 AD, the geochemical record to date does not record this activity, at least in concentration data. This indicates that early mining probably took place in small select areas distant to Xing Yun. Another possibility is that there is a lag in the watershed system due to the temporary storage of metals. Historical records are ambiguous as to when the technique of refining silver and gold using cupellation first began

(Golas, 1999). While it may have been used as early as 600 BC, explicit mention of cupellation in texts does not occur until roughly 900 AD (Golas, 1999). Xing Yun may be registering atmospheric deposition of the waste products of cupellation which was in wide use by 900 AD.

Metal flux decreases at the beginning of the Ming Dynasty and as southwestern China enters the cold and arid LIA. However, it is unlikely that the LIA had a great impact on mining activities since flux rises again with the onset of the Qing Dynasty even as the climate remains dry. As historical accounts indicate, the mines in Yunnan were especially prone to flooding and had to frequently be pumped to remove excess water, so it is possible that reduced monsoon strength (and less precipitation) was actually beneficial to the miners (Golas, 1999). Another consideration that because the Qing Dynasty encouraged migration into the Yunnan Province, the increased flux may be attributed to the sheer increase in mining labor rather than an increase in the scale of mining operations. This is plausible since Chinese mines relied on manual labor to haul the ores out of the mine (Golas, 1999). As Yunnan entered the peak of mining in 1700 AD, there is a corresponding rise in flux as metals reach their peak during this time period.

Additional proxies such as carbon to nitrogen ratio, sedimentation rate, and magnetic susceptibility indicate that the Xing Yun watershed experienced changes as early as 1400 AD which increased substantially by 1700 AD (Figure 3-7). This is the time period where immigrants increased in number and began intensively working the land with terracing (Giersch, 2006). Terracing likely increased the runoff, lithogenic, and nutrient input to the lake which caused eutrophication and algal blooms as evidenced by the increased sedimentation and decreasing carbon to nitrogen ratio. Eutrophication decreases the amount of dissolved oxygen in the water column, which caused Xing Yun to become enriched in reduced iron. The high magnetic susceptibility values, post depositional precipitated pyrite, and rapid oxygenation of the

core at the surface all support this interpretation. Increased terracing of the land does not necessarily imply increased deforestation of the watershed, since carbon to nitrogen ratios typically increase with deforestation (Kaushal and Binford, 1999). With increased deforestation, there is an increase in sedimentary terrestrial carbon delivered to the watershed, which results in a high carbon to nitrogen ratio.

After 1790 AD, lead reached a peak whereas bismuth, chromium, antimony, and zinc continued to increase. As the Qing dynasty came to power, focus shifted from silver to copper (Yang, 2009). This is likely why lead reached a peak and began to decrease even though mining activity in Yunnan was still extensive. Subsequent decline in flux is likely due to the political instability in the region. As the Qing dynasty fell, Yunnan was subject to foreign and indigenous takeover and after the Chinese republic was formed, the Yunnan province was no longer of national interest. The declining metal flux is due to declining interest in mining and what flux remains is due to pollution from human activities in the watershed.

Principal component analysis (PCA) supports the above interpretations. PCA suggests that component 1 defines the gradient between those elements that originate lithogenically from the landscape and those that are the result of human activity (Cooke et al., 2009). Elements of the landscape bedrock such as calcium, magnesium, selenium, and strontium plot negatively for component 1. Arranging the samples in stratigraphic order, component 1 and 2 scores appear inversely correlated (Figure 3-8). The decrease in component 1 scores takes place in the year 930 AD, which indicates that the elements associated with bedrock input increase and become more dominant through time. This demonstrates the increasing runoff being delivered to the lake, which is likely the result of increased human activity. Component 2 also seems to play a role in identifying elements of anthropogenic origin, but it is more ambiguous, since elements

such as chromium, cobalt, and iron plot negatively, while antimony and lead plot positively. However, component 2 scores do increase beginning around 1900 AD which may be the rise of modern industrial China.

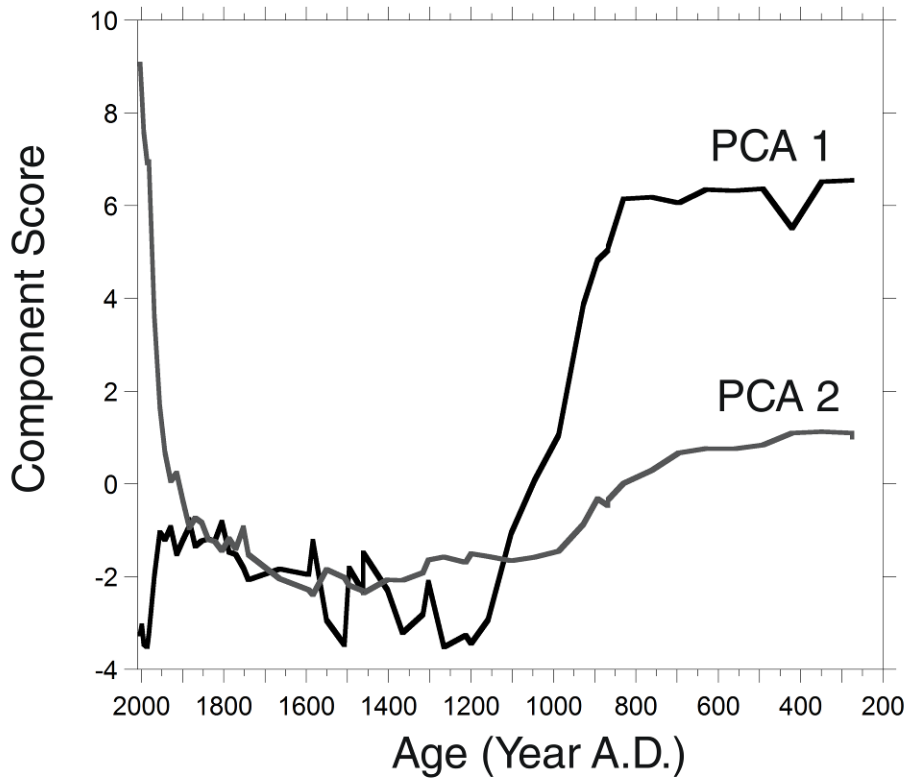


Figure 3-8- Fifty six samples plotted with component 1 and 2 scores from Xing Yun A-09.

3.5 CONCLUSION

Performing trace metal analysis on 56 samples spanning a time period of roughly 1,800 years gives valuable insight into the timing and extent of the metallurgy activities of the early Yunnan people. While historical records suggest that Yunnan people were mining by 800 BC, the record from Xing Yun does not pick up this activity, which indicates that early mining

probably took place in small select areas not near Xing Yun Lake. The Yunnan Province has traditionally been isolated from the Chinese government, but once the Chinese dynasties took an interest in Yunnan's ores, mining intensified to such an extent that the pollution is seen in Xing Yun Lake. More importantly, this record shows that the encouragement by the Qing Dynasty to migrate into Yunnan had a drastic impact on the magnitude of mining activities and the subsequent pollution to the watershed. An unexpected finding is that modern day metal enrichment values are roughly half of the enrichment values at the peak of mining activity.

Future work is to measure Hg concentration and Pb isotopes at the same intervals as the other trace metals. Measuring Pb isotopes has the potential to reveal the source of the ore used for smelting which could help explain why Xing Yun does not show the impact of mining prior to 930 AD. Taking these proxies and combining them with other environmental indicators is essential to understanding how people interacted with their environment in the past and what this can say about interaction today.

4.0 THE INTERACTION BETWEEN HUMAN ACTIVITY AND LANDSCAPE DEVELOPMENT

History teaches us that those who ignore the environment and its changing climate can often face devastating consequences. There are numerous examples, but none more striking than the Mayan civilization whose collapse was likely influenced by the intensification of drought (Brenner et al., 2001). Throughout our work in southwestern China, it is clear that no society is immune to the impact of rapid climate change. While some would make the claim that Chinese history and dynastic transitions have been directly impacted by changing climate patterns, what we see is a much more subtle impact on society (Zhang et al., 2008).

Using the stable isotopes of authigenic carbonate from Xing Yun Lake, it is clear that southwestern China has experienced several dramatic shifts in climate in the last 2,500 years. Due to precessional forcing, the strength of the AM was slowly weakening for at least 1,500 years of Xing Yun's record. Several speleothem records have interpreted small shifts in $\delta^{18}\text{O}$ as evidence of drastically changing monsoon strength, but Xing Yun puts these shifts into perspective and suggests that many of the shifts are small. Using the trace metal record to track mining and other human activity, it appears that the slowly shifting monsoon strength had a negligible impact on society in southwestern China. As James Scott (2009) has proposed, the Yunnan Province also appears insensitive to the political chaos of dynastic China since trace metal flux continued to rise despite government instability. If this increase in trace metal flux

were purely the result of increased land clearance and erosional input to the watershed, evapotranspiration would decrease, increasing water flow to the lake, and causing oxygen isotopes values to decrease (Rosenmeier et al., 2002). However, this is not the case for the oxygen isotopes of the Xing Yun throughout the initial period of metal enrichment.

The anomalous period of increased monsoon strength from 1140-1360 AD is the first major perturbation in an otherwise stable period. This is also a period of time when trace metal flux stops dramatically increasing. It is possible that these wetter conditions flooded the mines in Yunnan which halted mining activity for several weeks or months. However, this is by no means an indication of environmental determinism. Other proxies indicate that society in the Yunnan Province continued to grow, even into the transition of drier climates. Additional investigation into this period may clarify this interpretation and indicate to what extent human activities changed Xing Yun lake level.

The transition into the Little Ice Age (LIA) as recorded in Xing Yun lake sediments is extraordinarily rapid, taking place within a human lifetime. The climate in southwestern China during the LIA matches well with what has been modeled; however the severity of the drought is far beyond what many speleothem records in this region record (Dykoski et al., 2005; Mann et al., 2009; Zhang et al., 2008). The dry LIA lasted for at least 500 years and likely had an impact on mining activities as trace metal flux takes a slight downturn. The values of trace metal flux still remain high and are comparable to previous values, but the increase is not as great as expected had flux continued on a similar increasing trajectory. Indeed, this is likely why trace metal flux begins to rise again as more Han immigrants meant more mining labor. It is also important to note that around the same time, the $\delta^{13}\text{C}$ record took an unprecedented negative shift and no longer matched the $\delta^{18}\text{O}$ record. Carbon to nitrogen ratio, magnetic susceptibility,

and stratigraphic characteristics all indicate that this was likely the result of increased nutrient delivery to the watershed producing eutrophication.

As the LIA ends in the nineteenth century conditions became wetter, but not as wet as they were roughly 1,000 years ago. Xing Yun indicates that present day monsoon strength is weak compared to the past 2,500 years. With this data set, it is impossible to predict what the future will hold for the AM, but regardless of the outcome there are important lessons to be learned from the past. With such a variable climate occurring in this small sector of the world, it is worth investigating how society responded to these changes. How were Yunnan people able to shift their lifestyles to accommodate a dry climate without major disruption to society? Do historical or archaeological records indicate these periods of drought? Were people consciously aware of their shifting environment or did they make unconscious adaptations? Additionally, it is important to note that environmental degradation has been taking place for hundreds of years. While we may traditionally think of the Industrial Revolution as the start of widespread pollution, instead we see that wherever humans cluster together for long periods of time, they can dramatically change their landscape. Learning lessons from past civilizations may prove to be the key to adapting to future climate change.

APPENDIX A

TABLE OF DATA FOR DRIVE 1

Total Depth (mm)	Core Depth (mm)	Age (years BP)	Cal Year	Corr. $\delta^{18}\text{O}$	Corr. $\delta^{13}\text{C}$	Magnetic Susceptibility ($\text{k} \times 10^{-5}$ SI)
5	5	-55	2005	-6.25	0.89	221.55
10	10	-53	2003	-6.23	0.77	198.55
15	15	-51	2001	-6.19	0.69	187.45
20	20	-49	1999	-6.16	0.67	219.30
25	25	-47	1997	-6.21	0.68	235.60
30	30	-45	1995	-6.14	0.67	229.15
35	35	-43	1993	-6.18	0.77	233.40
40	40	-41	1991	-6.16	0.59	241.65
45	45	-39	1988	-6.16	0.69	240.85
50	50	-36	1986	-6.14	0.60	235.65
55	55	-34	1984	-6.30	0.44	247.00
60	60	-32	1982	-6.17	0.37	250.20
65	65	-30	1980	-6.15	0.41	245.70
70	70	-28	1978	-6.18	0.59	241.70
75	75	-26	1976	-6.15	0.52	237.30
80	80	-24	1974	-6.18	0.20	239.75
85	85	-22	1972	-6.21	0.29	236.60
90	90	-20	1969	-6.27	0.32	235.70
95	95	-17	1967	-6.15	0.04	231.10
100	100	-15	1965	-6.01	-0.14	226.40
105	105	-13	1963	-6.03	-0.94	218.90
110	110	-11	1961	-5.95	-0.87	213.15
115	115	-9	1959	-6.03	-1.20	216.35
120	120	-6	1956	-6.02	-1.10	208.85
125	125	-4	1954	-5.95	-1.16	200.10
130	130	-2	1952	-6.07	-1.18	204.55
135	135	0	1950	-6.29	-1.49	200.00
140	140	3	1947	-6.23	-1.72	200.10
145	145	5	1945	-6.46	-2.41	191.15
150	150	7	1943	-6.13	-1.73	181.85
155	155	9	1941	-6.15	-1.75	179.10

160	160	12	1938	-6.44	-1.86	178.35
165	165	14	1936	-6.33	-2.16	176.80
170	170	16	1934	-6.13	-1.89	171.80
175	175	19	1931	-6.12	-1.95	170.30
180	180	21	1929	-6.17	-1.90	191.90
185	185	23	1927	-6.10	-1.95	193.90
190	190	26	1924	-6.16	-2.08	205.20
195	195	28	1922	-6.05	-1.88	226.55
200	200	30	1920	-6.05	-1.39	222.60
205	205	33	1917	-6.34	-2.15	216.00
210	210	35	1915	-6.25	-2.29	222.75
215	215	37	1912	-6.17	-2.23	215.60
220	220	40	1910	-6.29	-1.85	222.00
225	225	42	1908	-6.01	-1.68	233.15
230	230	45	1905	-6.34	-2.44	249.05
235	235	47	1903	-6.38	-2.02	254.80
240	240	50	1900	-6.42	-2.59	246.75
245	245	52	1898	Sample lost		229.90
250	250	54	1895	-6.41	-2.30	231.25
255	255	57	1893	-6.47	-2.66	244.25
260	260	59	1890	-6.72	-3.13	243.70
265	265	62	1888	-6.44	-2.67	254.65
270	270	64	1885	-6.48	-2.71	254.25
275	275	67	1883	-6.49	-2.67	263.25
280	280	70	1880	-6.36	-2.57	265.60
285	285	72	1878	-6.44	-3.27	272.50
290	290	75	1875	-6.71	-3.37	275.85
295	295	77	1873	-6.51	-2.86	282.20
300	300	80	1870	-6.07	-1.91	287.00
305	305	82	1867	-6.52	-3.31	283.95
310	310	85	1865	-6.41	-3.50	277.95
315	315	87	1862	-6.41	-3.10	273.10
320	320	90	1860	-6.09	-2.63	281.95
325	325	93	1857	-6.42	-3.26	279.90
330	330	95	1854	-6.49	-3.02	279.20
335	335	98	1852	-6.47	-3.31	293.95
340	340	101	1849	-6.02	-2.71	300.20
345	345	103	1846	-5.99	-1.38	299.85
350	350	106	1844	-5.92	-3.03	303.70
355	355	109	1841	-6.42	-4.04	304.40
360	360	111	1838	-6.32	-4.21	305.15
365	365	114	1836	-6.07	-3.92	309.75
370	370	117	1833	-5.80	-2.58	309.00
375	375	119	1830	-5.88	-2.61	304.35

380	380	122	1827	-5.36	-2.16	306.20
385	385	125	1825	-5.30	-2.16	307.40
390	390	128	1822	-4.83	-0.70	302.45
395	395	130	1819	-5.37	-1.67	301.25
400	400	133	1816	-4.71	-0.51	297.10
405	405	136	1814	-5.17	-1.68	298.75
410	410	139	1811	-5.38	-2.98	307.45
415	415	142	1808	-5.51	-2.49	309.00
420	420	144	1805	-5.09	-1.82	309.25
425	425	147	1802	-5.11	-1.06	311.45
430	430	150	1800	-5.52	-3.50	315.25
435	435	153	1797	-6.12	-4.58	311.50
440	440	156	1794	-5.33	-2.58	314.75
445	445	159	1791	-5.09	-2.02	312.85
450	450	161	1788	-5.93	-5.26	310.45
455	455	164	1785	-5.43	-3.58	315.60
460	460	167	1782	-5.06	-2.31	316.30
465	465	170	1780	-5.35	-2.87	314.60
470	470	173	1777	-5.47	-3.15	314.40
475	475	176	1774	-5.89	-3.32	305.55
480	480	179	1771	-5.54	-3.56	294.10
485	485	182	1768	-5.06	-2.52	291.90
490	490	185	1765	-5.52	-2.76	292.70
495	495	188	1762	-5.49	-4.55	287.80
500	500	191	1759	-4.95	-1.81	280.60
505	505	194	1756	-5.53	-3.73	286.45
510	510	197	1753	-5.45	-3.36	284.10
515	515	200	1750	-4.94	-2.28	289.20
520	520	203	1747	-4.85	-2.85	289.45
525	525	206	1744	-4.61	-0.59	289.15
530	530	209	1741	-5.10	-1.42	286.55
535	535	212	1738	-5.48	-2.31	287.00
540	540	215	1735	-5.08	-2.02	289.00
545	545	218	1732	-5.03	-1.60	287.95
550	550	221	1729	-5.15	-1.73	292.65
555	555	224	1726	-5.59	-2.76	291.15
560	560	227	1722	-5.16	-1.94	292.75
565	565	230	1719	-5.25	-2.56	289.15
570	570	233	1716	-4.82	-1.77	294.10
575	575	236	1713	-5.10	-2.18	293.20
580	580	240	1710	-5.09	-1.30	289.90
585	585	243	1707	-5.00	-1.56	287.45
590	590	246	1704	-4.73	-1.30	277.75
595	595	249	1701	-5.33	-2.96	266.50

600	600	252	1697	-5.23	-2.67	260.65
605	605	255	1694	-5.38	-3.18	258.75
610	610	259	1691	-5.45	-1.84	253.90
615	615	262	1688	-4.92	-1.86	246.10
620	620	265	1685	-4.60	-1.39	223.90
625	625	268	1681	-4.74	-1.51	208.15
630	630	271	1678	-4.41	-0.84	214.55
635	635	275	1675	-4.53	-0.98	226.90
640	640	278	1672	-4.63	-0.96	233.90
645	645	281	1668	-4.82	-1.79	247.85
650	650	284	1665	-4.79	-1.16	262.85
655	655	288	1662	-4.87	-1.50	268.70
660	660	291	1658	-4.93	-1.52	272.45
665	665	294	1655	-4.95	-1.36	279.45
670	670	298	1652	-4.66	-0.94	276.20
675	675	301	1649	-5.01	-1.84	274.20
680	680	304	1645	-5.35	-2.18	277.05
685	685	308	1642	-4.77	-1.32	278.40
690	690	311	1639	-5.10	-1.76	278.60
695	695	314	1635	-4.69	-1.11	279.00
700	700	318	1632	-5.06	-1.87	282.55
705	705	321	1628	-5.19	-2.23	287.40
710	710	324	1625	-5.23	-2.28	289.20
715	715	328	1622	-5.18	-2.02	289.55
720	720	331	1618	-5.19	-2.01	292.10
725	725	335	1615	-4.73	-1.43	291.00
730	730	338	1611	-4.47	-0.48	288.15
735	735	341	1608	-4.47	-0.09	284.40
740	740	345	1604	-4.89	-2.08	297.35
745	745	348	1601	-4.64	-0.40	297.10
750	750	352	1598	-5.36	-2.45	295.60
755	755	355	1594	-5.23	-2.57	293.50
760	760	359	1591	-5.89	-2.74	289.95
765	765	362	1587	-5.63	-1.86	287.75
770	770	366	1584	-5.61	-2.91	285.00
775	775	369	1580	-5.60	-2.67	285.60
780	780	373	1576	-5.40	-2.43	289.70
785	785	376	1573	-5.23	-2.32	288.30
790	790	380	1569	-5.22	-1.90	287.85
795	795	384	1566	-5.21	-2.02	286.85
800	800	387	1562	-5.30	-1.61	293.20
805	805	391	1559	-5.20	-1.96	299.95
810	810	394	1555	-4.65	-1.00	300.60
815	815	398	1551	-5.35	-1.85	301.40

820	820	401	1548	-5.33	-2.18	295.45
825	825	405	1544	-5.36	-2.49	290.90
830	830	409	1541	-5.22	-1.79	286.85
835	835	412	1537	-4.91	-1.05	279.95
840	840	416	1533	-4.91	-1.37	275.95
845	845	420	1530	-5.00	-1.38	274.15
850	850	423	1526	-4.92	-1.61	279.65
855	855	427	1522	-5.55	-2.62	281.05
860	860	431	1519	-5.17	-1.29	282.40
865	865	434	1515	-5.19	-1.83	280.20
870	870	438	1511	-5.21	-1.83	278.75
875	875	442	1507	-5.26	-1.95	279.05
880	880	446	1504	-4.96	-0.43	279.20
885	885	449	1500	-5.40	-1.78	276.70
890	890	453	1496	-4.93	-1.28	276.40
895	895	457	1492	-5.02	-1.45	269.00
900	900	461	1489	-4.81	-0.74	263.25
905	905	464	1485	-4.63	-0.64	264.60
910	910	468	1481	-4.60	-0.38	269.15
915	915	472	1477	-4.58	-0.23	274.65
920	920	476	1473	-4.62	0.10	272.60
925	925	480	1470	-4.39	1.32	267.90
930	930	483	1466	-4.78	0.40	261.30
935	935	487	1462	-4.72	0.44	258.70
940	940	491	1458	-4.50	0.66	255.45
945	945	495	1454	-4.60	0.25	253.75
950	950	499	1450	-4.61	0.49	253.50
955	955	503	1446	-4.65	0.46	251.55
960	960	507	1443	-4.45	0.88	247.35
965	965	510	1439	-4.66	0.11	243.60
970	970	514	1435	-4.71	0.20	246.00
975	975	518	1431	-4.78	-0.03	247.90
980	980	522	1427	-4.82	0.01	249.10
985	985	526	1423	-4.56	0.57	220.45
990	990	530	1419	-4.59	0.62	211.65
995	995	534	1415	-4.33	0.74	261.00
1000	1000	538	1411	-4.55	1.02	260.15
1005	1005	542	1407	-4.44	0.83	259.15
1010	1010	546	1403	-4.56	0.67	262.00
1015	1015	550	1399	-4.48	0.80	260.50
1020	1020	554	1395	-4.52	0.46	254.95
1025	1025	558	1391	-4.63	0.44	258.80
1030	1030	562	1387	-4.57	0.19	257.45
1035	1035	566	1383	-5.02	-0.28	261.25

1040	1040	570	1379	-5.23	-1.25	264.40
1045	1045	574	1375	-5.33	-1.44	254.30
1050	1050	578	1371	-5.52	-2.17	236.85
1055	1055	582	1367	-5.59	-1.98	201.10
1060	1060	586	1363	-5.98	-3.10	157.80
1065	1065	591	1359	-6.43	-2.53	121.20
1070	1070	595	1354	-6.92	-2.00	113.05
1075	1075	599	1350	-6.83	-1.36	110.70
1080	1080	603	1346	-6.89	-1.61	102.40
1085	1085	607	1342	-6.90	-1.43	90.75
1090	1090	611	1338	-6.93	-1.50	80.05
1095	1095	615	1334	-6.88	-1.37	70.60
1100	1100	619	1330	-6.96	-1.44	62.60
1105	1105	624	1325	-7.02	-1.70	58.20
1110	1110	628	1321	-6.86	-1.13	57.25
1115	1115	632	1317	-7.00	-1.35	56.00
1120	1120	636	1313	-6.93	-1.43	54.65
1125	1125	640	1309	-6.99	-1.53	53.70
1130	1130	645	1304	-7.04	-2.17	52.30
1135	1135	649	1300	-6.96	-1.84	51.05
1140	1140	653	1296	-6.97	-1.59	51.20
1145	1145	657	1292	-6.99	-1.66	51.50
1150	1150	662	1287	-7.04	-1.44	52.10
1155	1155	666	1283	-6.94	-1.42	55.85
1160	1160	670	1279	-6.90	-1.39	60.65
1165	1165	675	1274	-6.91	-1.67	70.15
1170	1170	679	1270	-7.43	-1.94	77.50
1175	1175	683	1266	-7.32	-1.92	83.25
1180	1180	688	1261	-7.41	-1.99	85.70
1185	1185	692	1257	-7.34	-1.75	84.50
1190	1190	696	1253	-7.46	-1.91	89.45
1195	1195	701	1248	-7.21	-1.64	92.70
1200	1200	705	1244	-7.40	-1.90	97.30
1205	1205	709	1240	-7.41	-1.81	107.70
1210	1210	714	1235	-7.30	-1.26	100.95
1215	1215	718	1231	-7.41	-2.15	72.85
1220	1220	723	1226	-7.27	-1.83	53.95
1225	1225	727	1222	-7.46	-2.14	59.80
1230	1230	731	1218	Sample lost		65.60
1235	1235	736	1213	-7.21	-1.75	66.60
1240	1240	740	1209	-6.88	-1.19	67.80
1245	1245	745	1204	-6.97	-1.20	65.30
1250	1250	749	1200	-6.91	-1.13	64.60
1255	1255	754	1195	-6.88	-1.01	59.40

1260	1260	758	1191	-6.94	-0.55	51.80
1265	1265	763	1186	-6.93	-0.96	39.75
1270	1270	767	1182	-7.02	-1.35	35.55
1275	1275	772	1177	-6.93	-1.21	33.90
1280	1280	776	1173	-7.01	-1.13	33.10
1285	1285	781	1168	-7.15	-1.51	30.30
1290	1290	785	1164	-7.11	-1.42	24.30
1295	1295	790	1159	-7.06	-1.74	23.00
1300	1300	794	1154	-6.84	-0.48	23.05
1305	1305	799	1150	-7.15	-1.53	22.95
1310	1310	804	1145	-7.11	-1.53	23.30
1315	1315	808	1141	-7.22	-1.65	23.15
1320	1320	813	1136	-7.18	-1.77	22.90
1325	1325	817	1131	-7.09	-1.82	22.90
1330	1330	822	1127	-7.07	-1.06	22.95
1335	1335	827	1122	-7.04	-0.83	22.90

APPENDIX B

TABLE OF DATA FOR DRIVE 2

Total Depth (mm)	Core Depth (mm)	Age (years BP)	Cal Year	Corr. $\delta^{18}\text{O}$	Corr. $\delta^{13}\text{C}$	Magnetic Susceptibility ($\text{k} \times 10^{-5}$ SI)
865	5	434	1515	-5.12	1.06	25.20
870	10	438	1511	-4.80	1.61	26.35
875	15	442	1507	-4.85	0.25	26.00
880	20	446	1504	-5.15	0.73	26.35
885	25	449	1500	-5.34	-0.10	26.50
890	30	453	1496	-5.11	-0.02	26.15
895	35	457	1492	-5.25	-0.21	25.00
900	40	461	1489	-4.81	0.61	26.05
905	45	464	1485	-4.56	-0.21	26.75
910	50	468	1481	-4.58	0.80	26.70
915	55	472	1477	-4.54	0.55	27.10
920	60	476	1473	-4.53	0.38	27.45
925	65	480	1470	-4.47	0.81	27.35
930	70	483	1466	-4.50	1.00	27.60
935	75	487	1462	-4.55	0.95	27.70
940	80	491	1458	-4.62	0.78	28.55
945	85	495	1454	-4.55	0.90	28.15
950	90	499	1450	-4.55	0.95	28.40
955	95	503	1446	-4.53	1.00	28.75
960	100	507	1443	-4.48	0.94	28.10
965	105	510	1439	-4.46	1.39	27.50
970	110	514	1435	-4.48	0.65	27.35
975	115	518	1431	-4.53	1.26	26.70
980	120	522	1427	-4.32	1.68	27.25
985	125	526	1423	-4.22	1.77	28.30
990	130	530	1419	-4.05	2.10	28.20
995	135	534	1415	-4.00	2.12	28.40
1000	140	538	1411	-4.22	1.73	29.10
1005	145	542	1407	-4.42	1.33	28.75
1010	150	546	1403	-4.49	0.34	28.60
1015	155	550	1399	-4.24	2.19	28.90

1020	160	554	1395	-4.47	1.23	28.80
1025	165	558	1391	-4.84	-0.45	28.40
1030	170	562	1387	-4.90	-0.45	25.60
1035	175	566	1383	-5.07	-0.89	23.05
1040	180	570	1379	-5.76	-1.83	22.45
1045	185	574	1375	-6.50	-1.32	21.40
1050	190	578	1371	-6.88	-1.02	19.80
1055	195	582	1367	-7.14	-1.39	20.15
1060	200	586	1363	-6.97	-1.46	21.35
1065	205	591	1359	-6.89	-0.81	21.50
1070	210	595	1354	-7.19	-1.13	21.20
1075	215	599	1350	-7.02	-1.23	22.50
1080	220	603	1346	-7.00	-0.61	19.65
1085	225	607	1342	-7.14	-0.89	17.35
1090	230	611	1338	-7.02	-1.16	14.45
1095	235	615	1334	-7.44	-1.67	10.05
1100	240	619	1330	-7.40	-1.05	6.50
1105	245	624	1325	-7.27	-0.85	6.85
1110	250	628	1321	-7.20	-1.40	9.20
1115	255	632	1317	-7.26	-0.83	10.30
1120	260	636	1313	-7.18	-1.11	11.40
1125	265	640	1309	-7.20	-1.20	12.75
1130	270	645	1304	-7.27	-0.99	13.45
1135	275	649	1300	-7.31	-0.60	13.55
1140	280	653	1296	-7.28	-0.80	13.60
1145	285	657	1292	-7.12	-0.88	15.95
1150	290	662	1287	-7.28	-0.83	16.50
1155	295	666	1283	-7.12	-1.06	16.40
1160	300	670	1279	-7.10	-1.13	15.60
1165	305	675	1274	-7.26	-1.30	15.80
1170	310	679	1270	-7.27	-0.73	16.35
1175	315	683	1266	-7.02	-1.03	15.45
1180	320	688	1261	-7.02	-0.95	12.90
1185	325	692	1257	-7.10	-0.97	12.05
1190	330	696	1253	-7.21	-0.71	12.90
1195	335	701	1248	-7.26	-1.32	12.00
1200	340	705	1244	-7.12	-0.91	10.50
1205	345	709	1240	-7.20	-1.31	9.00
1210	350	714	1235	-7.05	-0.88	8.15
1215	355	718	1231	-6.90	-0.73	7.70
1220	360	723	1226	-6.87	-0.66	7.55
1225	365	727	1222	-6.59	-0.14	6.80
1230	370	731	1218	-6.88	-0.60	6.20
1235	375	736	1213	-6.67	-0.26	5.70

1240	380	740	1209	-6.41	0.09	5.35
1245	385	745	1204	-6.19	0.51	5.20
1250	390	749	1200	-6.03	0.87	5.20
1255	395	754	1195	-6.20	0.39	5.15
1260	400	758	1191	-6.25	0.38	5.35
1265	405	763	1186	-6.22	0.23	5.40
1270	410	767	1182	-6.30	0.39	5.30
1275	415	772	1177	-6.45	0.19	5.20
1280	420	776	1173	-6.35	0.21	4.95
1285	425	781	1168	-6.39	0.16	4.35
1290	430	785	1164	-6.42	0.35	5.50
1295	435	790	1159	-6.24	0.43	13.95
1300	440	794	1154	-6.18	0.36	16.00
1305	445	799	1150	-6.21	0.46	15.45
1310	450	804	1145	-6.38	0.25	17.65
1315	455	808	1141	-6.31	0.35	20.90
1320	460	813	1136	-6.17	0.66	21.75
1325	465	817	1131	-6.47	0.48	22.10
1330	470	822	1127	-6.27	0.71	23.05
1335	475	827	1122	-6.23	0.80	23.40
1340	480	831	1117	-6.41	0.55	22.55
1345	485	836	1113	-6.46	0.41	22.55
1350	490	841	1108	-6.31	0.65	22.05
1355	495	845	1103	-6.54	0.30	21.85
1360	500	850	1099	-6.45	0.46	22.25
1365	505	855	1094	-6.52	0.33	22.00
1370	510	859	1089	-6.46	0.25	22.15
1375	515	864	1085	-6.72	0.15	22.15
1380	520	869	1080	-6.61	-0.03	20.85
1385	525	874	1075	-6.63	0.01	17.95
1390	530	878	1070	-6.60	-0.04	14.85
1395	535	883	1066	-6.71	0.06	14.15
1400	540	888	1061	-6.71	-0.03	15.40
1405	545	893	1056	-6.70	-0.08	14.70
1410	550	897	1051	-6.59	0.07	14.80
1415	555	902	1046	-6.74	-0.04	15.85
1420	560	907	1042	-6.63	-0.01	16.40
1425	565	912	1037	-6.66	0.00	15.95
1430	570	917	1032	-6.67	0.00	15.70
1435	575	922	1027	-6.72	-0.29	15.10
1440	580	926	1022	-6.93	-0.59	14.35
1445	585	931	1017	-6.87	-0.62	13.70
1450	590	936	1013	-6.83	-0.55	13.80
1455	595	941	1008	-6.89	-0.56	14.20

1460	600	946	1003	-6.99	-0.53	14.55
1465	605	951	998	-6.99	-0.72	13.75
1470	610	956	993	-6.98	-0.59	11.95
1475	615	961	988	-7.03	-0.61	11.15
1480	620	966	983	-7.03	-0.79	11.10
1485	625	970	978	-7.08	-0.76	10.85
1490	630	975	973	-7.03	-0.69	10.55
1495	635	980	968	-7.10	-0.77	10.60
1500	640	985	963	-7.13	-0.66	10.30
1505	645	990	958	-6.94	-0.73	9.70
1510	650	995	953	-7.09	-0.84	9.50
1515	655	1000	948	-7.09	-0.75	8.40
1520	660	1005	943	-7.05	-0.80	7.75
1525	665	1010	938	-7.09	-0.82	7.65
1530	670	1015	933	-7.02	-0.72	7.95
1535	675	1020	928	-7.15	-0.83	7.65
1540	680	1025	923	-7.13	-0.88	7.60
1545	685	1031	918	-7.14	-0.79	8.15
1550	690	1036	913	-7.05	-0.77	7.55
1555	695	1041	908	-7.17	-0.82	6.95
1560	700	1046	903	-7.15	-0.68	7.00
1565	705	1051	898	-7.13	-0.71	7.25
1570	710	1056	893	-7.14	-0.84	7.30
1575	715	1061	888	-7.16	-0.77	6.90
1580	720	1066	882	-7.17	-0.76	6.55
1585	725	1071	877	-7.16	-0.84	6.55
1590	730	1077	872	-7.09	-0.77	7.10
1595	735	1082	867	-7.13	-0.87	7.50
1600	740	1087	862	-7.01	-0.75	7.15
1605	745	1092	857	-7.10	-0.79	6.70
1610	750	1097	851	-7.09	-0.68	6.75
1615	755	1102	846	-7.15	-0.67	6.80
1620	760	1108	841	-7.35	-0.75	6.20
1625	765	1113	836	-7.14	-0.73	5.95
1630	770	1118	830	-7.29	-0.92	6.80
1635	775	1123	825	-7.17	-0.68	6.05
1640	780	1129	820	-7.03	-0.81	5.50
1645	785	1134	815	-7.05	-0.76	5.10
1650	790	1139	809	-7.02	-0.64	4.85
1655	795	1144	804	-7.17	-0.91	4.40
1660	800	1150	799	-6.98	-0.84	3.60
1665	805	1155	794	-6.99	-0.91	3.30
1670	810	1160	788	-7.02	-0.84	3.00
1675	815	1166	783	-6.96	-0.86	3.25

1680	820	1171	778	-6.92	-0.83	2.80
1685	825	1176	772	-7.13	-0.89	2.50
1690	830	1182	767	-7.09	-0.89	2.30
1695	835	1187	762	-7.00	-0.90	2.35
1700	840	1192	756	-6.97	-0.83	2.10
1705	845	1198	751	-7.01	-0.76	2.05
1710	850	1203	745	-7.11	-0.80	3.05
1715	855	1208	740	-7.18	-0.85	2.75
1720	860	1214	735	-7.02	-0.72	2.40
1725	865	1219	729	-7.17	-0.88	2.00
1730	870	1225	724	-7.11	-0.92	1.85
1735	875	1230	718	-7.12	-0.85	1.95
1740	880	1236	713	-7.06	-0.89	1.90
1745	885	1241	707	-6.98	-0.77	1.30
1750	890	1247	702	-7.35	-1.05	0.60
1755	895	1252	696	-7.04	-0.73	0.10
1760	900	1258	691	-7.02	-0.78	0.10
1765	905	1263	685	-6.96	-0.77	0.15
1770	910	1269	680	-7.23	-0.90	-0.05
1775	915	1274	674	-7.36	-1.09	0.00
1780	920	1280	669	-7.32	-0.86	-0.10

APPENDIX C

TABLE OF DATA FOR DRIVE 3

Total Depth (mm)	Core Depth (mm)	Age (years BP)	Cal Year	Corr. $\delta^{18}\text{O}$	Corr. $\delta^{13}\text{C}$	Magnetic Susceptibility ($\text{k} \times 10^{-5}$ SI)
1685	5	1176	772	-7.11	-0.95	6.70
1690	10	1182	767	-7.21	-0.87	7.45
1695	15	1187	762	-7.05	-0.67	7.55
1700	20	1192	756	-7.07	-0.83	6.25
1705	25	1198	751	-7.21	-0.92	6.30
1710	30	1203	745	-7.03	-0.73	8.95
1715	35	1208	740	-7.07	-0.88	12.30
1720	40	1214	735	-7.06	-0.80	14.50
1725	45	1219	729	-7.05	-0.83	15.00
1730	50	1225	724	-7.00	-0.68	15.25
1735	55	1230	718	-7.14	-0.76	16.10
1740	60	1236	713	-7.20	-1.01	15.55
1745	65	1241	707	-7.39	-0.94	16.50
1750	70	1247	702	-7.14	-0.89	15.90
1755	75	1252	696	-7.27	-0.87	15.65
1760	80	1258	691	-7.18	-0.90	14.70
1765	85	1263	685	-7.14	-0.99	14.35
1770	90	1269	680	-7.23	-0.81	14.30
1775	95	1274	674	-7.38	-1.08	14.80
1780	100	1280	669	-7.54	-1.11	12.75
1785	105	1285	663	-7.43	-1.11	10.20
1790	110	1291	658	-7.34	-1.19	9.15
1795	115	1296	652	-7.37	-1.30	10.90
1800	120	1302	647	-7.20	-0.76	9.85
1805	125	1307	641	-7.25	-0.83	10.70
1810	130	1313	635	-7.35	-1.13	12.25
1815	135	1319	630	-7.58	-1.52	12.35
1820	140	1324	624	-7.27	-1.29	11.90
1825	145	1330	619	-7.53	-1.49	11.25
1830	150	1335	613	-7.63	-1.62	10.70
1835	155	1341	607	-7.38	-1.45	10.65
1840	160	1347	602	-7.74	-1.54	10.75
1845	165	1352	596	-7.72	-1.58	10.90
1850	170	1358	590	-7.54	-1.48	10.60
1855	175	1364	585	-7.54	-1.44	10.40
1860	180	1369	579	-7.69	-1.54	9.85

1865	185	1375	573	-7.41	-0.99	8.95
1870	190	1381	568	-7.53	-1.42	8.80
1875	195	1387	562	-7.71	-1.70	8.90
1880	200	1392	556	-7.57	-1.59	8.00
1885	205	1398	550	-7.56	-1.61	7.45
1890	210	1404	545	-7.66	-1.65	7.90
1895	215	1409	539	-7.63	-1.71	8.15
1900	220	1415	533	-7.65	-1.62	9.25
1905	225	1421	527	-7.66	-1.62	9.15
1910	230	1427	521	-7.70	-1.60	8.80
1915	235	1433	516	-7.90	-1.75	8.65
1920	240	1438	510	-7.60	-1.67	8.65
1925	245	1444	504	-7.74	-1.75	8.20
1930	250	1450	498	-7.66	-1.70	8.35
1935	255	1456	492	-7.52	-1.57	8.45
1940	260	1462	487	-7.75	-1.59	8.50
1945	265	1468	481	-7.80	-1.62	8.20
1950	270	1473	475	-7.81	-1.62	8.15
1955	275	1479	469	-7.86	-1.83	7.65
1960	280	1485	463	-7.69	-1.63	7.70
1965	285	1491	457	-7.63	-1.59	8.50
1970	290	1497	451	-7.82	-1.73	8.05
1975	295	1503	445	-7.89	-1.72	8.25
1980	300	1509	439	-7.87	-1.76	8.05
1985	305	1515	433	-7.75	-1.62	8.25
1990	310	1521	427	-7.96	-1.77	8.30
1995	315	1527	421	-7.89	-1.74	8.15
2000	320	1533	416	-7.97	-1.73	7.80
2005	325	1539	410	-8.19	-1.84	5.60
2010	330	1545	404	-7.96	-1.80	4.45
2015	335	1551	398	-8.09	-1.75	1.55
2020	340	1557	392	-8.18	-1.94	0.65
2025	345	1563	385	-8.05	-1.70	0.60
2030	350	1569	379	-8.17	-1.83	1.90
2035	355	1575	373	-8.01	-1.74	2.25
2040	360	1581	367	-8.17	-1.84	3.35
2045	365	1587	361	-8.09	-1.66	4.35
2050	370	1593	355	-7.96	-1.83	7.70
2055	375	1599	349	-8.31	-1.92	7.75
2060	380	1605	343	-8.07	-1.89	7.35
2065	385	1611	337	-8.14	-1.87	7.45
2070	390	1617	331	-8.12	-1.78	7.80
2075	395	1623	325	-8.03	-1.96	7.45
2080	400	1630	319	-8.07	-1.74	7.90
2085	405	1636	312	-8.17	-1.93	7.40
2090	410	1642	306	-7.98	-1.75	7.55
2095	415	1648	300	-8.05	-1.79	7.60
2100	420	1654	294	-8.01	-1.80	7.75
2105	425	1660	288	-8.26	-1.79	7.90
2110	430	1667	282	-8.37	-2.13	7.50
2115	435	1673	275	-8.21	-1.84	7.40
2120	440	1679	269	-8.22	-1.86	8.25

2125	445	1685	263	-8.07	-1.82	8.00
2130	450	1691	257	-8.19	-1.75	8.05
2135	455	1698	250	-8.27	-1.89	7.80
2140	460	1704	244	-8.17	-1.77	7.35
2145	465	1710	238	-8.10	-1.72	6.95
2150	470	1716	232	-8.13	-1.69	6.95
2155	475	1723	225	-8.15	-1.76	6.60
2160	480	1729	219	-8.33	-1.93	4.45
2165	485	1735	213	-8.17	-1.83	5.85
2170	490	1742	206	-8.22	-1.78	7.25
2175	495	1748	200	-8.27	-1.83	7.25
2180	500	1754	194	-8.28	-1.67	7.50
2185	505	1761	187	-8.04	-1.67	7.75
2190	510	1767	181	-8.16	-1.69	6.95
2195	515	1773	175	-8.22	-1.74	6.85
2200	520	1780	168	-8.26	-1.77	6.55
2205	525	1786	162	-8.15	-1.81	6.15
2210	530	1792	156	-8.10	-1.74	6.75
2215	535	1799	149	-8.24	-1.75	6.95
2220	540	1805	143	-8.30	-1.69	6.85
2225	545	1812	136	-8.15	-1.71	7.20
2230	550	1818	130	-8.03	-1.69	6.85
2235	555	1825	123	-8.16	-1.68	6.60
2240	560	1831	117	-8.18	-1.70	6.20
2245	565	1837	111	-8.17	-1.65	7.00
2250	570	1844	104	-8.05	-1.65	8.15
2255	575	1850	98	-8.04	-1.65	7.80
2260	580	1857	91	-8.07	-1.69	7.25
2265	585	1863	85	-8.06	-1.61	6.95
2270	590	1870	78	-8.24	-1.83	7.30
2275	595	1876	72	-8.07	-1.71	7.95
2280	600	1883	65	-8.25	-1.81	7.50
2285	605	1889	59	-8.14	-1.68	6.45
2290	610	1896	52	-8.08	-1.69	4.95
2295	615	1903	45	-7.95	-1.68	5.05
2300	620	1909	39	-8.07	-1.74	5.50
2305	625	1916	32	-8.13	-1.77	5.35
2310	630	1922	26	-8.08	-1.65	5.55
2315	635	1929	19	-8.00	-1.64	6.10
2320	640	1936	12	-8.27	-1.76	6.40
2325	645	1942	6	-8.21	-1.79	5.65
2330	650	1949	-1	-8.24	-1.81	3.65
2335	655	1955	-7	-8.14	-1.67	2.55
2340	660	1962	-14	-7.84	-1.62	2.20
2345	665	1969	-21	-8.11	-1.77	1.65
2350	670	1975	-27	-8.13	-1.75	1.50
2355	675	1982	-34	-8.37	-1.92	1.30
2360	680	1989	-41	-8.10	-1.81	1.50
2365	685	1995	-48	-8.18	-1.74	1.80
2370	690	2002	-54	-8.02	-1.69	1.50
2375	695	2009	-61	-8.20	-1.84	1.35
2380	700	2016	-68	-8.27	-1.84	1.30

2385	705	2022	-74	-8.42	-1.98	1.25
2390	710	2029	-81	-8.22	-1.82	1.30
2395	715	2036	-88	-8.28	-1.74	0.95
2400	720	2043	-95	-8.30	-1.90	1.05
2405	725	2049	-102	-8.15	-1.74	0.75
2410	730	2056	-108	-8.38	-1.90	0.95
2415	735	2063	-115	-8.34	-1.94	1.00
2420	740	2070	-122	-8.39	-1.87	0.80
2425	745	2077	-129	-8.25	-1.74	0.65
2430	750	2083	-136	-8.26	-1.82	0.95
2435	755	2090	-142	-8.43	-1.79	0.95
2440	760	2097	-149	-8.33	-1.75	0.75
2445	765	2104	-156	-8.23	-1.81	0.75
2450	770	2111	-163	-8.43	-1.78	1.15
2455	775	2118	-170	-8.35	-1.81	1.40
2460	780	2125	-177	-8.32	-1.76	1.15
2465	785	2132	-184	-8.39	-1.98	0.85
2470	790	2138	-191	-8.39	-1.84	0.50
2475	795	2145	-198	-8.42	-1.83	0.55
2480	800	2152	-204	-8.33	-1.72	0.40
2485	805	2159	-211	-8.35	-1.74	0.20
2490	810	2166	-218	-8.43	-1.96	0.25
2495	815	2173	-225	-8.50	-1.78	0.50
2500	820	2180	-232	-8.41	-1.75	0.65
2505	825	2187	-239	-8.47	-1.81	0.65
2510	830	2194	-246	-8.31	-1.66	0.70
2515	835	2201	-253	-8.34	-1.80	0.95
2520	840	2208	-260	-8.37	-1.70	0.95
2525	845	2215	-267	-8.50	-1.78	0.70
2530	850	2222	-274	-8.32	-1.63	0.75
2535	855	2229	-281	-8.37	-1.63	0.85
2540	860	2236	-288	-8.24	-1.60	0.80
2545	865	2243	-296	-8.32	-1.74	0.95
2550	870	2250	-303	-8.33	-1.68	0.90
2555	875	2257	-310	-8.44	-1.85	0.95
2560	880	2264	-317	-8.24	-1.59	1.20
2565	885	2272	-324	-8.24	-1.61	1.30
2570	890	2279	-331	-8.29	-1.61	1.20
2575	895	2286	-338	-8.18	-1.57	1.25
2580	900	2293	-345	-8.27	-1.59	1.05
2585	905	2300	-352	-8.33	-1.65	0.80
2590	910	2307	-360	-8.45	-2.00	1.00
2595	915	2314	-367	-8.21	-1.55	0.95
2600	920	2322	-374	-8.26	-1.52	0.95
2605	925	2329	-381	-8.19	-1.54	1.00
2610	930	2336	-388	-8.13	-1.46	1.05
2615	935	2343	-395	-8.29	-1.75	0.90
2620	940	2350	-403	-8.20	-1.44	0.50
2625	945	2358	-410	-8.13	-1.44	0.05
2630	950	2365	-417	-8.16	-1.54	0.00
2635	955	2372	-424	-8.17	-1.56	0.10
2640	960	2379	-432	-8.17	-1.47	0.10

APPENDIX D

TABLE OF TRACE METAL DATA

Drive	Total Core Depth (cm)	Cal Year	Na (ppm)	Mg (ppm)	Al (ppm)	P (ppm)	K (ppm)	Ca (ppm)	Sc (ppm)
D1	1.0	2003	223.71	5259	1911	1961	513	90220	1.29
D1	2.0	1999	193.35	5008	1718	2125	499	84875	1.25
D1	3.0	1995	163.53	4908	1855	2171	477	75598	1.30
D1	5.0	1986	146.78	4981	2069	2000	462	71584	1.36
D1	6.0	1982	144.63	4805	1791	2033	439	71366	1.24
D1	9.0	1969	122.73	4198	1794	1460	416	50071	1.49
D1	12.0	1956	97.66	3664	1618	989	404	37604	1.54
D1	15.0	1943	88.54	3121	1824	875	397	21945	1.70
D1	18.0	1929	79.67	3094	1745	798	371	20543	1.75
D1	21.0	1915	81.45	3209	1957	935	358	20159	2.09
D1	24.0	1900	84.06	3143	2137	813	346	17301	2.16
D1	27.0	1885	70.23	2924	2073	774	324	13802	2.19
D1	27.0	1885	67.28	2900	1966	773	323	13841	2.13
D1	30.0	1870	77.08	3234	2389	892	355	14862	2.49
D1	33.0	1854	66.01	3150	2182	897	336	13713	2.40
D1	36.0	1838	56.98	2950	2383	840	334	10576	2.37
D1	39.0	1822	57.12	2865	2313	858	317	9147	2.37
D1	42.0	1805	55.43	2691	2247	841	311	8139	2.24
D1	45.0	1788	56.64	2817	2484	884	308	7933	2.47
D1	48.0	1771	55.97	2647	2631	869	304	6864	2.49
D1	51.0	1753	55.17	2546	2503	1266	318	6676	2.37
D1	53.0	1741	53.07	2684	2589	948	302	6503	5.05
D1	65.0	1665	43.33	2297	2480	883	279	6522	4.99
D2	75.5	1594	32.15	2384	2388	861	251	7143	5.09
D1	77.0	1584	39.06	2100	2304	812	262	6374	4.61
D2	81.5	1551	35.68	2539	2671	914	244	7932	5.56
D2	87.5	1507	43.52	2189	2705	774	264	10386	5.50
D1	89.0	1496	49.02	2463	2491	864	241	6849	5.07
D2	93.5	1462	34.82	2796	2840	647	264	25845	5.37
D2	93.5	1462	33.79	2660	2405	620	257	25852	4.84
D2	99.5	1415	39.42	3059	2700	693	268	28079	5.19
D1	101.0	1403	42.94	2312	2471	817	235	6981	5.28
D2	105.5	1367	34.45	3008	2845	1006	239	18549	6.06
D2	111.5	1317	34.28	2982	2347	917	231	20261	5.65

D1	113.0	1304	39.64	2754	2446	1111	276	25527	4.95
D2	117.5	1266	31.88	3176	2548	913	230	22555	5.83
D2	123.5	1213	33.33	3061	2501	815	242	25322	5.81
D1	125.0	1200	41.80	3081	2520	1119	269	20164	6.08
D2	129.5	1159	35.60	3084	2372	1061	246	28355	5.65
D2	135.5	1103	39.00	3488	2154	982	243	44850	4.63
D2	141.5	1046	44.41	3715	1947	781	247	58071	3.98
D2	147.5	988	47.13	4007	1732	670	244	70522	3.38
D2	153.5	928	56.21	5027	1221	525	195	118251	2.04
D3	157.0	893	64.46	5442	1059	521	193	146317	1.69
D2	159.5	867	62.79	5491	987	481	181	144507	1.51
D2	159.5	867	63.79	5495	964	494	185	149269	1.53
D3	163.0	830	66.13	5913	713	469	175	172717	1.09
D3	169.5	762	69.94	5937	682	534	182	183080	1.15
D3	175.5	696	72.47	6154	828	579	205	191240	1.41
D3	181.5	630	68.54	6051	639	575	202	192239	1.11
D3	187.5	562	65.33	5922	719	567	203	188555	1.20
D3	193.5	492	67.68	5979	701	581	185	186788	1.15
D3	199.5	421	73.10	6031	1055	571	280	184558	1.99
D3	205.5	349	70.14	6091	664	578	196	187001	1.07
D3	211.5	275	72.05	6110	696	566	185	181593	1.11
D3	211.5	275	72.08	6036	694	558	182	177489	1.07

Drive	Total Core Depth (cm)	Cal Year	Ti (ppm)	V (ppm)	Cr (ppm)	Mn (ppm)	Fe (ppm)	Co (ppm)	Ni (ppm)
D1	1.0	2003	54.81	45.60	11.17	649.27	13619.47	5.72	15.06
D1	2.0	1999	54.23	43.06	9.70	695.56	13075.88	5.08	13.07
D1	3.0	1995	54.34	43.05	10.22	695.36	13572.89	5.45	12.15
D1	5.0	1986	51.74	44.47	10.91	657.44	14142.10	5.74	11.58
D1	6.0	1982	50.41	42.63	9.61	689.46	13681.89	5.22	11.23
D1	9.0	1969	42.65	43.26	8.22	600.19	12367.41	5.72	8.70
D1	12.0	1956	34.24	38.94	6.82	560.32	10910.26	5.59	6.91
D1	15.0	1943	28.34	39.77	6.94	527.83	9923.67	6.26	5.99
D1	18.0	1929	25.96	37.89	6.34	506.42	9297.89	6.80	5.69
D1	21.0	1915	30.21	41.56	7.09	572.74	11480.06	7.14	5.94
D1	24.0	1900	26.51	39.97	7.41	558.73	11921.07	7.52	5.96
D1	27.0	1885	26.44	38.62	7.44	466.00	11779.76	7.06	5.53
D1	27.0	1885	26.35	38.06	7.04	466.61	11287.88	6.90	5.35
D1	30.0	1870	27.70	42.49	8.54	522.95	13373.45	7.69	6.11
D1	33.0	1854	30.58	41.10	7.88	475.11	12606.45	7.11	5.69
D1	36.0	1838	27.18	40.24	8.33	419.29	12595.84	7.24	5.77
D1	39.0	1822	27.83	40.37	8.29	401.30	12462.89	7.34	5.68
D1	42.0	1805	23.63	37.02	7.81	366.57	10836.63	7.07	5.26
D1	45.0	1788	25.02	39.52	8.87	447.27	12108.56	7.65	5.73
D1	48.0	1771	22.85	39.74	9.41	438.91	12531.33	7.72	5.71
D1	51.0	1753	23.99	38.47	9.06	590.17	12982.80	7.77	5.47
D1	53.0	1741	23.75	38.54	9.53	573.36	12610.59	7.80	4.56
D1	65.0	1665	25.89	40.04	10.07	408.54	12386.79	7.29	4.39
D2	75.5	1594	28.94	42.44	9.92	408.01	13653.70	6.41	4.33
D1	77.0	1584	25.12	37.53	9.19	328.63	11552.99	6.31	4.03
D2	81.5	1551	33.00	47.26	10.97	633.28	17544.12	6.89	5.43
D2	87.5	1507	39.27	48.61	10.57	497.36	16853.50	6.93	5.19
D1	89.0	1496	26.77	42.93	10.28	401.79	13073.97	7.04	4.42
D2	93.5	1462	53.51	47.84	10.64	336.75	17791.37	7.38	5.78
D2	93.5	1462	52.57	43.51	8.48	308.68	15031.28	6.30	5.09
D2	99.5	1415	60.55	48.07	9.61	325.14	16386.78	6.54	5.17
D1	101.0	1403	30.63	43.10	9.67	669.57	16936.50	6.44	4.31
D2	105.5	1367	49.64	53.55	12.09	320.76	15921.19	8.07	6.14
D2	111.5	1317	48.60	49.62	10.23	589.47	16946.22	6.86	5.25
D1	113.0	1304	58.43	45.27	9.03	371.52	16011.72	6.33	4.94
D2	117.5	1266	55.45	51.31	10.74	842.14	20548.94	7.56	5.80
D2	123.5	1213	55.50	51.69	10.18	809.92	19684.90	7.37	6.02
D1	125.0	1200	50.92	53.25	11.21	591.00	17436.32	8.26	5.97
D2	129.5	1159	60.66	49.95	9.56	670.77	17835.65	6.62	5.44
D2	135.5	1103	57.54	42.12	8.09	322.29	12359.96	5.42	5.17
D2	141.5	1046	55.67	35.29	6.68	265.62	10355.70	4.29	4.81
D2	147.5	988	52.08	29.98	5.39	256.91	8529.16	3.43	4.57
D2	153.5	928	31.25	16.60	3.03	299.35	5049.20	1.99	4.84
D3	157.0	893	23.35	11.23	2.64	380.56	4196.83	1.71	5.37
D2	159.5	867	20.69	10.53	2.55	350.49	3882.64	1.58	5.17

D2	159.5	867	21.24	10.67	2.45	354.72	3824.85	1.53	5.39
D3	163.0	830	14.40	6.26	1.84	412.66	2835.58	1.18	5.92
D3	169.5	762	14.26	5.12	1.97	432.94	2696.08	1.28	6.46
D3	175.5	696	13.24	4.49	2.37	467.56	2861.42	1.53	7.30
D3	181.5	630	12.94	4.82	1.73	447.25	2194.49	1.19	7.57
D3	187.5	562	11.76	3.97	1.82	422.26	2081.93	1.31	8.13
D3	193.5	492	12.22	4.59	1.64	418.00	1947.83	1.27	8.41
D3	199.5	421	27.88	5.02	2.34	412.51	2314.65	1.41	9.04
D3	205.5	349	12.16	4.31	1.54	422.94	1837.33	1.31	9.37
D3	211.5	275	11.77	3.92	1.66	416.88	1742.79	1.27	9.65
D3	211.5	275	11.33	3.81	1.61	407.35	1708.11	1.26	9.82

Drive	Total Core Depth (cm)	Cal Year	Cu (ppm)	Zn (ppm)	As (ppm)	Se (ppm)	Sr (ppm)	Y (ppm)	Zr (ppm)
D1	1.0	2003	30.25	57.92	8.60	5.63	74.64	15.48	1.49
D1	2.0	1999	28.45	52.20	8.57	4.65	70.94	15.02	1.49
D1	3.0	1995	29.36	49.84	7.93	3.84	64.05	15.30	1.60
D1	5.0	1986	29.82	49.04	7.52	3.73	61.77	15.50	1.61
D1	6.0	1982	28.75	46.22	7.61	3.55	61.53	15.25	1.63
D1	9.0	1969	29.67	30.66	4.97	2.70	41.14	15.70	1.49
D1	12.0	1956	30.63	19.44	3.86	2.13	27.97	16.47	1.36
D1	15.0	1943	31.56	18.60	2.82	1.46	17.17	17.69	1.17
D1	18.0	1929	37.27	17.07	2.50	1.48	15.45	17.86	1.13
D1	21.0	1915	35.48	17.13	2.75	1.44	15.12	19.68	1.28
D1	24.0	1900	35.40	16.64	2.11	1.32	12.98	19.53	1.09
D1	27.0	1885	35.05	16.15	2.00	1.15	10.60	19.40	1.08
D1	27.0	1885	34.65	15.67	2.00	1.11	10.51	19.24	1.06
D1	30.0	1870	37.57	18.01	2.07	1.29	10.96	20.38	0.92
D1	33.0	1854	37.56	17.22	2.35	1.22	10.17	20.55	1.09
D1	36.0	1838	36.76	18.10	1.97	1.16	8.77	19.92	1.02
D1	39.0	1822	37.40	18.58	2.01	1.20	8.14	20.18	1.09
D1	42.0	1805	36.63	18.04	1.80	1.17	7.39	20.11	1.00
D1	45.0	1788	38.69	19.42	2.05	1.25	7.52	20.92	1.07
D1	48.0	1771	38.46	19.49	1.86	1.21	6.97	20.78	1.07
D1	51.0	1753	38.27	18.63	1.93	1.18	6.84	20.64	1.09
D1	53.0	1741	39.33	19.44	2.08	1.63	7.18	22.88	1.25
D1	65.0	1665	38.25	18.12	2.01	1.72	6.92	22.13	1.41
D2	75.5	1594	41.13	20.10	2.03	1.16	6.57	19.83	1.48
D1	77.0	1584	38.94	17.34	1.91	1.61	6.50	20.31	1.37
D2	81.5	1551	43.78	22.29	2.12	1.29	7.09	20.22	1.52
D2	87.5	1507	43.76	21.25	2.12	1.30	8.26	18.42	2.65
D1	89.0	1496	40.82	19.34	1.98	1.78	6.67	20.54	1.41
D2	93.5	1462	40.50	22.63	2.07	1.03	14.27	16.97	1.20
D2	93.5	1462	39.57	20.13	2.01	0.92	14.26	16.56	1.15
D2	99.5	1415	41.61	21.92	2.14	1.15	15.14	17.56	1.23
D1	101.0	1403	42.48	20.59	1.95	1.59	6.70	19.32	1.40
D2	105.5	1367	46.31	24.65	2.09	0.81	11.86	20.10	1.53
D2	111.5	1317	45.83	22.67	1.87	0.81	12.10	18.79	1.59
D1	113.0	1304	39.83	20.32	2.62	1.37	14.42	16.83	1.29
D2	117.5	1266	47.22	23.66	2.21	0.84	13.31	18.29	1.54
D2	123.5	1213	48.46	23.18	1.89	0.88	14.42	18.40	1.44
D1	125.0	1200	45.54	24.05	2.13	1.03	12.50	19.76	1.64
D2	129.5	1159	46.84	21.74	2.06	0.90	15.53	17.97	1.44
D2	135.5	1103	39.66	17.91	2.02	0.99	21.17	15.92	1.19
D2	141.5	1046	36.00	15.65	2.21	1.11	25.47	13.99	1.06
D2	147.5	988	33.34	13.76	2.16	1.18	29.45	12.02	0.92
D2	153.5	928	22.99	9.37	2.58	2.23	43.60	8.13	0.61
D3	157.0	893	18.86	8.08	2.81	3.23	48.88	6.40	0.49
D2	159.5	867	18.75	8.26	2.75	3.01	49.85	6.15	0.46
D2	159.5	867	18.81	8.15	2.80	3.28	50.53	6.14	0.45
D3	163.0	830	14.76	6.26	2.71	4.23	55.17	4.82	0.36
D3	169.5	762	15.10	6.33	2.64	4.75	57.59	5.09	0.42

D3	175.5	696	15.52	7.29	2.50	5.30	60.66	5.51	0.42
D3	181.5	630	15.27	5.78	2.58	5.77	60.31	5.66	0.44
D3	187.5	562	14.69	5.83	2.53	5.90	59.19	6.00	0.41
D3	193.5	492	15.22	5.58	2.55	6.08	59.00	6.18	0.40
D3	199.5	421	15.72	6.81	2.46	6.02	58.15	6.11	0.60
D3	205.5	349	13.68	4.97	2.63	6.61	59.06	6.00	0.43
D3	211.5	275	13.44	5.03	2.60	6.69	57.97	5.92	0.44
D3	211.5	275	13.12	4.90	2.49	6.45	56.16	5.79	0.42

Drive	Total Core Depth (cm)	Cal Year	Mo (ppm)	Cd (ppm)	Sn (ppm)	Sb (ppm)	La (ppm)	Ce (ppm)	Pr (ppm)
D1	1.0	2003	0.32	0.92	<	0.28	9.6	29.0	3.27
D1	2.0	1999	0.30	0.91	<	0.28	9.5	29.4	3.28
D1	3.0	1995	0.29	0.92	<	0.29	9.8	30.8	3.45
D1	5.0	1986	0.28	0.89	<	0.29	10.3	32.0	3.59
D1	6.0	1982	0.28	0.91	<	0.31	10.1	31.7	3.51
D1	9.0	1969	0.23	0.56	<	0.23	10.8	34.8	3.88
D1	12.0	1956	0.24	0.38	<	0.23	11.7	37.4	4.21
D1	15.0	1943	0.18	0.36	<	0.23	12.4	40.1	4.61
D1	18.0	1929	0.16	0.38	<	0.20	12.1	40.0	4.56
D1	21.0	1915	0.16	0.38	<	0.20	13.1	43.4	4.97
D1	24.0	1900	0.13	0.37	<	0.15	13.0	42.1	4.90
D1	27.0	1885	0.12	0.35	<	0.14	13.3	42.0	4.92
D1	27.0	1885	0.12	0.34	<	0.14	13.0	41.3	4.81
D1	30.0	1870	0.13	0.33	<	0.11	13.2	40.8	4.72
D1	33.0	1854	0.14	0.32	<	0.13	14.0	42.9	4.97
D1	36.0	1838	0.11	0.31	<	0.12	14.5	43.1	5.06
D1	39.0	1822	0.12	0.32	<	0.11	15.1	44.9	5.19
D1	42.0	1805	0.09	0.34	<	0.10	15.2	45.1	5.22
D1	45.0	1788	0.10	0.36	<	0.11	15.3	45.8	5.27
D1	48.0	1771	0.08	0.35	<	0.10	15.2	45.3	5.23
D1	51.0	1753	0.11	0.35	<	0.11	14.6	43.9	5.07
D1	53.0	1741	0.11	0.38	0.08	0.11	16.2	43.7	5.64
D1	65.0	1665	0.09	0.33	0.08	0.13	16.0	44.2	5.62
D2	75.5	1594	0.13	0.32	0.08	0.14	14.6	42.6	5.17
D1	77.0	1584	0.08	0.31	0.08	0.12	15.7	43.1	5.43
D2	81.5	1551	0.14	0.33	0.09	0.14	14.6	42.9	5.15
D2	87.5	1507	0.14	0.29	0.10	0.14	14.2	42.5	5.07
D1	89.0	1496	0.09	0.32	0.08	0.12	14.7	42.0	5.21
D2	93.5	1462	0.16	0.26	0.07	0.10	12.1	36.6	4.35
D2	93.5	1462	0.17	0.25	0.07	0.11	11.8	36.4	4.25
D2	99.5	1415	0.22	0.26	0.08	0.11	11.7	36.0	4.24
D1	101.0	1403	0.11	0.31	0.09	0.12	14.3	41.6	5.03
D2	105.5	1367	0.19	0.30	0.10	0.15	12.4	39.2	4.64
D2	111.5	1317	0.17	0.30	0.09	0.14	11.9	37.9	4.45
D1	113.0	1304	0.15	0.26	0.09	0.14	11.9	36.4	4.26
D2	117.5	1266	0.19	0.29	0.09	0.14	12.3	38.5	4.61
D2	123.5	1213	0.15	0.29	0.08	0.13	13.0	40.5	4.73
D1	125.0	1200	0.15	0.29	0.10	0.17	12.5	38.6	4.59
D2	129.5	1159	0.14	0.28	0.08	0.14	12.8	40.1	4.71
D2	135.5	1103	0.14	0.27	0.06	0.13	12.0	36.0	4.29
D2	141.5	1046	0.13	0.24	<	0.11	11.6	33.5	4.02
D2	147.5	988	0.13	0.23	<	0.11	10.8	30.4	3.67
D2	153.5	928	0.11	0.16	<	0.07	8.35	22.5	2.69
D3	157.0	893	0.14	0.15	<	0.05	6.62	17.7	2.07
D2	159.5	867	0.12	0.14	<	0.05	6.85	18.2	2.16
D2	159.5	867	0.11	0.14	<	0.05	7.02	18.5	2.17
D3	163.0	830	0.11	0.12	<	0.03	5.35	14.2	1.64
D3	169.5	762	0.09	0.12	<	0.03	5.80	15.2	1.77

D3	175.5	696	<	0.14	<	0.03	6.38	16.8	1.94
D3	181.5	630	<	0.12	<	0.03	6.70	17.6	2.02
D3	187.5	562	<	0.13	<	0.04	7.39	19.2	2.23
D3	193.5	492	<	0.14	<	0.04	7.74	20.2	2.32
D3	199.5	421	<	0.13	<	0.04	7.89	20.5	2.33
D3	205.5	349	0.11	0.13	<	0.04	7.82	20.5	2.30
D3	211.5	275	<	0.13	<	0.03	7.85	20.5	2.31
D3	211.5	275	<	0.13	<	0.03	7.73	20.2	2.27

Drive	Total Core Depth (cm)	Cal Year	Nd (ppm)	Sm (ppm)	Eu (ppm)	Gd (ppm)	Tb (ppm)	Dy (ppm)
D1	1.0	2003	14.11	3.02	0.77	4.84	0.46	2.06
D1	2.0	1999	13.78	3.04	0.77	4.85	0.46	2.09
D1	3.0	1995	14.65	3.18	0.81	5.16	0.49	2.21
D1	5.0	1986	15.15	3.36	0.85	5.27	0.51	2.31
D1	6.0	1982	14.88	3.29	0.82	5.17	0.51	2.27
D1	9.0	1969	16.52	3.62	0.88	5.72	0.57	2.51
D1	12.0	1956	17.94	3.97	0.94	6.56	0.62	2.73
D1	15.0	1943	20.00	4.44	1.05	7.22	0.71	3.09
D1	18.0	1929	19.83	4.46	1.07	7.24	0.71	3.15
D1	21.0	1915	21.58	4.87	1.17	7.73	0.77	3.44
D1	24.0	1900	21.46	4.82	1.16	7.92	0.77	3.41
D1	27.0	1885	21.34	4.72	1.14	7.82	0.75	3.39
D1	27.0	1885	20.70	4.65	1.12	7.52	0.74	3.29
D1	30.0	1870	20.40	4.53	1.09	7.45	0.73	3.22
D1	33.0	1854	21.31	4.71	1.12	7.83	0.76	3.31
D1	36.0	1838	21.59	4.67	1.12	7.85	0.74	3.29
D1	39.0	1822	22.00	4.79	1.13	8.01	0.76	3.29
D1	42.0	1805	21.92	4.76	1.10	8.19	0.76	3.28
D1	45.0	1788	22.36	4.89	1.13	8.27	0.78	3.37
D1	48.0	1771	22.30	4.85	1.12	8.25	0.76	3.34
D1	51.0	1753	21.72	4.76	1.11	8.08	0.75	3.27
D1	53.0	1741	25.97	5.38	1.21	5.93	0.71	3.70
D1	65.0	1665	25.38	5.33	1.19	5.80	0.70	3.57
D2	75.5	1594	23.10	4.87	1.10	5.44	0.66	3.25
D1	77.0	1584	24.64	5.02	1.14	5.53	0.66	3.30
D2	81.5	1551	22.98	4.83	1.11	5.39	0.66	3.28
D2	87.5	1507	22.54	4.67	1.08	5.16	0.63	3.08
D1	89.0	1496	23.47	4.87	1.11	5.48	0.66	3.32
D2	93.5	1462	19.43	4.05	0.95	4.51	0.57	2.79
D2	93.5	1462	18.91	3.99	0.94	4.38	0.55	2.76
D2	99.5	1415	19.71	4.12	0.97	4.61	0.56	2.92
D1	101.0	1403	23.19	4.77	1.07	5.23	0.63	3.18
D2	105.5	1367	21.38	4.60	1.07	5.17	0.64	3.36
D2	111.5	1317	20.87	4.38	1.03	4.88	0.60	3.11
D1	113.0	1304	19.07	4.00	0.93	4.53	0.56	2.76
D2	117.5	1266	21.05	4.47	1.06	5.01	0.61	3.09
D2	123.5	1213	21.70	4.57	1.08	5.14	0.62	3.19
D1	125.0	1200	21.21	4.48	1.06	5.05	0.64	3.14
D2	129.5	1159	21.47	4.57	1.08	5.11	0.60	3.14
D2	135.5	1103	19.41	4.14	0.97	4.51	0.55	2.78
D2	141.5	1046	17.66	3.76	0.86	4.09	0.50	2.51
D2	147.5	988	16.09	3.41	0.79	3.63	0.44	2.18
D2	153.5	928	11.12	2.40	0.56	2.47	0.30	1.45
D3	157.0	893	8.62	1.88	0.45	1.91	0.25	1.09
D2	159.5	867	9.00	1.92	0.45	1.95	0.24	1.11
D2	159.5	867	9.08	1.95	0.45	1.93	0.24	1.10
D3	163.0	830	6.78	1.49	0.36	1.50	0.19	0.84
D3	169.5	762	7.30	1.60	0.38	1.58	0.19	0.92

D3	175.5	696	8.04	1.72	0.41	1.76	0.21	0.99
D3	181.5	630	8.44	1.85	0.44	1.87	0.21	1.04
D3	187.5	562	9.30	1.98	0.47	2.03	0.23	1.12
D3	193.5	492	9.51	2.08	0.49	2.11	0.23	1.16
D3	199.5	421	9.70	2.07	0.49	2.16	0.23	1.18
D3	205.5	349	9.55	2.08	0.49	2.14	0.22	1.16
D3	211.5	275	9.49	2.09	0.49	2.16	0.23	1.16
D3	211.5	275	9.36	2.04	0.49	2.11	0.23	1.17

Drive	Total Core Depth (cm)	Cal Year	Ho (ppm)	Er (ppm)	Tm (ppm)	Yb (ppm)	Lu (ppm)	Pb (ppm)	Bi (ppm)
D1	1.0	2003	0.40	1.22	0.14	0.88	0.13	36.15	0.17
D1	2.0	1999	0.40	1.23	0.15	0.88	0.13	36.78	0.17
D1	3.0	1995	0.42	1.29	0.15	0.94	0.14	37.45	0.17
D1	5.0	1986	0.44	1.34	0.16	0.98	0.14	38.28	0.17
D1	6.0	1982	0.44	1.32	0.16	0.96	0.14	37.40	0.17
D1	9.0	1969	0.47	1.46	0.17	1.04	0.15	31.24	0.13
D1	12.0	1956	0.52	1.58	0.18	1.14	0.16	27.29	0.13
D1	15.0	1943	0.58	1.78	0.21	1.28	0.18	28.71	0.15
D1	18.0	1929	0.59	1.81	0.21	1.28	0.19	26.17	0.09
D1	21.0	1915	0.64	1.95	0.23	1.40	0.20	26.46	0.10
D1	24.0	1900	0.64	1.94	0.23	1.38	0.20	24.66	0.09
D1	27.0	1885	0.64	1.93	0.22	1.36	0.20	22.77	0.08
D1	27.0	1885	0.62	1.88	0.22	1.35	0.20	22.20	0.08
D1	30.0	1870	0.61	1.86	0.22	1.34	0.19	20.80	0.09
D1	33.0	1854	0.62	1.91	0.22	1.36	0.20	22.09	0.09
D1	36.0	1838	0.61	1.88	0.21	1.32	0.19	22.52	0.08
D1	39.0	1822	0.61	1.89	0.21	1.33	0.19	23.07	0.08
D1	42.0	1805	0.60	1.90	0.21	1.32	0.19	23.00	0.07
D1	45.0	1788	0.63	1.94	0.22	1.37	0.20	24.59	0.08
D1	48.0	1771	0.62	1.94	0.22	1.36	0.20	24.03	0.07
D1	51.0	1753	0.62	1.90	0.21	1.35	0.19	22.63	0.07
D1	53.0	1741	0.72	2.08	0.26	1.55	0.22	23.97	0.09
D1	65.0	1665	0.70	2.02	0.24	1.50	0.22	20.48	0.09
D2	75.5	1594	0.63	1.81	0.22	1.34	0.19	20.09	0.09
D1	77.0	1584	0.64	1.86	0.23	1.37	0.20	18.58	0.08
D2	81.5	1551	0.64	1.84	0.23	1.35	0.19	22.41	0.10
D2	87.5	1507	0.59	1.69	0.21	1.26	0.18	22.91	0.10
D1	89.0	1496	0.65	1.88	0.23	1.38	0.19	19.26	0.08
D2	93.5	1462	0.54	1.57	0.19	1.15	0.16	20.32	0.09
D2	93.5	1462	0.52	1.51	0.19	1.12	0.16	19.76	0.09
D2	99.5	1415	0.57	1.63	0.21	1.21	0.17	20.72	0.12
D1	101.0	1403	0.62	1.77	0.22	1.28	0.18	20.53	0.09
D2	105.5	1367	0.66	1.90	0.23	1.39	0.20	21.09	0.12
D2	111.5	1317	0.61	1.76	0.22	1.30	0.19	20.08	0.12
D1	113.0	1304	0.53	1.53	0.19	1.12	0.16	18.36	0.09
D2	117.5	1266	0.60	1.72	0.21	1.23	0.17	20.62	0.12
D2	123.5	1213	0.61	1.74	0.21	1.25	0.18	20.32	0.12
D1	125.0	1200	0.62	1.77	0.22	1.29	0.19	18.23	0.11
D2	129.5	1159	0.59	1.68	0.20	1.22	0.17	20.51	0.12
D2	135.5	1103	0.53	1.49	0.18	1.09	0.15	19.20	0.10
D2	141.5	1046	0.47	1.35	0.16	0.96	0.13	18.61	0.09
D2	147.5	988	0.41	1.16	0.14	0.81	0.11	17.69	0.08
D2	153.5	928	0.27	0.75	0.09	0.53	0.07	13.39	0.02
D3	157.0	893	0.20	0.57	0.07	0.41	0.06	11.15	0.03
D2	159.5	867	0.20	0.58	0.07	0.40	0.06	10.96	0.01
D2	159.5	867	0.20	0.58	0.07	0.40	0.06	10.50	0.01
D3	163.0	830	0.15	0.42	<	0.30	0.04	8.23	<
D3	169.5	762	0.17	0.47	<	0.32	0.05	8.28	<

D3	175.5	696	0.18	0.51	0.06	0.36	0.05	9.36	<
D3	181.5	630	0.19	0.54	0.07	0.38	0.05	9.60	<
D3	187.5	562	0.21	0.59	0.07	0.41	0.06	10.27	<
D3	193.5	492	0.22	0.61	0.07	0.44	0.06	10.60	<
D3	199.5	421	0.22	0.63	0.07	0.44	0.06	11.0	<
D3	205.5	349	0.22	0.61	0.07	0.44	0.06	10.3	<
D3	211.5	275	0.22	0.60	0.07	0.44	0.06	10.5	<
D3	211.5	275	0.21	0.61	0.07	0.43	0.06	10.4	<

< indicates that sample was below detection limit

Ag, In, W, Os, Ir, Au, Tl were below detection limit for all samples

APPENDIX E

TABLE OF CARBON TO NITROGEN RATIO DATA

Drive	Total Core Depth (cm)	Cal Year	Corr. $\delta^{15}\text{N}$	%N	Corr. $\delta^{13}\text{C}$	%C	C (%) / N (%)
D1	2	1999	7.40	0.80	-25.13	6.67	8.34
D1	4	1991	6.75	0.67	-25.52	5.66	8.45
D1	6	1982	6.20	0.66	-25.68	5.59	8.47
D1	8	1974	6.05	0.63	-25.60	5.29	8.40
D1	10	1965	5.56	0.45	-26.64	3.62	8.04
D1	12	1956	4.85	0.31	-27.52	2.59	8.35
D1	14	1947	5.19	0.23	-27.82	1.96	8.52
D1	16	1938	5.06	0.22	-28.02	1.86	8.45
D1	18	1929	4.98	0.20	-27.56	1.70	8.50
D1	20	1920	4.65	0.17	-27.49	1.46	8.59
D1	22	1910	4.47	0.16	-27.50	1.43	8.94
D1	24	1900	4.45	0.16	-27.60	1.36	8.50
D1	26	1890	4.48	0.15	-27.68	1.32	8.80
D1	28	1880	4.24	0.14	-27.47	1.29	9.21
D1	30	1870	4.28	0.15	-27.46	1.36	9.07
D1	32	1860	4.17	0.15	-27.31	1.34	8.93
D1	34	1849	4.25	0.14	-27.14	1.30	9.29
D1	36	1838	4.22	0.14	-26.90	1.22	8.71
D1	38	1827	4.37	0.13	-26.44	1.09	8.38
D1	40	1816	4.38	0.12	-26.39	1.05	8.75
D1	42	1805	4.57	0.12	-26.24	0.97	8.08
D1	44	1794	4.57	0.11	-25.96	0.90	8.18
D1	46	1782	4.85	0.11	-25.57	0.82	7.45
D1	48	1771	4.93	0.10	-25.18	0.73	7.30
D1	50	1759	4.94	0.10	-25.42	0.73	7.30
D1	52	1747	5.12	0.10	-25.27	0.71	7.10
D1	54	1735	5.30	0.09	-24.72	0.68	7.56
D1	56	1722	5.50	0.09	-24.62	0.66	7.33
D1	58	1710	5.36	0.09	-24.62	0.65	7.22
D1	60	1697	4.95	0.09	-24.90	0.68	7.56
D1	62	1685	5.06	0.09	-24.87	0.68	7.56
D1	64	1672	5.21	0.09	-24.81	0.67	7.44
D1	66	1658	5.29	0.09	-24.54	0.67	7.44
D1	68	1645	5.30	0.09	-24.67	0.68	7.56
D1	70	1632	5.23	0.09	-24.67	0.66	7.33

D1	72	1618	5.22	0.09	-24.69	0.65	7.22
D1	74	1604	5.08	0.09	-24.77	0.68	7.56
D1	76	1591	5.36	0.09	-24.80	0.68	7.56
D1	78	1576	5.13	0.09	-24.81	0.66	7.33
D1	80	1562	5.32	0.09	-24.53	0.67	7.44
D1	82	1548	5.32	0.09	-24.71	0.67	7.44
D1	84	1533	5.30	0.09	-24.70	0.69	7.67
D1	86	1519	5.26	0.09	-24.88	0.69	7.67
D1	88	1504	5.26	0.10	-24.88	0.71	7.10
D1	90	1489	5.40	0.10	-24.92	0.72	7.20
D1	92	1473	5.38	0.10	-24.86	0.72	7.20
D1	94	1458	5.22	0.10	-24.74	0.75	7.50
D1	96	1443	5.10	0.10	-24.80	0.75	7.50
D1	98	1427	5.26	0.10	-24.82	0.77	7.70
D1	100	1411	5.19	0.11	-24.77	0.86	7.82
D1	102	1395	4.39	0.10	-24.78	0.87	8.70
D1	104	1379	3.93	0.12	-24.87	1.02	8.50
D1	106	1363	3.93	0.13	-25.12	1.18	9.08
D1	108	1346	3.72	0.17	-26.43	1.75	10.29
D1	110	1330	3.81	0.19	-26.65	1.99	10.47
D1	112	1313	3.88	0.19	-26.80	2.06	10.84
D1	114	1296	4.01	0.14	-26.12	1.32	9.43
D1	116	1279	4.07	0.15	-26.29	1.50	10.00
D1	118	1261	3.95	0.18	-26.76	1.81	10.06
D1	120	1244	3.99	0.20	-27.12	2.13	10.65
D1	122	1226	3.76	0.20	-27.04	2.09	10.45
D1	124	1209	4.07	0.14	-26.01	1.29	9.21
D1	126	1191	4.38	0.14	-26.04	1.33	9.50
D1	128	1173	4.69	0.14	-25.99	1.28	9.14
D1	130	1154	4.32	0.15	-26.07	1.39	9.27
D1	132	1136	4.18	0.14	-26.19	1.34	9.57
D2	134	1117	4.69	0.15	-26.02	1.51	10.07
D2	136	1099	5.08	0.15	-26.09	1.54	10.27
D2	138	1080	4.89	0.15	-26.12	1.56	10.40
D2	140	1061	5.07	0.16	-26.16	1.61	10.06
D2	142	1042	4.91	0.16	-26.12	1.67	10.44
D2	144	1022	4.50	0.18	-26.50	1.65	9.17
D2	146	1003	4.69	0.17	-26.23	1.81	10.65
D2	148	983	4.50	0.18	-26.53	1.98	11.00
D2	150	963	4.20	0.22	-26.57	2.67	12.14
D2	152	943	4.18	0.22	-26.20	2.34	10.64
D2	154	923	3.82	0.23	-26.15	2.39	10.39
D2	156	903	3.96	0.24	-26.69	2.50	10.42
D2	158	882	3.64	0.27	-26.82	2.89	10.70
D2	160	862	3.57	0.29	-26.85	3.13	10.79
D2	162	841	3.61	0.29	-26.94	3.18	10.97
D2	164	820	3.40	0.32	-26.94	3.51	10.97
D2	166	799	3.25	0.43	-27.10	4.70	10.93
D2	168	778	3.22	0.45	-27.32	4.99	11.09
D2	170	756	3.10	0.54	-27.49	6.06	11.22

D2	172	735	2.98	0.56	-27.55	6.23	11.13
D2	174	713	2.86	0.61	-27.69	7.57	12.41
D2	176	691	2.80	0.57	-27.78	6.49	11.39
D3	178	669	3.03	0.57	-27.65	6.49	11.39
D3	180	647	3.67	0.48	-27.42	5.41	11.27
D3	182	624	2.98	0.56	-27.78	6.26	11.18
D3	184	602	2.76	0.60	-27.86	6.71	11.18
D3	190	533	3.55	0.45	-27.43	5.00	11.11
D3	192	510	3.60	0.49	-27.37	5.37	10.96
D3	194	487	3.55	0.49	-27.35	5.48	11.18
D3	196	463	3.76	0.48	-26.77	5.37	11.19
D3	198	439	3.66	0.42	-26.58	4.58	10.90
D3	200	416	3.69	0.42	-26.51	4.53	10.79
D3	202	392	3.65	0.42	-26.48	4.55	10.83
D3	204	367	3.63	0.36	-26.23	3.72	10.33
D3	206	343	3.36	0.38	-26.21	4.06	10.68
D3	208	319	3.76	0.37	-26.20	3.95	10.68
D3	210	294	3.69	0.37	-26.21	3.91	10.57
D3	212	269	3.74	0.38	-26.21	3.97	10.45
D3	214	244	3.67	0.39	-26.21	4.19	10.74
D3	216	219	3.83	0.38	-26.16	3.93	10.34
D3	218	194	3.79	0.38	-26.17	3.87	10.18
D3	220	168	3.71	0.39	-26.16	4.12	10.56
D3	222	143	3.67	0.40	-26.15	4.25	10.63
D3	224	117	3.74	0.39	-26.12	4.15	10.64
D3	226	91	3.72	0.38	-26.14	4.04	10.63
D3	228	65	3.71	0.37	-26.11	3.88	10.49
D3	230	39	4.03	0.38	-26.34	3.54	9.32
D3	232	12	3.96	0.37	-26.05	3.90	10.54
D3	234	-14	4.15	0.36	-26.08	3.86	10.72
D3	236	-41	4.11	0.34	-26.14	3.66	10.76
D3	238	-68	4.41	0.36	-26.02	3.86	10.72
D3	240	-95	4.26	0.35	-25.96	3.80	10.86
D3	242	-122	4.25	0.34	-26.05	3.67	10.79
D3	244	-149	4.55	0.34	-25.90	3.72	10.94
D3	246	-177	4.56	0.35	-25.84	3.88	11.09
D3	248	-204	4.76	0.36	-25.85	3.81	10.58
D3	250	-232	4.79	0.35	-25.76	3.81	10.89
D3	252	-260	4.88	0.35	-25.83	3.85	11.00
D3	254	-288	5.14	0.36	-25.80	3.87	10.75
D3	256	-317	4.98	0.36	-25.63	3.92	10.89
D3	258	-345	5.18	0.38	-25.58	4.18	11.00
D3	260	-374	4.87	0.39	-25.58	4.25	10.90
D3	262	-403	4.90	0.40	-25.52	4.39	10.98
D3	264	-432	4.83	0.40	-25.50	4.42	11.05

BIBLIOGRAPHY

- Abbott, M.B., and Stafford, T.W., 1996, Radiocarbon Geochemistry of Modern and Ancient Arctic Lake Systems, Baffin Island, Canada: *Quaternary Research*, v. 45, p. 300-311.
- Abbott, M.B., and Wolfe, A.P., 2003, Intensive Pre-Incan Metallurgy Recorded by Lake Sediments from the Bolivian Andes: *Science*, v. 301, p. 1893-1895.
- Appleby, P.G., and Oldfield, F., 1983, The assessment of ^{210}Pb data from sites with varying sediment accumulation rates: *Hydrobiologia*, v. 103, p. 29-35.
- Braganza, K., Gergis, J.L., Power, S.B., Risbey, J.S., and Fowler, A.M., 2009, A multiproxy index of the El Niño-Southern Oscillation, A.D. 1525-1982.: *Journal of Geophysical Research (Atmospheres)*, v. 114.
- Brenner, M., Hodell, D.A., Curtis, J.H., Rosenmeier, M., and Abbott, M.B., 2001, A abrupt Climate Change and Pre-Columbian Cultural Collapse, *in* Markgraf, V., ed., *Interhemispheric climatic linkages*, Academic Press, p. 87-103.
- Chang, C.-P., 2004, *East Asian Monsoon*, World Scientific Series on Meteorology of East Asia, Volume 2: Hackensack, NJ, World Scientific Publishing Co. Pte. Ltd.
- Cook, E.R., Anchukaitis, K.J., Buckley, B.M., D'Arrigo, R.D., Jacoby, G.C., and Wright, W.E., 2010, Asian Monsoon Failure and Megadrought During the Last Millennium: *Science*, v. 328, p. 486-489.
- Cooke, C.A., Wolfe, A.P., and Hobbs, W.O., 2009, Lake-sediment geochemistry reveals 1400 years of evolving extractive metallurgy at Cerro de Pasco, Peruvian Andes: *Geology*, v. 37, p. 1019-1022.
- Dean, W., 1974, Determination of carbonate and organic matter in calcareous sediments and sedimentary rocks by loss on ignition: Comparison with other methods: *Journal of Sedimentary Petrology*, v. 44, p. 242-248.
- Dearing, J.A., Jones, R.T., Shen, J., Yang, X., Boyle, J.F., Foster, G.C., Crook, D.S., and Elvin, M.J.D., 2008, Using multiple archives to understand past and present climate-human-environment interactions: the lake Erhai catchment, Yunnan Province, China: *Journal of Paleolimnology*, v. 40, p. 3-31.

- DeEr, Z., Li, H.-C., Ku, T.-L., and Lu, L., 2009, On linking climate to Chinese dynastic change: Spatial and temporal variations of monsoonal rain: *Chinese Science Bulletin*, v. 55, p. 77-83.
- Deevey, E.S., Gross, M.S., Hutchinson, G.E., and Kraybill, H.L., 1954, The Natural C14 Contents of Materials From Hard-water Lakes: *Geology*, v. 40, p. 285-288.
- Dykoski, C., Edwards, R., Cheng, H., Yuan, D., Cai, Y., Zhang, M., Lin, Y., Qing, J., An, Z., and Revenaugh, J., 2005, A high-resolution, absolute-dated Holocene and deglacial Asian monsoon record from Dongge Cave, China: *Earth and Planetary Science Letters*, v. 233, p. 71-86.
- Eberhard, W., 1967, *A history of China*, Plain Label Books.
- Esper, J., Frank, D.C., and Luterbacher, J., 2007, On Selected Issues and Challenges in Dendrochronology, *in* Kienast, F., Wildi, O., and Ghosh, S., eds., *A Changing World. Challenges for Landscape Research*, p. 113-132.
- Fairbank, J.K., 1983, Volume 12 Part 1 Republican China, 1912–1949 New York, Cambridge University Press.
- Fairbank, J.K., and Liu, K.-C., 1980, Volume 11 Part 2 Late Ch'ing, 1800–1911: New York, Cambridge University Press.
- Giersch, C.P., 2006, *Asian borderlands: the transformation of Qing China's Yunnan frontier*, Harvard University Press.
- Golas, P.J., 1999, Volume 5 Chemistry and Chemical Technology Part XIII: Mining, *in* Needham, J., ed., *Science and Civilisation in China, Volume 5: Cambridge United Kingdom*, Cambridge University Press.
- He, F., Ge, Q., Dai, J., and Rao, Y., 2008, Forest change of China in recent 300 years: *Journal of Geographical Sciences*, v. 18, p. 59-72.
- Higham, C., 1996, *The Bronze Age of Southeast Asia*: Cambridge, Cambridge University Press.
- Hodell, D.A., Brenner, M., Kanfoush, S.L., Curtis, J.H., Stoner, J.S., Xueliang, S., Yuan, W., and Whitmore, T.J., 1999, Paleoclimate of Southwestern China for the Past 50,000 yr Inferred from Lake Sediment Records: *Quaternary Research*, v. 52, p. 369-380.
- Hu, C., Henderson, G., Huang, J., Xie, S., Sun, Y., and Johnson, K., 2008, Quantification of Holocene Asian monsoon rainfall from spatially separated cave records: *Earth and Planetary Science Letters*, v. 266, p. 221-232.
- Kaushal, S., and Binford, M.W., 1999, Relationship between C:N ratios of lake sediments, organic matter sources, and historical deforestation in Lake Pleasant, Massachusetts, USA: *Journal of Paleolimnology*, v. 22, p. 439-442.

- Kinter, J.L., Miyakoda, K., and Yang, S., 2002, Recent Change in the Connection from the Asian Monsoon to ENSO: *American Meteorological Society*, v. 15, p. 1203-1215.
- Lachniet, M.S., 2009, Climatic and environmental controls on speleothem oxygen-isotope values: *Quaternary Science Reviews*, v. 28, p. 412-432.
- Lau, N.-C., and Nath, M.J., 2006, ENSO Modulation of the Interannual and Intraseasonal Variability of the East Asian Monsoon—A Model Study: *Journal of Climate*, v. 19, p. 4508-4530.
- Lee, J., 1982, Food Supply and Population Growth in Southwest China, 1250-1850: *Journal of Asian Studies*, v. 41, p. 711-746.
- Li, H.-C., and Ku, T.-L., 1997, $\delta^{13}\text{C}$ - $\delta^{18}\text{O}$ covariance as a paleohydrological indicator for closed-basin lakes: *Palaeogeography, Palaeoclimatology, Palaeoecology*, v. 133, p. 69-80.
- Li, R., Dong, M., Zhao, Y., Zhang, L., Cui, Q., and He, W., 2007, Assessment of Water Quality and Identification of Pollution Sources of Plateau Lakes in Yunnan (China): *Journal of Environment Quality*, v. 36, p. 291.
- Mann, M.E., Zhang, Z., Rutherford, S., Bradley, R.S., Hughes, M.K., Shindell, D., Ammann, C., Faluvegi, G., and Ni, F., 2009, Global Signatures and Dynamical Origins of the Little Ice Age and Medieval Climate Anomaly: *Science*, v. 326, p. 1256-1260.
- Myers, P.A., 1994, Preservation of elemental and isotopic source identification of sedimentary organic matter: *Chemical Geology*, v. 114, p. 289-302.
- Needham, J., and Gwei-djen, L., 1974, Volume 5 Chemistry and Chemical Technology Part II: Spagyric Discovery and Invention: Magisteries of Gold and Immortality: Chemistry and Chemical Technology, in Needham, J., ed., *Science and Civilisation in China, Volume 5*: Cambridge United Kingdom, Cambridge University Press.
- Nelson, D.B., Abbott, M.B., Steinman, B., Polissar, P.J., Stansell, N.D., Ortiz, J.D., Rosenmeier, M.F., Finney, B.P., and Riedel, J., 2011, Drought variability in the Pacific Northwest from a 6,000-yr lake sediment record: *Proceedings of the National Academy of Sciences of the United States of America*, v. 108, p. 3870-3875.
- Pacific, U.N.E.a.S.C.f.A.a.t., 2010, Yunnan, Volume 2010.
- Qian, and W., 2002, Little Ice Age Climate near Beijing, China, Inferred from Historical and Stalagmite Records: *Quaternary Research*, v. 57, p. 109-119.
- Rosenmeier, M.F., Hodell, D.A., Brenner, M., Curtis, J.H., Martin, J.B., Anselmetti, F.S., Ariztegui, D., and Guilderson, T.P., 2002, Influence of vegetation change on watershed hydrology: implications for paleoclimatic interpretation of lacustrine $\delta^{18}\text{O}$ records: *Journal of Paleolimnology*, v. 27, p. 117-131.

- Scott, J.C., 2009, *The art of not being governed: an anarchist history of upland Southeast Asia*, Yale University.
- Shen, J., Jones, R.T., Yang, X., Dearing, J.A., and Wang, S., 2006, The Holocene vegetation history of Lake Erhai, Yunnan province southwestern China: the role of climate and human forcings: *The Holocene*, v. 16, p. 265-276.
- Stuiver, M., Reimer, P., and Reimer, R., 2010, CALIB 6.0, Volume 2010.
- Wang, B., Wu, R., and Fu, X., 2000, Pacific-East Asian Teleconnection: How Does ENSO Affect East Asian Climate?: *Journal of Climate*, v. 13, p. 1517-1536.
- Wang, Y., Cheng, H., Edwards, R.L., He, Y., Kong, X., An, Z., Wu, J., Kelly, M.J., Dykoski, C.A., and Li, X., 2006, Dongge Cave Stalagmite High-Resolution Holocene $\delta^{18}O$ Data., *in* Program, N.N.P., ed.: Boulder, CO, IGBP PAGES/World Data Center for Paleoclimatology
- Whitmore, T.J., Brenner, M., Engstrom, D.R., and Xueliang, S., 1994, Accelerated soil erosion in watersheds of Yunnan Province, China: *Journal of Soil and Water Conservation*, v. 49, p. 67-72.
- Whitmore, T.J., Brenner, M., Jiang, Z., Curtis, J.H., Moore, A.M., Engstrom, D.R., and Wu, Y., 1997, Water quality and sediment geochemistry in lakes of Yunnan Province, southern China: *Environmental Geology*, v. 32, p. 45-55.
- Wright, H.E., Mann, D.H., and Glaser, P.H., 1984, Piston Corers for Peat and Lake Sediments: *Ecology*, v. 65, p. 657-659.
- Yafeng, S., Tandong, Y., and Bao, Y., 1999, Decadal climatic variations recorded in Guliya ice core and comparison with the historical documentary data from East China during the last 2000 years: *Science in China Series D*, v. 42, p. 91-100.
- Yang, B., 2009, *Between winds and clouds: the making of Yunnan (second century BCE to twentieth century CE)*: New York, Columbia University Press.
- Yao, A., 2010, Recent Developments in the Archaeology of Southwestern China: *Journal of Archaeological Research*, v. 18, p. 203-239.
- Yim, S.-Y., Yeh, S.-W., Wu, R., and Jhun, J.-G., 2008, The Influence of ENSO on Decadal Variations in the Relationship between the East Asian and Western North Pacific Summer Monsoons: *Journal of Climate*, v. 21, p. 3165-3179.
- Zhang, P., Cheng, H., Edwards, R.L., Chen, F., Wang, Y., Yang, X., Liu, J., Tan, M., Wang, X., Liu, J., An, C., Dai, Z., Zhou, J., Zhang, D., Jia, J., Jin, L., and Johnson, K.R., 2008, A Test of Climate, Sun, and Culture Relationships from an 1810-Year Chinese Cave Record: *Science*, v. 322, p. 940-942.

Zhong, H., Shi, H., Qi, X.-B., Xiao, C.-J., Jin, L., Ma, R.Z., and Su, B., 2010, Global distribution of Y-chromosome haplogroup C reveals the prehistoric migration routes of African exodus and early settlement in East Asia: *Journal of Human Genetics*, v. 55, p. 428-435.

Zhu, and R., 2003, Magnetostratigraphic dating of early humans in China: *Earth-Science Reviews*, v. 61, p. 341-359.